DISSERTATION

SUBMITTED TO THE

COMBINED FACULTIES FOR THE NATURAL SCIENCES

AND FOR MATHEMATICS

OF THE

RUPERTO-CAROLA UNIVERSITY OF

HEIDELBERG, GERMANY

FOR THE DEGREE OF

DOCTOR OF NATURAL SCIENCES

PRESENTED BY:

MARIYA VASILEVA, M.SC. IN MOLECULAR BIOTECHNOLOGY

BORN IN: CHIRPAN, BULGARIA

ORAL-EXAMINATION: .....

FUNCTION OF SYNAPSIN PROTEINS IN THE SYNAPTIC TRANSMISSION AT A GIANT CNS SYNAPSE

Referees: Prof. Dr. Thomas Kuner

Prof. Dr. Stephan Frings

Summary

At chemical synapses synaptic vesicles are functionally segregated into distinct pools depending on their mobility and release probability in response to action potentials. At most synapses synapsin proteins cluster and immobilize reserve pool vesicles within the cytoskeletal network, distally from the active zones. Activity-dependent phosphorylation of synapsins releases synaptic vesicles from the complex meshwork of the cytoskeletal components and renders them freely mobile and able to undergo vesicle cycling. There are three synapsin genes in mammals and their alternative splicing results in more than ten isoforms whose functional differences in maintaining synaptic transmission are not fully elucidated.

In this study we examined the involvement of synapsins in synaptic transmission using two independent approaches. First, we established the structure-function relationship at synapses, overexpressing synapsin I isoforms (synapsin Ia or synapsin Ib). Second, synaptic transmission and structural integrity of synapses in mice, lacking all three synapsin genes (triple knock-out (TKO)) were examined. The calyx of Held, a giant glutamatergic synapse located in the auditory brain stem, was utilized as a model system.

Synapsin I isoforms overexpression was accomplished through transduction of globular bushy cells (GBCs), located in the ventral cochlear nucleus, with recombinant adeno-associated viral particles. The GBCs are projection neurons, which give rise to the calyx of Held in the medial nucleus of the trapezoid body. 10 days after the transduction, overexpression of synapsin I isoforms resulted in a redistribution of SV within the calyx of Held, without changing the size and the overall structure of the perturbed synapses. Ultrastructural analysis, using serial sectioning scanning electron microscopy (S^3EM) revealed that synapsin Ia overexpression resulted in decreased numbers of SVs at the active zone without altering the total vesicle number. Therefore, we could conclude that synapsin Ia overexpression was followed by vesicle redistribution within the presynaptic terminal. On the functional level, the overexpression of both synapsin I isoforms had no effect on the properties of spontaneous and evoked EPSCs. However, repeated stimulation at frequencies exceeding 10 Hz led to accelerated short-term depression (STD). Overexpression of either isofroms led also to accelerated recovery from depression after strong stimulation.

Brain lysates from synapsin TKO mice revealed a strong reduction in the level of several synaptic vesicle proteins, while proteins of the active zone cytomatrix or of the postsynaptic density remained unaffected. Accordingly, TKO calyces had lower amounts of vGluT1 immunoreactivity while the level of the active zone marker bassoon was unchanged

as shown via 3D reconstructions of TKO calyces. The S^3EM analysis confirmed these results revealing a 50 % reduction in the number of synaptic vesicles in TKO calyces. The structural alterations resulting in the absence of synapsins led to accelerated and more pronounced STD at stimulation at frequencies above 100 Hz. Synapsin deletion, contrary to synapsin overexpression, slowed down the recovery of depression. This might prove that synapsin-dependent SVs contribute to the faster replenishment of the readily releasable pool, which maintains synaptic transmission under basic conditions. Despite the structural defects and the alterations in the short-term depression, transmission failures were not observed during the high-frequency trains. These results reveal that in wild-type synapses the synapsin-dependent vesicles account only for a small fraction of the SVs that enter the RRP.

In conclusion, synapsins maintain of a specific vesicle population at CNS synapses. However, these vesicles are dispensable from normal basal synaptic transmission and are recruited only when the synapse is exposed to long-lasting high-frequency activity. The synapsin-dependent vesicles are fed into the readily releasable pool to counteract the effects of presynaptic depression and aid the faster recovery of the synapse. Although synapsins may be required for normal synaptic vesicle biogenesis, trafficking and immobilization, they are not essential for sustained synaptic transmission at the calyx of Held.

Zusammenfassung

An chemischen Synapsen, werden synaptische Vesikel an Hand ihrer Mobilität und Freisetzungswahrscheinlichkeit verschiedenen funktionellen Pools zugeordnet. Die synaptischen Vesikel des Reservepools werden in den meisten Synapsen durch Synapsine an das Zytoskelett in Regionen entfernt von den aktiven Zonen gebunden. Synapsine können in Abhängigkeit von synaptischer Aktivität phosphoryliert werden, was zu einer Loslösung der Vesikel vom Zytoskelett führt. Die dann freibeweglichen Vesikel können am synaptischen Vesikelzyklus teilnehmen. In Säugern existieren drei Synapsingene die alternativ gespleißt werden, was zu mehr als zehn verschiedenen Isoformen führt. Die funktionellen Unterschiede der verschiedenen Isoformen bei der Regulation der synaptischen Transmission sind bis jetzt nur unzureichend verstanden.

Die funktionellen Eigenschaften der Synapsine wurden in der vorliegenden Arbeit in zwei verschiedenen Ansätzen untersucht. Zum einem wurden Struktur und Funktion von Synapsen untersucht in denen eine Synapsin-I-Isoform (Synapsin Ia oder Synapsin Ib) überexprimiert wurde, zum anderen die synaptische Transmission und die strukturelle Integrität von Synapsen bei denen alle drei Synapsingene ausgeschaltet wurden (*triple knock-out* (TKO)). Als Modelsynapse für beide Ansätze diente der Held'sche Calyx, eine glutamaterge Riesensynapse im auditorischen Hirnstamm.

Eine Überexpression von Synapsin-I-Isoformen wurde durch Transduktion von *globular bushy cells* (GBCs) im ventralen choclearen Nucleus mit rekombinanten adeno-assoziierten viralen Partikel erreicht. GBCs sind Projektionsneurone die im medialen Kern des kontralateralen Trapezkörpers die Held'schen Calyces bilden. Zehn Tage nach der Transduktion führte die Überexpression zu einer Umverteilung der synaptischen Vesikel innerhalb des Held'schen Calyx, dessen allgemeine Struktur nicht verändert wurde. Die ultrastrukturelle Analyse mittels *serial sectioning scanning* Elektronenmikroskopie (S^3EM) ergab dass weniger synaptische Vesikel in unmittelbarer Nähe zur aktiven Zone vorhanden waren. Da die Gesamtanzahl der synaptischen Vesikel nicht verändert war, ergab sich also eine Umverteilung der Vesikel bei Synapsin I Überexpression. Auf der funktionellen Ebene hatte die Überexpression von Synapsin I keinen Effekt auf spontane oder aktionspotentialabhängige Vesikelfreisetzung. Lediglich bei wiederholter Stimulation mit mehr als 10 Hz wurde eine beschleunigte Kurzzeitermüdung beobachtet. Die Erholung von dieser Ermüdung wurde allerdings auch durch beide Synapsin I Isoformen beschleunigt.

Bei der Untersuchung der Gehirne von TKO-Mäusen wurde eine starke Reduktion mehrer vesikulärer Proteine festgestellt, während Proteine der aktiven Zone und der

postsynaptischen Dichte nicht betroffen waren. Dementsprechend wiesen auf Immunfluoreszenz basierende 3D Rekonstruktionen von TKO-Calyces reduzierte Mengen des synaptischen Proteins vGluT1 aber nicht des aktiven Zonen-Markers Bassoon auf. Die ultrastrukturelle Analyse mittels S^3EM bestätigte diese Befunde, da TKO-Calyces eine um 50% reduzierte Anzahl von synaptischen Vesikeln aufwiesen. Diese strukturellen Veränderungen in der Abwesenheit von Synapsinen resultierten in einer beschleunigten und ausgeprägteren Kurzzeitermüdung bei Stimulationsfrequenzen über 100 Hz. Die Erholung von der Kurzzeitermüdung war, im Gegensatz zu Calyces die Synapsin I überexprimieren, in TKO-Calyces verlangsamt. Dies lässt vermuten, dass die Synapsin-abhängigen Vesikel zum schnellen Auffüllen des *readily-releasable* Pools, der die Vesikel zur Aufrechterhaltung der synaptischen Transmission stellt, beitragen. Trotz der strukturellen Defekte und der veränderten Kurzzeitermüdung wurde auch bei hohen Stimulationsfrequenzen kein Versagen der synaptischen Transmission beobachtet, was darauf hindeutet, dass der Anteil der Synapsin-abhängigen synaptischen Vesikel am *readily*-releasable Pool begrenzt ist.

Zusammenfassend lässt sich sagen, dass Synapsine für die Aufrechterhaltung einer spezifischen Vesikelpopulation an ZNS Synapsen nötig sind. Diese Vesikel sind allerdings während normaler synaptischer Transmission entbehrlich und werden erst bei dauerhafter, hochfrequenter Aktivität rekrutiert. Eine Erweiterung des *readily-releasable* Pools um diese Vesikelpopulation minimiert die präsynaptische Kurzzeitermüdung da mehr Vesikel zur Verfügung stehen die zur Erholung beitragen können. Trotz eine eindeutige Beteiligung der Synapsine an der normalen Biogenese der synaptischen Vesikel, deren Transport und Immobilization sind Synapsine nicht notwendig um eine hochfrequente, anhaltende und verlässliche synaptische Transmission im Held'schen Calyx zu gewährleisten.

Hereby, I officially declare that this dissertation has been conducted and written independently. It contains, to the best of my knowledge and belief, neither material previously published by another person nor material previously submitted for the award of any other degree or diploma of university or other institute of higher learning, except where due acknowledgment has been made in the text.

Heidelberg, 25.05.2012 …….

Mariya Vasileva

Table of Contents

1. Introduction 9
1.1. Chemical synapses – functional units of neuronal communication 10
1.2. Synaptic vesicles and synaptic vesicle recycling 13
1.2.1. Targeted transport of synaptic vesicles to the active zone 14
1.2.2. Synaptic vesicle cycle 15
1.3. Synaptic vesicle biogenesis and transport of presynaptic precursor molecules 16
1.4. Synaptic vesicle pools 17
1.5. Neurotransmitter release 19
1.5.1. Evoked release 19
1.5.2. Spontaneous release 19
1.5.3. Neuronal plasticity 20
1.5.4. Short-term facilitation 21
1.5.5. Post-tetanic potentiation 21
1.5.6. Short-term depression 22
1.6. Calyx of Held 23
1.6.1. The calyx of Held as a model synapse 23
1.6.2. Vesicle dynamics at the calyx of Held 25
1.7. Synapsins 26
1.7.1. Synapsin trafficking to the presynaptic terminal 28
1.7.2. Pre-docking function of synapsins 29
1.7.3. Putative functions of synapsins during the later stages of the SV cycle 30
1.7.4. Summary – synapsins function at the presynaptic terminal 31
1.8. Aim of the study 32

2. Materials and Methods 34
2.1. Animals 34
2.2. Plasmid cloning 34
2.3. Virus preparation 35
2.3.1. Cultivation of and transfection of AAV 239 cells 36
2.3.2. Recombinant adeno-associated virus production 36
2.4. Stereotaxic injection of recombinant adeno-associated viral particles 37
2.4.1. Stereotaxic setup 37
2.4.2. Injection capillaries 37
2.4.3. Injection procedure 37
2.5. Perfusion 39
2.6. Immunohistochemistry 39
2.7. Antibodies 40
2.8. Confocal imaging 40
2.8.1. Dye separation 41
2.8.2. Excision of Calyx-specific immunosignals and visualization of 3D image data 42
2.9. ELISA 42
2.10. Photooxidation and electron microscopy 42
2.10.1. Photooxidation 42
2.10.2. Tissue preparation for EM 43
2.10.3. Block preparation and serial sectioning 43
2.10.4. Preparation of the silicon wafer strip 43
2.10.5. SEM Imaging 44
2.10.6. Data Analysis 44
2.11. Electrophysiology 45
2.11.1 Rat experiments 45
2.11.2 Mice experiments 46
2.12. Statistics 47

3. Results 48
3.1. Structural and functional consequences of the overexpression of synapsin I isoforms in the rat calyx of Held 48
3.1.1. Identification and distribution of endogenous synapsin isoforms in the rat calyx of Held 48
3.1.2. Colocalization of synapsin isoforms with synaptic vesicles within the calyx of Held .. 52
3.1.3. Proper targeting of acutely overexpressed synapsin Ia/Ib to the calyx of Held 53
3.1.4. Redistribution of SVs within perturbed terminals upon overexpression of both synapsin I isoforms 56
3.1.5. Basal transmission at the calyx of Held is independent of synapsin I isoforms 58
3.1.6. Synapsin I isoforms control the use-dependent synaptic plasticity at the calyx of Held without changing the size of the readily releasable pool 61
3.1.7. Accelerated recovery from depression in calyces overexpressing synapsin I isoforms 65
3.1.9. Ultrastructural alterations at the calyx of Held upon overexpression of synapsin Ia . 67
3.1.10. Summary – overexpression of synapsin I isoforms leads to structural redistribution at the active zone, which underlies increased short-term depression at the calyx of Held synapse 73
3.2. Structure – function relationship at the calyx of Held in TKO mice 74
3.2.1. Distribution of endogenous synapsin isoforms in the mouse MNTB 74
3.2.2. Deletion of synapsin genes results in downregulation of SV associated proteins 76
3.2.3. Deletion of synapsin results in decreased levels of vGluT1 immunofluorescence within the calyx of Held 77
3.2.4. Electron microscopy revealed decreased number of SVs within the bulk volume of the TKO calyx of Held 81
3.2.5. Increased AZ areas and SV diameters in calyces lacking synapsins 84
3.2.6. Synapsin deletion spares basal synaptic transmission at the calyx of Held 88
3.2.7. Synapsins control short-term depression at the calyx of Held 91
3.2.8. Synapsins contribute to replenishment of the readily releasable pool 93
3.2.9. Synapsins control the fast component of recovery from depression 95
3.2.10. Summary – synapsins control the biogenesis and immobilization of synaptic vesicles and hence maintain the replenishment of the readily releasable pool during high-frequency transmission at the calyx of Held 96
4. Discussion 98
4.1. Subcellular localization of endogenous synapsin isoforms within the rodent calyx of Held 100
4.2. Effects of overexpression of synapsin I isoforms on the structure of the calyx of Held 102
4.2.1. Redistribution of SVs upon overexpression of synapsin I isoforms 102
4.2.2. Ultrastructure of the calyx of Held upon overexpression of synapsin Ia 103
4.2.3. Synapsin I overexpression does not affect basal neurotransmitter release and RRP function 104
4.2.4. Synapsin I isoforms accelerate short-term depression 105
4.2.5. Accelerated recovery from depression after EYFP-synapsin Ia/Ib overexpression . 106
4.2.6. Synapsin Ia/Ib overexpression and the synapsin dimerization hypotheis 107
4.3. Consequences of synapsin gene deletion that ensue at the mature calyx of Held. 108
4.3.1. Synapsins define the resting pool of SVs and may function upstream of presynaptic terminals 108
4.3.2. Synapsins do not control calyx maturation and morphology 110
4.3.3. Normal synaptic vesicle organization at active zones and putative compensatory effects 111
4.3.4. Basal synaptic transmission – largely unaltered by the deletion of synapsins 112
4.3.5. Altered short-term plasticity at the calyx of Held in TKO animals 113
4.4 Summary – mechanisms of synapsins action at the calyx of Held 114

4.5. Outlook **115**

5. Appendix **117**

5.1. Supplementary figures **117**

5.2. Abbreviations **120**

5.3. Acknowledgements **123**

5.4. References **124**

1. Introduction

The human brain is the most sophisticated organ in nature and allows us to discriminate an insurmountable variety of events in the environment. The activity of the brain underlies not only simple motor behaviors such as movement and food consumption, but all complex cognitive and emotional functions that we believe are ultimately human: thinking, speaking, creating of works of art and a sophisticated environment. The remarkable range of human behavior depends on an elaborate array of sensory inputs to the brain, which are organized in perceptions and then into appropriate behavioral responses. All this is accomplished by utilizing the capabilities of the nerve cells and their connections - synapses. There are 10^{11} nerve cells in the human brain and each of them receives on average 10^3 connections, which communicate in a precisely directed and timed manner. The number of synapses formed between two neurons determines the reliability and strength of the connection and thereby the properties of the underlying neuronal circuit (reviewed in (Atwood and Karunanithi, 2002)).

Although the nerve cells can be classified in various different types, all of them share similar basic architecture – they are polarized structures with four morphologically and functionally defined regions – cell body, dendrites, axon and presynaptic terminals. From the cell body (soma), which contains the nucleus and the major cytoplasmic organelles, a variable number of dendrites emanates and ramifies over certain volume of gray matter. The axon extends away from the cell body and is the main conducting unit of signals to other neurons. These electrical signals, called action potentials, are rapid, transient, all-or-none impulses (Hodgkin and Huxley, 1945). They are generated at a specialized trigger region – the axon initial segment and are successfully propagated towards the presynaptic terminals – the communication sites with the other neurons.

Neuronal communication is underlined by complex molecular processes, which control the precisely timed generation and transmission of the action potential from one cell to the next. A highly regulated interplay between various proteins maintains the release of neurotransmitter from small clear-core vesicles at the site of connection between two neuronal cells. Although decades of scientific research have led to a comprehensive understanding of these processes, the exact *in vivo* function of the separate molecular players has not been unraveled. Therefore, it is crucial to examine protein function within intact properly matured synapses, whose structural and functional properties are well established.

1.1. Chemical synapses – functional units of neuronal communication

Neuron-to-neuron communication is maintained through multiple synaptic contacts, which determine the strength of the connection between the two cells. There are two types of synapses: electrical and chemical. At electrical synapses ionic current passes through gap junction pores from one neuron to another. The neuron into which the current is generated is the presynaptic neuron and the neuron into which the current flows is the postsynaptic neuron.

At chemical synapses structural continuity does not exist between the presynaptic and postsynaptic compartments, which are separated by the synaptic cleft. The presynaptic elements contain multiple synaptic vesicles (SVs) filled with neurotransmitters, which when bound to the postsynaptic receptors control the probability of a given cell to reach the threshold for action potential (AP) firing. There are two major types of chemical synapses, depending on the effect of their neurotransmitter on the postsynaptic cell – excitatory and inhibitory synapses. The excitatory (gray type I or asymmetric) synapses are characterized by the presence of a pronounced postsynaptic density and a wide synaptic cleft, while the inhibitory (gray type II or symmetric) synapses have less prominent postsynaptic densities.

Signal transduction at chemical synapses depends entirely on the precisely regulated secretion of neurotransmitters from the presynaptic cell and the presence of specific receptors on the surface of the postsynaptic cell. The arrival of the action potential at a chemical synapse induces the opening of voltage-gated Ca^{2+} channels (primarily P/Q and N-type) and the resulting pulse of Ca^{2+} ions into the compartment stimulates the propagation of the presynaptic response (Fig. 1.1 A). It was shown that the amplitude of the response to an action potential varies by a multiple of stereotyped quanta (Katz, 1971), which proved to be synaptic vesicles (Heuser and Reese, 1981; Heuser et al., 1979). Synaptic vesicles fuse with the membrane and release neurotransmitter in the synaptic cleft where it activates postsynaptic receptors. Ca^{2+} influx triggers two components of release that are probably mechanistically distinct – a fast, synchronous phasic component, rapidly induced within 50 μs after a Ca^{2+} transient develops (Sabatini and Regehr, 1996) and a slower asynchronous component, which continues for more than 1 s as an increase in the rate of spontaneous release after the AP (Atluri and Regehr, 1998; Barrett and Stevens, 1972) Both components are highly Ca^{2+} dependent but change differentially upon repetitive stimulation (for review see (Südhof, 2004)). Figure 1.1 B describes the changes in membrane responses during the process of signal transduction at chemical synapses. When an AP invades the presynaptic terminal, the Ca^{2+} current (I_{Ca2+}) begins at the peak of the action potential, reaches its maximum during the descending phase of the AP, and ends before the terminal is fully

repolarized. The immediate drop down in the Ca^{2+} transient immediately terminates release but the neurotransmitters released in the presynaptic cleft activate postsynaptic receptors to elicit a postsynaptic response (eEPSC) and an AP in the postsynaptic cell, which propagates further on.

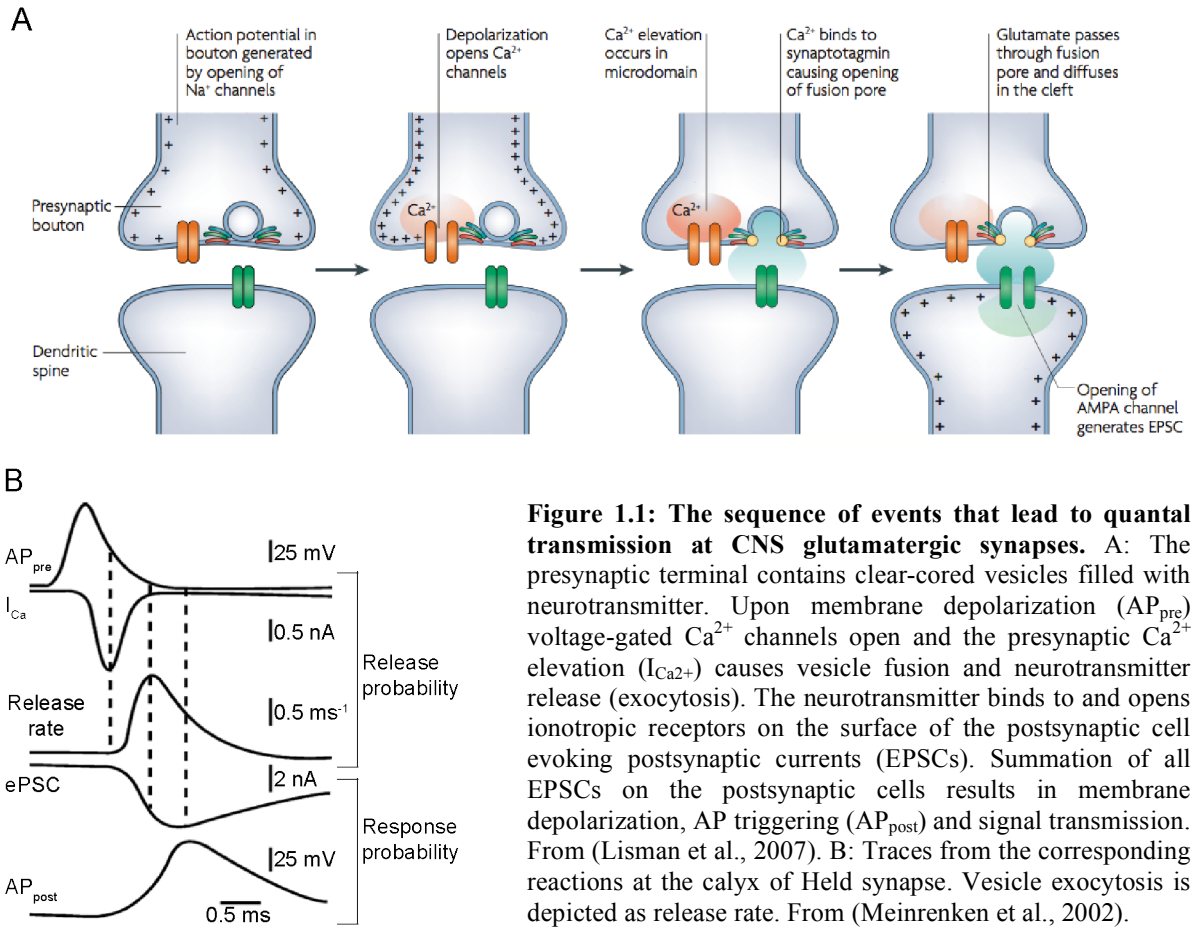

Figure 1.1: The sequence of events that lead to quantal transmission at CNS glutamatergic synapses. A: The presynaptic terminal contains clear-cored vesicles filled with neurotransmitter. Upon membrane depolarization (AP_{pre}) voltage-gated Ca^{2+} channels open and the presynaptic Ca^{2+} elevation (I_{Ca2+}) causes vesicle fusion and neurotransmitter release (exocytosis). The neurotransmitter binds to and opens ionotropic receptors on the surface of the postsynaptic cell evoking postsynaptic currents (EPSCs). Summation of all EPSCs on the postsynaptic cells results in membrane depolarization, AP triggering (AP_{post}) and signal transmission. From (Lisman et al., 2007). B: Traces from the corresponding reactions at the calyx of Held synapse. Vesicle exocytosis is depicted as release rate. From (Meinrenken et al., 2002).

The release evoked by an AP is proportional to both the size of the vesicle pool available for immediate release and the fraction of this pool, which is actually released by the action potential (Liley and North, 1953). However, neither the fraction of the released vesicles (Betz, 1970) nor the rate of replenishment of the releasable pool is constant (Kusano and Landau, 1975). Instead, they both are consequence of the inherently stochastic nature of molecular and cellular processes that drive exocytosis. Activity-dependent, complex molecular and structural processes transform synapses into plastic structures and influence their abilities to store and relay information on different time scales – ranging from milliseconds to days and weeks (Feldman, 2009; Zucker and Regehr, 2002). Therefore, it is crucial to study the events that determine synaptic activity under different conditions, understand their basic mechanisms and identify their molecular components.

The asymmetric structure and the molecular components of the pre- and postsynaptic components result from the directional nature of synaptic transmission. Presynaptic compartments are characterized by the presence of a large number of neurotransmitter-filled vesicles and active zones (AZs) – specialized patches of the presynaptic plasma membrane where SVs dock, prime, fuse and release neurotransmitter into the synaptic cleft. The active zone is characterized by the presence of the cytoskeletal matrix (CAZ) – electron-dense matrix of proteins, which is thought to facilitate and regulate the SV translocation to the presynaptic plasma membrane and to define the site of SV docking and fusion. Figure 1.2 gives a summary of the multiple proteins involved in the formation and function of the AZs. The proteins that define the AZ are grouped in distinct complexes depending on their function and molecular structure. The first complex is largely structural with main function to develop and hold the active zone opposite to the postsynaptic density (PSD), and to cluster Ca^{2+} channels within the plasma membrane. It comprises of cell adhesion molecules such as neuroligin, neurexin, N-cadherin, SynCAM and NCAM. Additionally, large scaffolding proteins such as piccolo, bassoon and ERC/Cast, and other cytoskeletal components such as liprin, CASK, velis, mint and spectrin belong to the complex.

The second group of AZ proteins encompasses proteins involved in SV docking and fusion. It contains components of the SNARE complex, Rim, Rab3a, Munc13 and Munc18, as well as N- and P/Q types of Ca^{2+} channels. The third complex involves proteins required for SV endocytosis and retrieval, including clathrin, dynamin and a family of SH3-domain containing adaptor proteins.

On the postsynaptic site, within the postsynaptic density large proteins, containing PDZ domains, such as SAP90/PSD95 are abundant and build specialized protein complexes around subclasses of ionotropic glutamate receptors (AMPA and NMDA receptors) and metabotropic receptors. Tyrosine kinase receptors (EphB) regulate the receptor recruitment from endosomal pools. Proteins such as NARP and ephrin-B probably promote the clustering of AMPA and NMDA receptors respectively (for review see (Ziv and Garner, 2004)).

The strength of synaptic connections is regulated by various molecular processes in the presynaptic terminal, which determine the number of vesicles in different functional states, their directional translocation to the active zone during activity, and the probability of release in response to a calcium signal.

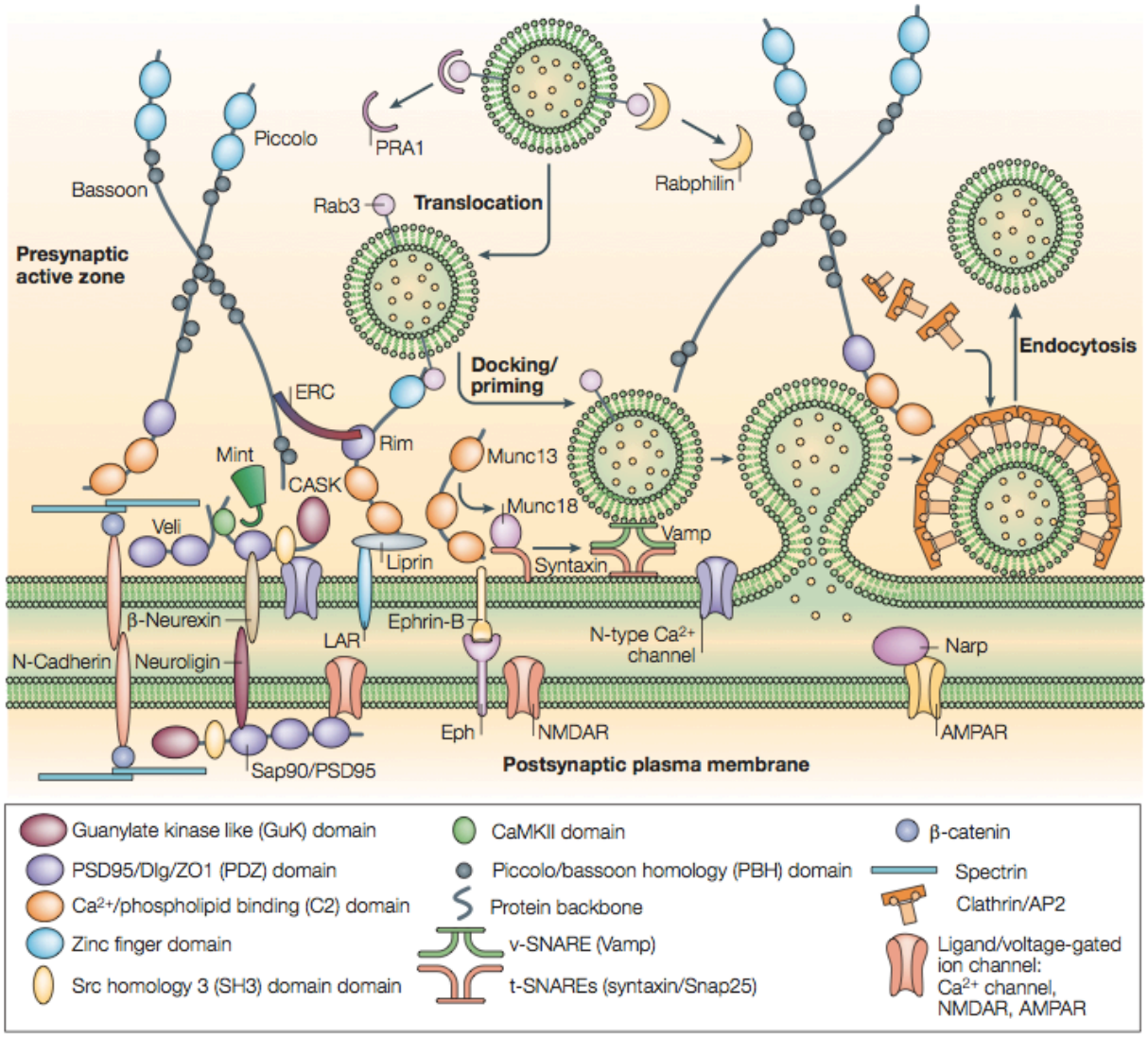

Figure 1.2: Molecular complexity of the glutamatergic central nervous system synapse. The presynaptic compartment is characterized by the presence of three distinct groups of proteins: (1) active zone proteins – large scaffolding molecules that hold the AZ aligned with the postsynaptic density; (2) proteins involved in the synaptic vesicle cycle; (3) postsynaptic proteins, including PDZ-domain-containing proteins and postsynaptic receptors. From (Ziv and Garner, 2004).

1.2. Synaptic vesicles and synaptic vesicle recycling

Synaptic vesicles (SVs) are uniformly small organelles of approximately 40 nm in diameter (Takamori et al., 2006) whose function is to take up and release neurotransmitter. In order to maintain high-fidelity synaptic transmission, exocytosed vesicles have to be retrieved from the presynaptic membrane and reconstructed. SVs participate in consecutive trials of exo- and endocytosis, known as the synaptic vesicle cycle. SVs are dispersed within the presynaptic terminal and contain two classes of obligatory components – (1) trafficking proteins, which participate in the SV endo- and exocytosis and (2) recycling and transport proteins involved in

neurotransmitter uptake. The trafficking proteome of the SV is complex and includes intrinsic membrane proteins, proteins associated with the SV membrane via posttranslational modifications and peripherally bound proteins. All these proteins function at precise steps of the SV cycle: targeted transport of synaptic vesicles to the active zone; tethering and docking of SVs onto the plasma membrane; SV priming; SV fusion with the presynaptic membrane; SV retrieval and recycling (Heuser and Reese, 1973).

1.2.1. Targeted transport of synaptic vesicles to the active zone

Although present within the complete volume of the presynaptic terminal and containing the same set of proteins, SVs are functionally organized into distinct clusters. The SVs, which are located away from the AZs form a reservoir of neurotransmitter-filled vesicles, which do not actively participate in neurotransmission and are anchored to actin filaments most probably via synapsins (Ferreira and Rapoport, 2002; Valtorta et al., 1992).

There are two models that describe the process of vesicle transport to the AZs: (1) directed movement towards the active zone, involving cytoskeletal tracks to guide vesicles to the AZ and (2) random diffusion. It is highly probable that actin could guide SVs towards the AZ. Actin filaments are strongly involved in the transport of newly endocytosed vesicles back into the cluster (Bloom et al., 2003; Shupliakov et al., 2002). However, less actin is found within the clusters and actin disruption experiments have produced diverse results. The most common effect was depression of neurotransmitter release, shown at the NMJ of Drosophila larvae and the calyx of Held (Kuromi and Kidokoro, 1998; Sakaba and Neher, 2003). Similar experiments in the goldfish bipolar terminals did not show any change in the release parameters (Job and Lagnado, 1998) and led to slight potentiation at hippocampal boutons (Sankaranarayanan et al., 2003)

Upon Ca^{2+}-dependent phosphorylation of synapsins SVs are set free from the cytoskeletal network (Hosaka et al., 1999). However, less than 15% of the available SVs participate actively in the SV cycle and the rest remains immobilized in the reserve pool (Denker et al., 2011; Harata et al., 2001). Small GTPases Rab3A and Rab3C most probably mediate SV transportation from the reserve pool to the active zone (Leenders et al., 2001). Synapsins and Rab3a interact with each other regulating the activity of the two proteins. Synapsins stimulate the Rab3a GTPase activity and recruitment to the SV membrane, while Rab3a inhibits the actin binding and vesicle clustering activity of synapsins (Giovedì et al., 2004a).

1.2.2. Synaptic vesicle cycle

After reaching the AZ the vesicles undergo multiple rounds of exo- and enocytosis. During the process of tethering SVs bind to the active zone where large scaffolding proteins like piccolo and bassoon spatially organize the vesicles (Gundelfinger et al., 2003). Priming is the mere process of SVs becoming fusion competent. During this process a SNARE complex is assembled, which mediates the interconnection of SVs and the pre-synaptic membrane. Recognition between v-SNAREs (synaptobrevin) and t-SNAREs (SNAP-25 and syntaxin) mediates SV docking. SM-family of proteins regulates the formation of the SNARE complex (Verhage et al., 2000). Munc 18-1 binds tightly to syntaxin 1 and competes with the formation of the SNARE complex, while Munc 13 counteracts this interaction. Complexin binding to the complex stabilizes the interaction between synaptobrevin and syntaxin and functions as a fusion clamp to seal SVs in a primed state (Giraudo et al., 2006; Schaub et al., 2006). The SNARE complex is disassembled by the ATPase activity of NSF.

Docking and priming brings vesicles in close proximity to presynaptic Ca^{2+} channels and the local increase of Ca^{2+} concentration proximal to the SV leads to the fusion event (Katz and Miledi, 1969a). Synaptotagmin 1 has been distinguished as a putative candidate for the Ca^{2+} sensor (Bai and Chapman, 2004). Ca^{2+} bound synaptotagmin 1 displaces complexin 1 from the membrane anchored SNARE complexes, allowing SVs to fuse with the presynaptic membrane (reviewed in (Rizo and Rosenmund, 2008; Rizo and Südhof, 2002)).

To allow the completion of the cycle, vesicles are retrieved from the membrane and recycled back into the presynaptic terminal. Three alternative pathways have been proposed: kiss-and-run (Ceccarelli et al., 1973), full fusion followed by classical clathrin-mediated endocytosis and full fusion mediated by bulk membrane retrieval (Heuser and Reese, 1973). According to the “kiss-and-run” mechanism, SVs, following the brief formation of a fusion pore, do not remain attached to the AZ and are immediately retrieved from the membrane, thus becoming available for another round of release. Full fusion is characterized by the complete SV membrane collapse into the presynaptic membrane as the content of neurotransmitter is released. To compensate for the resulting membrane enlargement, endocytosis takes place. The mechanism of clathrin-dependent endocytosis involves recruitment of clathrin coat by adaptor proteins, acquisition of curvature mediated by endophilin, epsin and other proteins and the subsequent scission of the nascent vesicle from the plasma membrane mediated by dynamin. Synaptic vesicle components retrieved by bulk endocytosis remain in contact with the plasma membrane on deep infoldings or are delivered to an endosome after the first budding from the membrane (reviewed in (Santos et al., 2009)).

The bulk endocytosis is classically viewed as an emergency mechanism, which operates when the other endocytotic pathways are exhausted (Ceccarelli and Hurlbut, 1980; Holt et al., 2004).

1.3. Synaptic vesicle biogenesis and transport of presynaptic precursor molecules

The specialized role of SVs relies on a restricted set of proteins (see above) that allows neurotransmitter storage and release. SV membrane proteins lack a common sorting motif and employ several strategies for targeting along the intracellular trafficking pathway from the soma to the presynaptic terminal. SV membrane proteins are synthesized and inserted in the membrane of the rough ER and are trafficked through the Golgi complex (Bonanomi et al., 2006; Hannah et al., 1999; Prado and Prado, 2002). Newly synthesized membrane proteins exit the Golgi complex either in constitutive secretory vesicles (CSV), common for all eukaryotic cells, or regulated secretory vesicles (RSV), typical for cells capable of regulated secretion (Blázquez and Shennan, 2000; Régnier-Vigouroux et al., 1991). An alternative hypothesis proposes the *de novo* formation of SVs, which might be formed directly from the TGN and are then transported down the axon to the presynaptic compartment (Holtzman, 1977; Janetzko et al., 1989). It is also shown that SVs can be formed locally at the presynaptic terminal after constitutive recycling of membrane carriers from endosomal intermediates (Ahmari et al., 2000). SV proteins in CSV might be delivered to the presynaptic membrane and go through several rounds of constitutive exo-endocytosis that may sort and cluster proteins (Barbosa et al., 2002; Régnier-Vigouroux et al., 1991; Santos et al., 2001).

During synaptogenesis distinct membrane carriers deliver functional sets of presynaptic proteins to the nascent synapse by fast axonal transport along microtubules (Hirokawa and Takemura, 2005). Scaffolding proteins of the AZ such as piccolo, bassoon and RIM are delivered on dense core vesicles, with a diameter of approximately 80 nm, which do not contain SV proteins such as synaptotagmin, synaptobrevin, synaptophysin. These vesicles termed piccolo/bassoon transport vesicles (PTVs) were suggested to be AZ precursor vesicles that lead to the rapid formation of new AZs on fusion with the presynaptic plasma membrane (Shapira et al., 2003; Zhai et al., 2001). PTVs carry also other presynaptic components, implicated in SV exocytosis: Munc 13, Munc 18, syntaxin, SNAP 25, N-type Ca^{2+} channels (Shapira et al., 2003). ERCs and α-liprins, which play role in the linking of the component of the CAZ have also been found on PTVs (Kim et al., 2003; Ohtsuka et al., 2002). Mobile PTVs are not associated with synaptic vesicles or with synapsin I.

SV proteins are transported down the axon in the form of tubulovesicular organelles as precursors and assembled as SVs in the presynaptic terminals. These precursor packages are different from the PTVs and contain vesicle-associated proteins such as synaptotagmin, synaptophysin, Rab3a but are lacking presynaptic membrane proteins (Ahmari et al., 2000).

1.4. Synaptic vesicle pools

In a typical synapse at rest only a small percentage of the available vesicles are attached at the membrane of the AZ, while the rest reside in the adjoining vesicle cluster. Apart from the relatively few SVs that are docked to the plasma membrane, the vast majority seems to constitute a single homogenous population without significant biochemical or morphological distinction. However, not all SVs are functionally equivalent but are organized in distinct SV pools depending on different kinetics of release and retrieval. The classical model of pool organization describes three distinctly localized pools of vesicles, which show differential release probabilities (Figure 1.3 A) – (1) readily releasable pool (RRP), (2) recycling pool and (3) reserve (resting) pool (reviewed in (Rizzoli and Betz, 2005)). Upon arrival of an AP the RRP SVs are released first, followed by release of recycling vesicles. Reserve vesicles are recruited only during continuous stimulation at high frequency (Figure 1.3 B).

The RRP includes approximately 1 % all SVs in the synapse. Various techniques have been implemented to measure the size of the RRP ranging from trains of 5 – 15 stimuli at high frequency (Elmqvist and Quastel, 1965; Richards et al., 2003; Schneggenburger et al., 1999) through a few milliseconds of depolarization (Mennerick and Matthews, 1996; Neves and Lagnado, 1999) to 1 s of hypertonic shock (Rosenmund and Stevens, 1996) and all of these methods result in the release of the same subset of vesicles. It is possible, however, that subpopulations of SVs with different release characteristics are present within the RRP. This has been proven for the calyx of Held and the hippocampus, where the RRP is divided into fast and slow release components (Hanse and Gustafsson, 2001; Hanse and Gustafsson, 2002; Sakaba and Neher, 2001a).

The recycling pool contains typically 5 – 20 % of all SVs, which are released upon moderate (physiological) stimulation. These SVs recycle constantly and newly recycled vesicles refill the recycling pool. Finally, at most synapses the reserve pool contains the majority SVs (80 – 90 % of all SVs in the terminal), which are reluctant to release and therefore are recruited only upon high-frequency stimulation when the capacity of recycling pool is exhausted. It is possible that the reserve vesicles are never recruited during physiological activity. The depletion of recycling SVs will trigger reserve pool mobilization

and release, although the underlying molecular mechanisms remain obscure (Kuromi and Kidokoro, 1998; Richards et al., 2000; Richards et al., 2003).

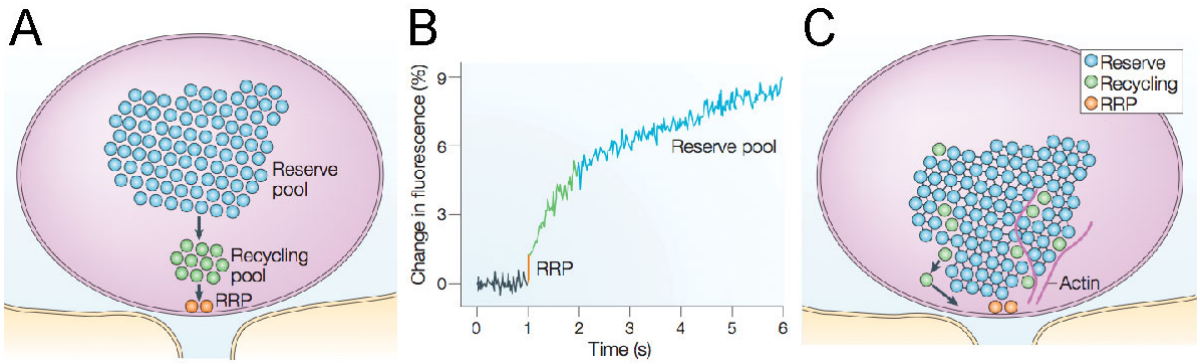

Figure 1.3: Three vesicle pools coexist at presynaptic terminals. A: The classic model of spatial segregation of reserve (RP), recycling and readily releasable pool (RRP). The RP makes up to 80 – 90 % of all SVs and form a cluster at the back of the terminal away from the release site, RRP vesicles, docked and primed for release, comprise only ~ 1 % of the total SV number. The remaining 10 – 15 % of the SVs constitute the recycling pool, which feed into the RRP. B: Release kinetics of the distinct pools at the goldfish bipolar cells. Vesicles belonging to the different pools have different release probabilities. C: Emerging model for spatial intermixing of vesicle pools. The RRP vesicles are docked and immobile, the reserve vesicles form most of the cluster and are tightly crosslinked by synapsin or other unknown synapsin-like proteins. The recycling vesicles are mobile and can to diffuse to the AZ (alternatively they might interact with cytoskeletal elements, which will direct them towards the AZ). From (Rizzoli and Betz, 2005).

The SVs in the RRP must, by definition, be able to undergo fusion immediately after stimulation, so that they must lie likely at or very close to the presynaptic membrane and consequently to voltage-gated Ca^{2+} channels. However, it might be possible that not all docked vesicles are available for immediate release (Denker et al., 2009; Rettig and Neher, 2002; Rizzoli and Betz, 2004). The vesicles that make up the other pools are recruited at a leisurely pace during repetitive stimulation and could be transported to release sites from any location within the presynaptic terminal, indicating that SVs in the recycling and reserve pools are intermixed to a large extent. According to this model SVs are spatially but not functionally intermixed (Fig. 1.3 C) (Rizzoli and Betz, 2005). The movement of the reserve vesicles might be restricted through binding to some scaffolding molecule, most probably synapsins. Additionally, a time-dependent exchange of SVs between the two pools might exist. The recycling vesicles are not as stably connected to the SV cluster as the reserve vesicles and with time they might mature into reserve vesicles by binding to the scaffolding molecules and integrating into the SV cluster (Gaffield et al., 2006). Conversely, reserve vesicles are not very likely to transform into recycling vesicles. The reserve vesicles appear to

become a part of the recycling pool only after exo- and endocytosis (Denker, 2010). In agreement with this model recently exocytosed vesicles are very mobile, whereas this mobility is lost with time as newly endocytosed vesicles integrate into the vesicle cluster (Kamin et al., 2010). This model of constant exchange between the recycling and reserve pool of vesicles requires specific molecular tags to define the pool affiliation. It is highly probable that synapsin family of phosphoproteins (see below) serves the role of a molecular tag, since it associates with vesicles in an activity dependent manner (Orenbuch et al., 2012b).

1.5. Neurotransmitter release

Fusion of synaptic vesicles and neurotransmitter release occurs on three different scales, either tightly coupled to action potentials (synchronous release), immediately following action potentials (asynchronous release) or as stochastic events in the absence of action potentials (spontaneous release). The different types of release are differentially coupled to the Ca^{2+} current invading the presynaptic terminal, with evoked release being Ca^{2+} dependent and spontaneous release being largely Ca^{2+} independent. It is possible that both types of transmission are supported by the same quanta, which means the evoked activity is merely a stimulus-enhanced probability of fusion for the very same SVs that are also fusing spontaneously.

1.5.1. Evoked release

Evoked release is tightly coupled to the AP and generates a postsynaptic response with a submillisecond delay. The process of evoked neurotransmitter release is non-uniform for every arriving action potential and is contingent on its preceding activity of the presynaptic terminal, i.e. the number of quanta released following a stimulus depends on the frequency and duration of previous stimulation. Both pre- and postsynaptic factors modulate neurotransmitter release, making it a highly dynamic and probabilistic phenomenon. The basic molecular mechanisms behind the process of evoked neurotransmitter release are described in detail in Chapter 1.2.

1.5.2. Spontaneous release

In the absence of neuronal stimulation, neurotransmitter release can still occur spontaneously, (Fatt and Katz, 1952). At rest the machinery responsible for SV fusion is active at very low release probability, giving rise to “miniature potentials”. These low release probability events correspond to the release of a single quantum that presumably originates from the fusion of a

single SV with the presynaptic membrane (Katz and Miledi, 1969b). Therefore, spontaneous release events provide information on the unitary properties of the synaptic transmission such as neurotransmitter content of individual vesicles and number of postsynaptic receptors that respond to a single vesicle release. The random unitary release events, known as "minis", are only loosely coupled to fluctuations in the intracellular Ca^{2+} concentration and Ca^{2+} modulators (Angleson and Betz, 2001). There are two major scenarios for the structural origin of spontaneous release: (1) spontaneous fusion may originate from the same pool as the evoked fusion (Groemer and Klingauf, 2007; Wilhelm et al., 2010) and therefore the extent of spontaneous release might reflect the number of readily releasable vesicles and spontaneous fusion will be a mere probabilistic event; (2) spontaneous release might result from the fusion of SVs belonging to a pool independent from the one mobilized during neuronal activity (Fredj and Burrone, 2009; Sara et al., 2005) and hence might require a distinct molecular machinery and might recycle uniquely from the SVs fusing in response to an AP. It is possible that non-canonical SNARE such as VAMP7 and Vti1 might maintain spontaneous release in its naïve form (Ramirez et al., 2012).

Both evoked and spontaneous fusion can be differentially affected by mutations or genetic ablations of molecules that are important for vesicle fusion. For example, knock out of synaptotagmin 1 or complexin results in greatly decreased evoked release without altering the spontaneous release (Maximov and Südhof, 2005; Reim et al., 2001). Additionally, deletion of SNARE components such as synaptobrevin or Munc 18-1 abolishes both modes of neurotransmitter (Schoch et al., 2001; Verhage et al., 2000), which combined with the phenotypes observed in the synaptotagmin and complexin knock-outs strongly argues against the idea of one release machinery for both types of fusion.

1.5.3. Neuronal plasticity

Neurons are able to modify their responses to incoming stimuli depending on the previous neuronal activity. Synaptic plasticity regulates the excitability of the neuronal network depending on the levels of network activity and can be roughly sub-divided into short-term and long-term plasticity (reviewed in (Timofeev, 2011)).

Short-term plasticity is a fast process, which occurs on millisecond to minute time scale. It functions on the network level to facilitate or prevent signal transmission and reflects a presynaptic change in neurotransmitter release (del Castillo and Katz, 1954; Katz and Miledi, 1968; Zucker and Regehr, 2002). Upon repetitive action potential activity, synapses do not respond uniformly but their release is augmented in time- and activity dependent

manner. This process can lead to presynaptic enhancement through two processes – facilitation (STF) and post-tetanic potentiation (PTP) or to reduction of neurotransmission, resulting in synaptic depression (STD), or to a mixture of both synaptic facilitation and depression. The magnitude of facilitation or depression varies between synapses depending on the stimulus frequency and the stage of development and maturation. All forms of presynaptic plasticity are Ca^{2+} dependent and the residual Ca^{2+} remaining in the synapse after an action potential augments synaptic transmission (Katz and Miledi, 1968; Zucker and Regehr, 2002).

Long-term plasticity represents the long-lasting augmentation of the communication between two neurons, which is based on the exact stimulation conditions and can be potentiating or depressing. It occurs on the scale of minutes and hours and is implicated in the formation of short-term memory including learning and forgetting The long-lasting changes of the synaptic connections between neurons can involve the making or breaking of synaptic contacts and morphological changes in the dendritic spines leading to larger injected synaptic currents and shorter time constant for Ca^{2+} compartmentalization (Yuste and Bonhoeffer, 2001).

1.5.4. Short-term facilitation

Short-term facilitation occurs at many synapses with low release probability, where repetitive stimulation at short intervals leads to transient increase in the neurotransmitter release. It is speculated that the residual Ca^{2+}, which remains in the presynaptic terminal following an AP, is involved in the synaptic facilitation. The residual Ca^{2+} enhances transmission via binding to a yet unknown high-affinity Ca^{2+} sensor different from synaptotagmin, which is responsible for SV fusion (Atluri and Regehr, 1996; Tang et al., 2000). Another mechanism that underlies synaptic facilitation might be the saturation of endogenous Ca^{2+} buffers (Blatow et al., 2003; Matveev et al., 2004; Neher, 1998). Finally, a use-dependent increase in Ca^{2+} currents would also increase the probability of release and contribute to facilitation (Inchauspe et al., 2004; Ishikawa et al., 2005).

1.5.5. Post-tetanic potentiation

Post-tetanic potentiation is observed after sustained high-frequency synaptic activation. It lasts for tens of seconds to minutes and becomes longer lasting when the stimulus frequency and duration are increased. The most probable mechanism behind the PTP is increased probability of release due to the increased level of residual Ca^{2+}, alteration of Ca^{2+} channels

and of vesicles. At the calyx of Held tetanic stimulation can increase the size of the RRP released by high frequency train (Lee et al., 2008). SVs located both proximally and distally to the voltage-gated Ca^{2+} channels would be recruited for the generation of large Ca^{2+} transients that lead to PTP (Müller et al., 2010; Sakaba, 2006).

1.5.6. Short-term depression

At many synapses repeated stimulation delivered at short time intervals leads to a transient decrease in the release probability, termed short-term depression. Various mechanisms have been attributed to maintain this type of synaptic plasticity (Fioravante and Regehr, 2011) including dramatic reduction in the vesicles immediately available for release (von Gersdorff and Borst, 2002). If an action potential releases a large fraction of the RRP, subsequent stimuli delivered before the replenishment of the pool will release fewer vesicles eliciting smaller response. Therefore, depression will increase if the initial release probability and frequency of activation are increased (Schneggenburger et al., 2002; Wang and Manis, 2008; Zucker and Regehr, 2002). Recovery from depression occurs within seconds and requires the vesicle replenishment of the RRP with either newly endocytosed vesicles or with vesicles from the reserve pool. Additionally, inactivation of release sites and reduction in Ca^{2+} influx might also lead to STD (von Gersdorff and Borst, 2002). The inactivation of the release site might last for seconds and might reflect the time that is needed to clear vesicular proteins that remain incorporated into the membrane after exocytosis (Neher and Sakaba, 2008). This might support the view that removal of vesicular proteins from the plasma membrane can alleviate the impediment and thereby speed recovery from depression (Hosoi et al., 2009). In this case the release sites will recover faster than if the proteins were removed by diffusion within the membrane. Endocytosis aids the recruitment of vesicles to the RRP and blocking endocytosis results in enhancement of the extent of depression and slows down the rate of recovery. Neurotransmitter release is highly dependent on Ca^{2+}, therefore, small activity-dependent changes in Ca^{2+} influx can lead to significant alterations in the synaptic plasticity (Neher and Sakaba, 2008). Inactivation of Ca^{2+} current might contribute to synaptic depression (Forsythe et al., 1998; Xu and Wu, 2005).

In conclusion, multiple mechanisms are involved in short-term plasticity at CNS synapses. Depending on the exact circumstances within a specific nerve terminal, certain mechanisms might contribute more than others. Different mechanisms are utilized at different stages of development and at different stimulation frequencies, allowing a dynamic modulation of synaptic properties.

1.6. Calyx of Held

The calyx of Held is a large axosomatic terminal in the auditory brainstem whose major function is sound localization. It was first characterized, using Golgi method in the cat auditory system by Hans Held in 1893 (Held, 1893). Auditory signals arriving to the cochlear are transmitted to the ipsilateral anterior ventral cochlear nucleus (aVCN) by excitatory synapses onto the globular and spherical bushy cells (Figure 1.4 A). Upon crossing the brainstem midline, the axons of the globular bushy cells make glutamatergic synapses with the principal cells of the medial nucleus of the trapezoid body (MNTB), forming the calyx of Held. The MNTB is organized in a tonotopic fashion, thus cells responding to high-frequency inputs are represented medially and cell responding to low frequencies – laterally (Sommer et al., 1993). Apart from the dominant calyceal input, the MNTB principal cells receive a somatic inhibitory input of unknown origin (Awatramani et al., 2004) and non-calyceal excitatory inputs (Hamann et al., 2003). The principal cells of the MNTB are glycenergic and send their inhibitory input to the lateral superior olive (LSO). The LSO receives also an excitatory input from the spherical bushy cells of the ipsilateral aVCN. Thus neurons in the LSO are strongly inhibited by auditory signals in the contralateral cochlear, but are excited by the input coming form the ipsilateral ear (reviewed in (Borst and Soria van Hoeve, 2012)). However, due to the large calyceal axon and the short delay at the calyx-to-MNTB principal cell synapse, the two signals arrive at the LSO almost at the same time, thus cells in the LSO use intensity differences between both ears to localize sounds (Grothe et al., 2010).

1.6.1. The calyx of Held as a model synapse

The calyx of Held is a high-fidelity relay synapse, which is specialized in preserving AP timing through specific pre- and postsynaptic specializations and fires efficiently at frequencies as high as several hundred Hz. This synapse a suitable model for studying the cellular mechanisms of neurotransmission due to its large size (10 – 20 μm), which allows simultaneous electrophysiological recordings from the pre- and the postsynaptic compartment. The synapse forms multiple thick fingers that wrap around a single principal cell, where multiple conventional active zones are localized (Figure 1.4 B). The presence of multiple active zones results in large quantal size, which affects the release probability of the presynaptic terminal and secures fast and reliable synaptic transmission. More than 100 SVs

can be released per AP (Borst and Sakmann, 1996). Therefore, the incoming AP does not fail to trigger an AP in the MNTB principal cell even at high input frequency.

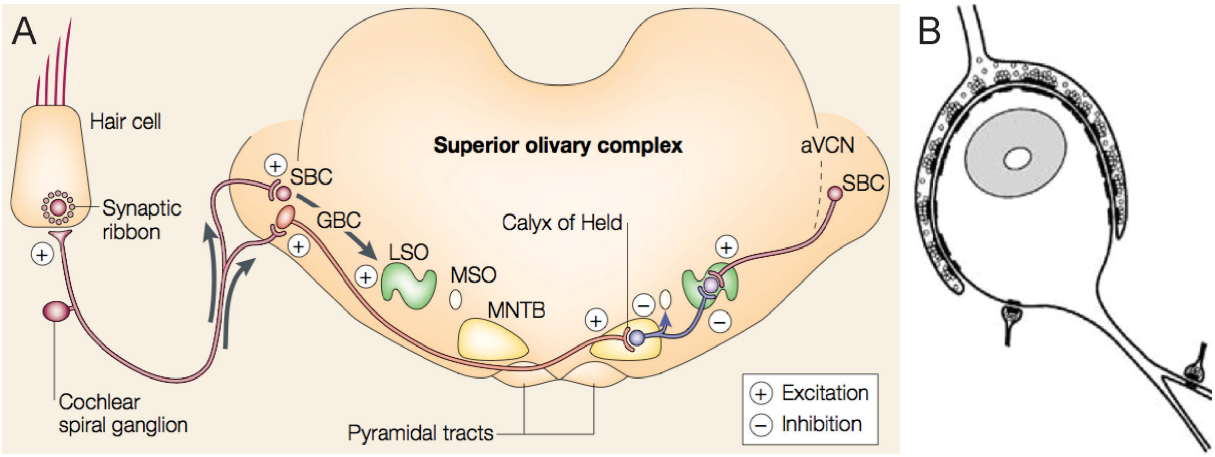

Figure 1.4: Localization of the calyx of Held within the superior olivary complex (SOC). A: Auditory signals arriving from the cochlear are transmitted to the ipsilateral aVCN by excitatory synapses on the spherical bushy cells (SBC) and globular bushy cells (GBC). The axons of the globular bushy cells cross the midline and form synapses with the principal cells of the contralateral MNTB to form the calyx of Held. The MNTB principal cells send inhibitory input to the lateral superior olive (LSO), which also receives an excitatory input from the SBC from the ipsilateral aVCN. Discharge trains evoked by sound at the two cochlea therefore converge on LSO neurons as ipsilateral excitation (through the aVCN) and contralateral inhibition (through the MNTB). The precise timing of the two inputs is crucial in determining the response of the LSO to interaural intensity differences. From (von Gersdorff and Borst, 2002). B: Schematic representation of a single calyx of Held synapsing onto a MNTB principal cell. The major input to the MNTB principal cell is the calyx of Held and it represents one-to-one connection between the GBC and the MNTB principal neuron. The MNTB cell also receives additional inhibitory and excitatory input through small bouton-like synapses. Multiple active zones are present at the calyx of Held, assuring a large EPSC in response to a single AP that rapidly depolarizes the postsynaptic cell. From (Schneggenburger and Forsythe, 2006).

The Ca^{2+} sensor in the calyx is synaptotgamin-2 (Sun et al., 2007), an isoform that mediates fast fusion of SVs (Xu et al., 2007). Release of glutamate from the calyx of Held triggers the activation of both AMPA and NMDA receptors with AMPA receptor mediated postsynaptic currents becoming faster and larger during maturation (Joshi and Wang, 2002) and the amplitude of the NMDA current being downregulated (Futai et al., 2001; Taschenberger and von Gersdorff, 2000).

Several alterations take place during the maturation of the presynaptic terminal. After the onset of hearing (p 10 – 12 in rodents) the calyx gradually becomes a fenestrated multi-digit structure that engulfs the larger part of the postsynaptic cell (Borst and Soria van Hoeve, 2012). The AZs become more in number but smaller in size without changing the density of the docked SVs. Therefore, the number of docked SVs per AZ decreases but the RRP is enlarged in order to compensate for the decrease in the release probability (Taschenberger et al., 2002). The quantal size, measured as the amplitude of miniature EPSCs, becomes significantly larger after the hearing onset (von Gersdorff and Borst, 2002). Consequently,

less SVs are needed to trigger the same conductance change in the adult principal cell as in the young neuron. The alterations during maturation decrease the release probability, which added to the enlarged size of the RRP, make the vesicle pool more resistant to depletion and the calyx a very reliable synapse.

1.6.2. Vesicle dynamics at the calyx of Held

The calyx of Held is a presynaptic terminal that shows pronounced STD when repeatedly stimulated *in vitro*. Reduction of size of RRP is the main mechanism contributing to STD. (von Gersdorff and Borst, 2002). The RRP at the calyx of Held has been estimated to contain between 600 – 5000 SVs depending on the used method (Neher and Sakaba, 2001; Sakaba and Neher, 2001a; Sakaba et al., 2002; Schneggenburger et al., 1999; Schneggenburger and Neher, 2000; Sun and Wu, 2001; Wölfel et al., 2007; Wölfel and Schneggenburger, 2003). Following pool depletion, the recovery of the RRP can be estimated by applying another stimulus at varying intervals. Such experiments have revealed heterogeneous release probability between vesicles of the RRP. At rest the RRP can be subdivided into a fast-releasing pool and a slow-releasing pool, which have different recovery kinetics – SVs with low release probability recover faster than SVs with high release probability. A lower Ca^{2+} sensitivity can contribute to the lower release probability of the slow-releasing pool (Wölfel et al., 2007). These SVs, however, should be located further away from the open Ca^{2+} channels (Wadel et al., 2007). The recovery from short-term depression represents both the replenishment of the RRP and an increase in the release probability.

The RRP replenishment is a use-dependent process since the release of the rapidly replenished, reluctant SVs depends to high extend on the buildup of residual Ca^{2+}. Additionally, accumulation of Ca^{2+} is shown to speed up the replenishment of the fast-releasing pool via binding to calmodulin (Sakaba and Neher, 2001a; Wang and Kaczmarek, 1998). The mechanisms that regulate the size of the fast-releasable pool are complex and cannot be explained only by the action of Ca^{2+}. Several presynaptic proteins, such as proteins kinase C, Munc 13, synaptotagmin-2 and myosin light-chain kinase, might be also involved in the regulation of SV release probability.

There is evidence that two kinetically distinct forms of endocytosis coexist at the calyx of Held – rapid and slow endocytosis, both of which involve dynamin and clathrin-dependent mechanisms (He et al., 2006; Yamashita et al., 2010). The rapid form, which takes place in order of a few seconds is used primarily during intense stimulation (Wu et al., 2005). Bulk endocytosis might take place upon very strong stimulation when SVs fuse with each other

before fusing with the plasma membrane (Wu and Wu, 2007). Especially after large stimuli release sites should be cleared before RRP replenishment can be completed (Neher, 2010).

To conclude, the cellular mechanisms that maintain the SV pool dynamics at the calyx of Held are not much different from that at small conventional synapses. The calyx of Held develops and matures in such a way to minimize the effects of short-term depression in response to high-frequency input. With its large size, well-established morphology and function the calyx of Held is an excellent system to study protein function and to characterize the effect of genetic perturbations leading to altered levels of presynaptic proteins on the neurotransmitter release. We utilized the calyx of Held to determine the function of synapsins in an intact CNS presynaptic terminal, which has developed and matured *in vivo*.

1.7. Synapsins

Synapsins are neuronal phosphoproteins, whose function in regulation of neurotransmission has remained obscure despite more than 20 years of intensive research. P. Greengard first described synapsin I as a substrate for cAMP-dependent protein kinase in synaptic fractions (Johnson et al., 1972; Ueda et al., 1973). Synapsins comprise approximately 6 % of the whole brain protein and are represented with 8.3 copies per SV (Takamori et al., 2006), making them one of the most ubiquitous brain proteins. Synapsins are a protein family, which is highly conserved across species and encompasses three genes in mammals – SYN I, SYN II and SYN III. The three genes are located in the human and mouse genome on chromosome X, chromosome 3 and chromosome 22 respectively (Kao et al., 1998; Li et al., 1995a; Yang-Feng et al., 1986). Alternative splicing of the three genes results in more than ten isoforms, which might have highly redundant functions. Synapsin I is expressed in two different isoforms – synapsin Ia and synapsin Ib of 86 and 80 kDa. Two isoforms of synapsin II have also been characterized – synapsin IIa (74 kDa) and synapsin IIb (55 kDa). Syanspin III was cloned and characterized much later (Kao et al., 1998) and exists in six isoforms (synapsin IIIa-f) (Porton et al., 1999). It has been shown that different members of the family exhibit distinct expression pattern in several brain regions: olfactory bulb, retina, thalamus (Kielland et al., 2006; Mandell et al., 1992; Mandell et al., 1990; Matus-Leibovitch et al., 1997; Stone et al., 1994; Südhof et al., 1989). Synapsin I and II are primarily localized in the presynaptic terminals and their expression levels rise with time (Ferreira et al., 2000; Fletcher et al., 1991). Synapsin III, on the contrary, is primarily enriched in cell bodies of immature neurons and growth cones as well as the presynaptic sites of a limited population of synapses and its expression decreases during development (Ferreira et al., 2000; Pieribone et al., 2002).

Therefore, synapsin I and II could be linked to SV production and maturation, while synapsin III might have a completely different function mainly maintaining the survival and proliferation of neuronal progenitor cells. However, the major function of all three synapsin genes is to immobilize SVs within presynaptic terminals via interaction with cytoskeletal components in a phosphorylation dependent manner (Cesca et al., 2010; Petrucci and Morrow, 1987). All synapsin isoforms form homo- or heterodimers, which aids their proper vesicle association (Gitler et al., 2004b; Hosaka and Südhof, 1999).

Synapsins share a similar domain-like structure with homologous N-terminal part and more variable C-terminal region (Fig. 1.5). The N-terminal region can be subdivided into 3 domains – A, B and C, which with exception of domain B are highly conserved among isoforms and species. The C-terminal portion of the proteins is more divergent and consists of splice variants of the domains (D – I) (Cesca et al., 2010; Porton et al., 1999; Südhof et al., 1989). Domain A is a short region located at the beginning of the N-terminus, contains a phophoryaltion site for proteins kinase A (PKA), calcium/calmodulin dependent kinase I (CaMKI) and IV (CaMIV). Phosphorylation at this site is involved in the reversible association with SV membranes. Domain B is considered as a linker region between domains A and C and its amino acid sequence varies from isoform to isoform. It contains two phosphorylation sites for mitogen-activated protein kinase (MAPK) and extracellular signal-regulated kinase (Erk). Domain C mediates the binding of synapsins to SVs and to the actin cytoskeleton as well as synapsin homo- and heterodimerization. It is a large domain, consisting of both hydrophobic and highly charged amino acids, which penetrate into the lipid bilayer and stabilize the interaction with the SVs. The region, which penetrates into the vesicle membrane is different from the region that mediates the dimerization of synapsins. This leads to the hypothesis that synapsins cluster SVs via homo and heterodimerization. Domain C hosts a single phosphorylation site, utilized by the tyrosine kinase c-Src, which also modulates the synapsin binding to both SVs and actin (Onofri et al., 2007). Additionally, domain C shares structural homology with bacterial ATP-dependent synthase. Therefore, it was suggested that either synapsins have enzymatic function or bind to ATP (Esser et al., 1998).

Synapsins bind to ATP with different Ca^{2+} sensitivity. Ca^{2+} promotes ATP binding to synapsin I, inhibits the reaction with synapsin III. ATP binding to synapsin II is Ca^{2+} independent (Hosaka and Südhof, 1998a, b). Binding to Ca^{2+} and ATP might aid the formation of synapsin I oligomers (Brautigam et al., 2004). Although, the C-terminal region of the synapsin is not preserved among isoforms, it contains a proline-rich motif – domain D

in synapsin Ia and Ib, domain G in synapsin IIa, domains G and H in synapsin IIb and finally domain J in synapsin IIIa. Domain D contains interaction sites for several protein kinases – CaMKII, p21-activated kinase, MAPK/Erk, Cdk1 and Cdk5. Additionally, domain D interacts with several proteins such as c-Src, Grb2, CAMKII and Rab3 (Benfenati et al., 1992; Giovedì et al., 2004b; McPherson et al., 1994; Onofri et al., 1997). Differentially spliced domains follow downstream of the proline-rich region. Domain E, which is common for all a-isoforms might mediate the synapsin targeting to presynaptic terminals (Gitler et al., 2004b) as well as synapsin oligomerization and SV cluster formation (Monaldi et al., 2010). Isoforms lacking the E-domain are still successfully trafficked to the presynaptic terminals via interaction with other isoforms (Gitler et al., 2004b).

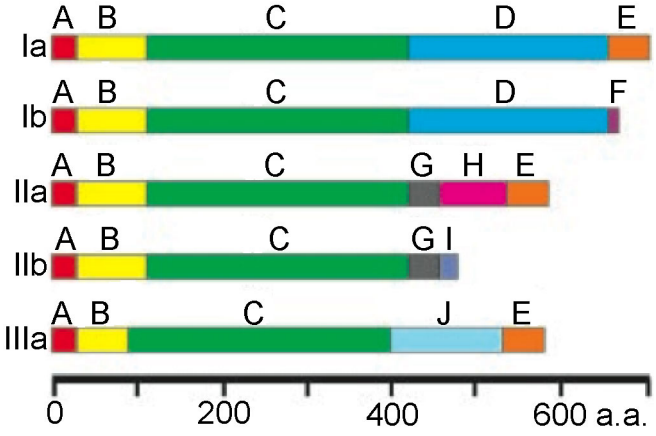

Figure 1.5: Domain-like structure of synapsins. All synapsin gene products share homologous N-terminal domains, which are implied in the maintenance of synapsin binding to SVs and cytoskeleton. The variable C-terminus might be responsible for the different functions of the separate isoforms. From (Gitler et al., 2004b).

1.7.1. Synapsin trafficking to the presynaptic terminal

After synthesis in the neuronal cell body synapsins are anterogradely transported to the presynaptic terminal. Synapsin I is transported to the presynaptic terminal as part of the slow component-b (Ahmari et al., 2000). Slow component-b transports more than 200 diverse proteins along axons at average rate between 2 and 8 mm/day. It includes presynaptic proteins such as synapsin I, α-synuclein, clathrin, motor proteins such as dynein and myosin, and cytoskeletal proteins such as actin and spectrin (Baitinger and Willard, 1987; Bourke et al., 2002; Dillman et al., 1996). At least some of the newly synthesized synapsin molecules are transported down the axon in association with cytoskeletal components (Baitinger and Willard, 1987). As a slow component-b protein, synapsin moves rapidly but infrequently with pauses during transit (Roy et al., 2007). The transport of slow component-b protein complexes might be powered by microtubule motors and not by actin filaments (Roy et al., 2008).

1.7.2. Pre-docking function of synapsins

Synapsin function has been studied in a variety of *in vitro* and *in vivo* preparations showing that synapsins keep the vesicle pool together in a phosphorylation dependent manner. Experiments interfering with the phosphorylation state of synapsin I showed that dephosphorylated synapsin I decreased the amplitude and the rate of rise of postsynaptic potentials at the squid giant synapse. However, presynaptic injection of phosphorylated or heat-inactivated dephosphorylated synapsin I remained without any detectable changes (Hackett et al., 1990; Llinás et al., 1985). In primary hippocampal cultures synapsin I dispersed from the SV cluster upon depolarization and reclustered following return to the resting membrane potential (Chi et al., 2001; Chi et al., 2003; Orenbuch et al., 2012b). However, at the frog neuromuscular junction synapsin dissociation is not a prerequisite for fusion. Some synapsin molecules remained associated with the SV membrane following exocytosis (Torri Tarelli et al., 1992; Torri-Tarelli et al., 1990).

The injection of an antibody recognizing synapsin E domain in the lamprey reticulospinal axons led to disappearance of the SVs distal to the AZs without affecting the docked SVs, which led to enhanced synaptic depression at high but not low stimulation frequencies (Pieribone et al., 1995). Both domains C and E are crucial for regulating the distal pool of vesicles as shown via injection of domain-derived peptides, which led to a decreased number of distally located SVs and increased rate and extent of synaptic depression at the squid giant synapse (Hilfiker et al., 2005; Hilfiker et al., 1998).

A dramatic decrease of SV density within the reserve pool as well as disassembly of SV clusters were detected in synapsin knock out animals, while the docked vesicles at the AZ were only poorly affected (Gitler et al., 2004a; Li et al., 1995b; Rosahl et al., 1995; Samigullin et al., 2004; Siksou et al., 2007; Takei et al., 1995). Accordingly, the level of SV-associated proteins was dramatically reduced, while that of proteins associated with the plasma membrane, or that of postsynaptic proteins was not impaired (Gitler et al., 2004a; Rosahl et al., 1995). This effect seemed to be mediated by synapsin I and synapsin II, since synapsin III knock out resulted in no change in the SV density but instead in an increase in the size of the recycling pool of vesicles and decreased level of depression (Feng et al., 2002). As expected, examination of SV recycling at individual synaptic boutons from synapsin I knock-out mice with FM-dyes revealed a strong reduction in both the number of exocytosed vesicles during a brief AP and the total number of SVs in the recycling pool, without altering the kinetics of endocytosis and vesicle repriming (Ryan et al., 1996). In the hippocampus the absence of synapsin I and II led to impairment of both the reserve and the readily releasable

pools and to accelerated STD (Rosahl et al., 1995). More recently, the physiological outcome of synapsin triple knock-out was studied in hippocampal autapses (Gitler et al., 2004a). At excitatory synapses normal basal transmission was observed, but the rate of synaptic depression was three-fold increased. These alterations were associated with a decrease in the number of reserve pool vesicles. Synapsins IIa is most probably the only isoform that can occlude the severe STD at hippocampal synapses (Gitler et al., 2008).

When the SV mobility in the NMJ of TKO mice was examined (Gaffield and Betz, 2007), it was shown that although decreased in number, SVs are not freely mobile and lack of synapsins does not impair neurotransmitter release. This led to the conclusion that at least in the motor neurons a phosphorylation target distinct from synapsins should be capable of controlling SV mobility. Contrary, at the *Drosophila* NMJ synapsins are required for the spatial segregation of RP and RRP, as well as for the mobilization of reserve pool vesicles during prolonged stimulation (Akbergenova and Bykhovskaia, 2007). Hence, the function of synapsins seems to be synapse specific and might be dependent on the role of the presynaptic terminal within the neuronal circuit.

At the calyx of Held of double knock-out mice, lacking synapsins I and II, the synaptic depression in response to high frequency stimulation was accelerated due to the reduction in the number of SVs released late in the train (Sun et al., 2006). It was proposed that in the wild type situation the residual Ca^{2+} that builds up during the train would trigger CaMKII-dependent phosphorylation of synapsins and would regulate the size of the RRP during prolonged stimulation.

1.7.3. Putative functions of synapsins during the later stages of the SV cycle

A small fraction (20 – 25 %) of the synapsin molecules remains attached to the SVs during recycling upon high-frequency stimulation (Torri Tarelli et al., 1992) and synapsins colocalize with actin at sites of intense endocytosis (Bloom et al., 2003). Synapsin E domain might interfere with the interaction of synapsins and actin cytoskeleton surrounding the AZ, which under normal conditions should control synaptic recycling. FM-dye imaging showed that the vesicle number in both the recycling vesicle pool and the RRP were decreased in synapsin I-deficient mice without altering the kinetics of endocytosis and vesicle reprimining (Ryan et al., 1996). This is consistent with the inhibition and slowing down of neurotransmitter release without altering the number of the docked SVs when peptides derived from the C- and E-domains were injected in the squid giant synapse (Hilfiker et al., 1998). These two domains specifically aid the binding of synapsin to actin but not to vesicles

suggesting that synspsin I interaction with actin might be important for exocytosis in the squid giant synapse (Hilfiker et al., 2005).

At the inhibitory purkinje-cell–nuclear-neuron synapse, however, overexpression of synapsin domain E increased synaptic efficiency by accelerating both the kinetics of exocytosis and the rate of synaptic vesicle cycling, and decreasing depression (Fassio et al., 2006). The effects of overexpression of domain E might lead to increased sensitivity of the postsynaptic neurons to inhibition and thereby control the level of network activity. CA3 pyramidal neurons from synapsin I knock-out mice exhibit reduced efficiency of inhibitory synaptic transmission due to less SVs being released during isolated APs (Terada et al., 1999). Additionally, the deletion of synapsin I induced a reduction of the eIPSC amplitude, attributable to reduced RRP and not impaired probability of release at hippocampal and cortical neurons (Baldelli et al., 2007; Chiappalone et al., 2009). Decease in the evoked IPSCs and the quantal content was also observed in cultured hippocampal autaptic neurons from synapsin III knock-out and TKO animal (Feng et al., 2002; Gitler et al., 2004a).

1.7.4. Summary – synapsins function at the presynaptic terminal

Synapsins function primarily downstream of SV docking and they aid the formation and maintaining of the reserve pool. This pool of immobile vesicles is utilized only upon depletion of the readily releasable and recycling pools, when sustained and repetitive release exhausts the endocytotic capacity of the presynaptic terminal (Cesca et al., 2010; Greengard et al., 1993; Hilfiker et al., 1999). In this scenario, homo- and/or heterodimerization of synapsins maintains SV clustering and the vesicle integration in the cytoskeletal network. In this way synapsins keep the SV pools segregated and prevent vesicles from unwanted fusion events and rapid turnover. Upon phosphorylation of synapsins, the vesicles in the distal pool become mobile and able to undergo exocytosis (Cesca et al., 2010; Hosaka et al., 1999; Pieribone et al., 1995).

The classical model of synapsin function proposes that synapsins detach from SVs upon stimulation (Orenbuch et al., 2012b). However, synapsins seem not to completely dissociate from vesicles during recycling and hence they might have an additional role in controlling events downstream of SV docking. They might play role in controlling the docked vesicles released in response to an AP. In order to fulfill this function, synapsins might interact with the actin at the active zone or with the SV protein Rab3a (Giovedì et al., 2004b). Figure 1.6 summarizes the possible action mechanism of synapsin at presynaptic terminals.

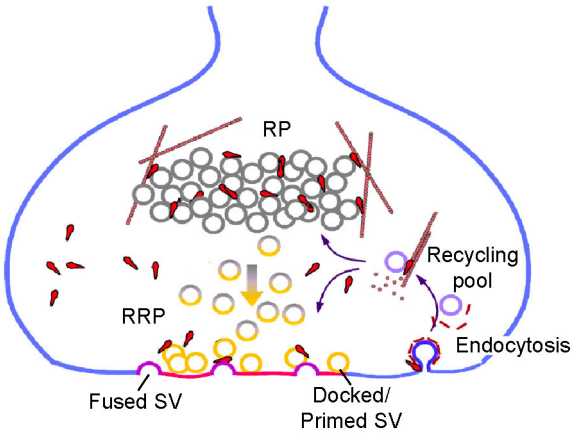

Figure 1.6: Model of the molecular interactions of synapsins within the presynaptic compartment. Synapsins (represented in red) might modulate different steps of SV cycle at CNS synapses. They link SVs within the RP to keep vesicles away from the presynaptic membrane. Synaptic activity phosphorylates synapsins thereby releasing a subset of SVs, which join the RRP and are exocytosed. It is possible that part of the synapsins remains associated with the SVs, which become part of the RRP. Synapsins might contribute to several steps in the vesicle cycle: docking, post-docking and fusion. During endocytosis synapsins might stimulate actin polymerization. Finally, synapsins might mediate the recruitment of recently endocytosed vesicles to the different vesicle pools. From (Cesca et al., 2010).

The different roles of synapsins are most probably synapse-type specific and might vary according to the neurotransmitter used. The functional differences might be caused by the differential expression pattern of the various synapsin isoforms and/or differences in the mechanisms of SV trafficking and quantal release in distinct neuronal populations (Evergren et al., 2006; Kielland et al., 2006; Südhof et al., 1989).

1.8. Aim of the study

The main goal of this study is to determine the impact of alterations in the organization and stabilization of the synaptic vesicle cluster on the function of the presynaptic terminal. For this purpose, we plan to elucidate the functional properties of synapsins at the calyx of Held – a giant glutamatergic synapse in the auditory brain stem involved in the precise sound localization. We will focus on the role of synapsins in maintaining the distribution and the functional properties of SVs within a properly developed CNS synapse.

The main question addressed in this study is the involvement of synapsins in the trafficking of SVs to the active zones and in the local recycling processes. We will examine the functional diversity of synapsin isoforms and the involvement of synapsin dimerization in the formation and stabilization of the SV cluster at the calyx of Held. The extensive molecular variability of the synapsin isoforms, in conjunction with their cross-interactions, would provide multiple regulatory junctions, all of which may contribute to the fine-tuning of presynaptic function. First we plan to determine which isoforms are present in the mature calyx of Held and then to examine their role in the control of neurotransmitter release. We aim to obtain a wide overview of the structural and functional consequences of perturbing

synapsin function at a CNS synapse. For this purpose we utilize two different genetic manipulations – viral gene transfer into the GBCs to induce overexpression of synapsin I isoforms and a global knock out mouse line lacking all three synapsin genes (Gitler et al., 2004a).

The calyx of Held with its exceptionally large size allows an excellent system to study the localization pattern of presynaptic proteins. Genetic labeling of the presynaptic terminal combined with immunohistochemistry against the separate synapsin will be used to unravel which isofroms are abundant within the calyx of Held. Consequently the molecular components of the GBCs will be altered via overexpression synapsin I isofroms. Finally, three dimensional imaging and electrophysiological methods will be applied on the acutely perturbed calyces and on triple knock out terminals to study the function of synapsins. The alterations in the vesicle number, distribution and function will help us to understand the interplay between synapsin isoforms composition and synaptic function.

2. Materials and Methods

2.1. Animals

TKO and TWT mice have been previously characterized (Gitler et al., 2004a). TKO mice were verified by genotyping using the following primers: 1. AGG GAG TTT CGT TAC TAC AGG TCC, 2. AGA TTG GCC ATG AAG TTG CTG TCC and 3. CTA CTT CCA TTT GTC ACG TCC TGC (synapsin I); 4. TTC AGG TCT CAG CAT ACA AGG TGC, 5. GGA AGT TCA TCA TCT GGC TTG AGG and 6. CTA CTT CCA TTT GTC ACG TCC TGC (synapsin II); 7. GTC TAG AGC AGA GTT GAA CCT GTG, 8. CCG CCC TGG ATG TTA AGA TCA GAT and 9. ACA CTG CTC GAC ATT GGG TGG AAA (synapsin III) and further confirmed by the absence of synapsin immunoreactivity in the MNTB (Supplementary Figure 2). We used three TKO and three WT mice, injected with rAAV at p 6 and sacrificed at p 16 – 18 for the three-dimensional immunofluorescence. We used two p 17 TKO mice and three p 17 WT mice for the ultrastructural analysis. For electrophysiological recordings we used p 14 – 18 mice from both genotypes. Additionally, we used p 6 Sprague Dawley rats to characterize the expression pattern of synapsin isoforms and to overexpress synapsin I isoforms in the calyx of Held. Rats were injected at p 6 with rAAVs and sacrificed at p 16 – 20 to perform morphological and functional analysis.

All experiments were conducted in accordance with the German welfare guidelines and were approved by the Regierungspräsidium Karlsruhe .

2.2. Plasmid cloning

All enzymes we purchased from New England Biolabs (Ipswich, MA 01938-2723) and used according to manufacturers' recommendations. The AAV plasmid was constructed as follows: EYFP-synapsin Ia was excised from pEYFP-synapsin Ia-C1 (Gitler et al., 2004b) via NheI/SpeI restriction endonucleases and inserted into pAM-AAV (MfeI/SpeI) containing CAG promoter – a combination of the CMV enhancer element and chicken ß-actin promoter to drive high levels of gene expression, the woodchuck post-transcriptional regulatory element (WPRE) and the bovine growth hormone poly-A (bGH) to generate pAM-CBA-EYFP-synapsinIa-WPRE-bGH. pAM-CBA-EGFP-synapsinIa-WPRE-bGH was obtain through the same procedure but utilizing EGFP-synapsin Ia fragment from pEGFP-synapsin

Ia-C1. pAM-CBA-EYFP-synapsinIb-WPRE-bGH was previously generated. Newly generated plasmids were sequenced. The used plasmids are listed in Figure 2.1 and Table 2.1.

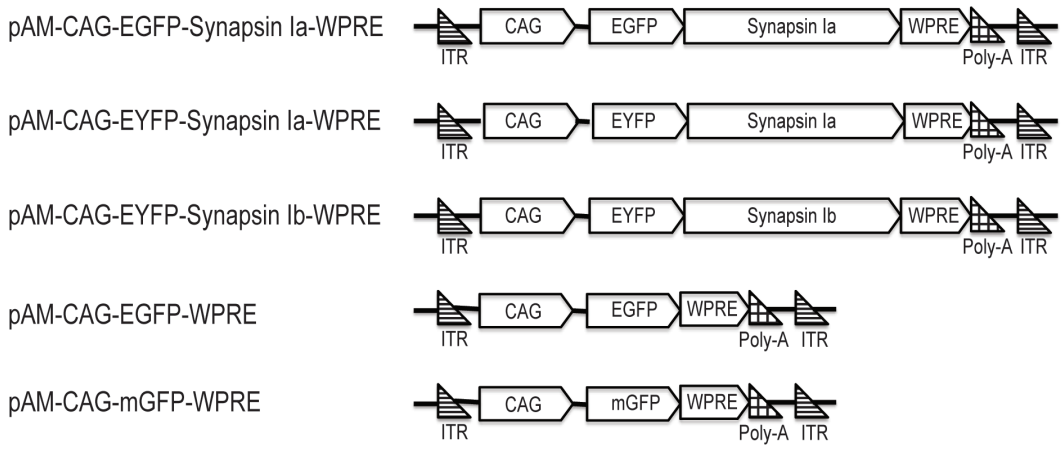

Figure 2.1: Plasmids used for production of rAAVs to modify the presynaptic composition of the calyx of Held.

Plasmid	Source
pAM-EGFP	provided by Michaela Kaiser
pAM-mGFP	provided by Michaela Kaiser
pEYFP-synapsin Ia-C1	provided by Daniel Gitler
pEGFP-synapsin Ia-C1	provided by Daniel Gitler
pAM-EYFP-synapsin Ib	constructed previously (M. Vasileva)
pAM-EYFP-synapsin Ia	constructed
pAM-EGFP-synapsin Ia	constructed
pDP1	PlasmidFactory, Bielefeld, Germany
pDP2	PlasmidFactory, Bielefeld, Germany

Table 2.1: List with the plasmids used in this study.

2.3. Virus preparation

A plasmid system, lacking all viral essential genes, was employed for generation of recombinant adeno-associated virus (rAAV) preparations. The system consists of a vector plasmid (pAM) in which the expression cassette is flanked by adeno-associated virus 2 (AAV2) inverted terminal repeats. Two helper plasmids carried all genes necessary for packaging the viral DNA into functional infectious particles. One helper plasmid (pDP1) encoded for the cap gene from AAV serotype 1 and the other (pDP2) for the cap gene of AAV serotype 2. Recombinant AAV chimeric viruses containing a 1:1 ratio of AAV1 and AAV2 capsid proteins and the foreign gene were generated as previously described (Grimm et al., 2003; Klugmann et al., 2005).

2.3.1. Cultivation of and transfection of AAV 239 cells

AAV 293 cells (Cat. No. 240073, Agilent Technologies, Böblingen, D-71034) were cultivated in DMEM medium (Gibco, Cat. No. 41965-039). 500 ml DMEM were supplemented with 50 ml Fetal bovine serum (Gibco, Cat. No. 10500-064), 10 ml 100x non-essential amino acids (Gibco, Cat. No. 11140-035), 10 ml 100x Sodium pyruvate (Gibco, Cat. No. 11360-039) and 5 ml penicillin/streptomycin (Gibco, Cat. No. 15140-122).

For rAAV production $4x10^6$ AAV 293 cells/plate were seeded in ten 14 cm culture plates in 20 ml cultivation medium. Cells were cultivated at 37°C in humidified atmosphere supplemented with 5% CO_2. Recombinant DNA was transfected in the cells one day after seeding via calcium phosphate method. For the purpose equimolar amounts of pAM and helper plasmids DNA were mixed to a final weight of 37.5 µg. Then 2000 µl H_2O and 100 µl 2.5 M $CaCl_2$ were mixed, added to the DNA and incubated for 60 s. 1000 µl HeBS buffer, containing in mM: 280 NaCl, 50 HEPES, 1.5 Na_2HPO_4, pH 7.05, adjusted with NaOH, pre-warmed to room temperature (RT), was directly added to the $H_2O/CaCl_2$/DNA mixture and mixed vigorously, and incubated for 90 s. The mixture was then added in a drop-wise fashion to the cells and the cell culture plates were returned to the incubator. Cell culture medium was exchanged on the following day.

2.3.2. Recombinant adeno-associated virus production

Four days after transfection cells were harvested at 200 g for 10 min, using Eppendorf centrifuge (5804R) with a swing bucket rotor (A-4-44), and resuspended in lysis buffer (1 ml/plate), containing in mM: 150 NaCl, 50 Tris-HCl, pH 8.5. Cells were lysed via three freeze-thaw cycles in dry ice ethanol bath and 37°C water bath. Cells were briefly vortexed between the cycles. Genomic DNA was digested by the application of benzonase (50 U/plate) (Sigma, Cat. No. E1014) for 2 h at 37°C. Cell debris was removed via centrigugation at 3645 g for 15 min at 4 °C. The supernatant, i.e. crude lysate was collected with a needle and syringe and filtered through 0.45 µm filter (Millex, 13 mm, Cat. No. SLHV013SL).

The crude lysate was purified on heparin columns (Biorad, Cat. No. 7321010). For this purpose, the columns were equilibrated with 10 ml equilibration buffer containing in mM: PBS (Gibco #14200), 1 $MgCl_2$, 2.5 KCl, pH 7.2. Heparin agarose (Sigma, Cat. No. H6508) (0.5 ml/plate) was added to the columns and mixed with equilibration buffer (4x volume of the heparin agarose). The agarose is let to sediment in the columns and the equilibration buffer is eluted with an elution buffer containing in mM: PBS (Gibco #14200), 1 $MgCl_2$, 2.5

KCl, 500 NaCl, pH 7.2. The crude lysate was loaded on the columns and incubated for 2 h at RT under constant agitation. The columns were washed with equilibration buffer and the crude lysate was eluted with 15 ml elution buffer and filled in an Amicon-ULTRA filter (Millipore, Cat. No. UFC9 100 24). The solution was centrifuged 30 min at 3000 g and the filter, containing the virus solution was washed three times with PBS to remove remaining salts. The virus solution was concentrated to 200 µl, filtered through a 0.22 µm filter (Millex, 4 mm #SLGV004SL), aliquoted and stored at 4°C until used.

2.4. Stereotaxic injection of recombinant adeno-associated viral particles

2.4.1. Stereotaxic setup

The SAS75 stereotaxic alignment system was used in combination with the EM70G manipulator (Kopf Instruments) and an angular injection adaptor (Wimmer et al., 2004). The anterio-posterior axis was referred as Y-axis, medio-lateral – as X-axis and ventro-lateral – as Z-axis. Prior to each injection the stereotaxic set up was calibrated according to manufacturer's guidelines. The centering scope was inserted and the cross hairs were fine adjusted over the cross of the calibration piece. At this position the three axes were set to zero and this point was regarded as reference point.

2.4.2. Injection capillaries

Injection capillaries were pulled on a P – 97 horizontal puller (Sutter, Novato CA) from micropipettes (5 µl, Blaubrand, intraMark, Brand GMBH, Wertheim, Germany). The elongated tips were manually trimmed to approximately 1 cm lenght. The 1 µl calibration bars on the pipette were used as a landmark for the injected volume.

2.4.3. Injection procedure

P6 mice/rats of both genotypes of either sex were stereotaxically injected with rAAV similarly to previous reports (Wimmer et al., 2004) using isoflurane inhalation anaesthesia (Dondzillo et al., 2010; Schwenger and Kuner, 2010) (HDG9623, Baxter, Unterschleißheim, Germany, vaporizer: Isotec4, Surgivet, Dublin, OH). Initially, the animals were anesthetized with 5 % isoflurane in O_2 for 2 – 4 min and afterwards the anaesthesia was decreased stepwise to 1 – 1.5 %, which was kept during the surgery. The breathing rate was monitored

optically and the isoflurane concentration was adjusted accordingly. When the animal was reflex-free it was fixed into the head-holder with ear bars attached to the os petrosium and the tongue pulled out of the mouth. The skin was disinfected with 70% CH_3CH_2OH and Lidocain (AlleMan Pharma GmbH, Rimbach, Germany) was injected subcutaneously. A small incision along the midline of the skull was done and the skin was retracted laterally. Two landmarks of the skull were used as reference points – bregma – the point of connection between the frontal bone and the parietal bones and lambda – between the occipital bone and the parietal bones. A craniotomy of approximately 2 – 3 mm in diameter was made with a dental driller (EXL-40 – drill: Komet, 1104005, Osada, Tokyo, Japan) in the area between the lambda and the occiput under binocular control (stereomicroscope – Leica MZ6). The bregma was positioned in the zero point of the stereotaxic setup (reference point – crossing of the Cartesian axes) and the two reference points were aligned along the Y-axis of the set up. The bregma – lambda distance was calibrated for each animal individually. Then the head was leveled in the sagital and coronal plane using an electronic leveling device (eLeVeLeR) (Wimmer et al., 2004) (Sigmann Elektronik). To align the head properly in the sagital plane the two aluminum bars are positioned onto the landmarks. Bregma and lambda were set on identical positions in the Z-dimension by turning the head in the X-axis until both probes reported identical distances. Then the eLeVeLeR was turned 90º without changing the distance between the two bars, positioning them at identical positions on both sides of the midline. Leveling in the coronal plane was performed through tilting the head in the Y-axis until the sensors reported identical distances. The injection capillary was attached to the angular adaptor and loaded with virus solution, using plastic tubing attached to a 50 ml syringe. The pipette tip was zeroed – brought to bregma and all controls were set to zero – and then brought to the first injection coordinates. For injections in the ventral cochlear nucleus approximately 2 µl virus solution was evenly distributed among injection sites with the coordinates relative to bregma and midline provided in table 2.2. Viral-mediated overexpression of synapsin I isoforms at the calyx of Held was synapse specific since the globular bushy cells that give rise to the calyx of Held project contralaterally. The injection and the target area are separated by several millimeters, leaving the MNTB unaffected by the virus injection and the fluorescence signal observed in the calyx of Held was due to the successful trafficking of the overexpressed proteins (Wimmer et al., 2004).

The animals recovered from the anaesthesia 2 – 5 min after the isoflurane ceased to be administered and were returned to the cage with the mother.

p6 Mice				p6 Rats			
X	Y	Z	Depth Ax	X	Y	Z	Depth Ax
0.50	-4.8	0.45	3.5 - 3.0	1.05	-9.00	0.45	1.5
0.45	-5.1	0.45	3.5 - 3.1	1.05	-8.70	0.45	1.5
0.60	-4.5	0.45	3.5 - 3.2	1.00	-8.40	0.45	1.5
0.55	-4.5	0.45	3.5 - 3.3	0.90	-9.10	0.45	1.5
0.55	-5.2	0.45	3.5 - 3.4	0.90	-8.80	0.45	1.5
				0.85	-8.50	0.45	1.5

Table 2.2: Injection coordinates for p 6 mice and p 6 rats. Coordinates are given as distance in (mm) relative to bregma.

2.5. Perfusion

10 – 12 days after injection both mice and rats were transcardially perfused with approximately 20 ml and 40 ml respectively phosphate buffered saline (PBS) (Bioline), followed by fixation with approximately 20 ml and 40 ml respectively 4% paraformaldehyde (PFA) in PBS, pH 7.4. For the purpose the animal was deeply anesthetized with isoflurane and the abdominal cavity and the thorax were opened. A 22G injection needle (BD Microlance^{TM} 3) was inserted in the left ventricle, a small opening in the right atrium was made and the solutions were infused one after another. Brains were immediately extracted and postfixed in 4 % paraformaldehyde/PBS overnight at 4 °C. The PBS was freshly prepared and contained in mM: 10 phosphate buffer, 0.27 KCl chloride, 140 NaCl with pH 7.4 at 25°C.

2.6. Immunohistochemistry

The brain stems were embedded in 3 % agarose and 50 μm-thick coronal sections, containing the medial nucleus of the trapezoid body (MNTB) were cut on a vibratome slicer HR2 (Sigmann Elektronik, Hüffenhardt, Germany)

Mouse tissue was permeabilized for 90 min at RT under constant shaking in a PBS-based solution containing 10 % normal goat serum (NGS) (Jackson Immunoresearch Laboratories), 1% bovine serum albumin (BSA) (Roth), 1 % Triton X-100 (Tx-100) and 0.1 % fish skin gelatin (Sigma). Rat brain sections were permeabilized in PBS containing 5 % NGS, 1 % TX-100. After 3x10 min washing steps in 0.01 M PBS, slices were stained with primary antibodies over night at RT. On the following day slices were washed 3x10 min in PBS and secondary antibodies were incubated for 90 min at RT, in the dark. Upon 3x10 min washing in PBS, the sections were rinsed with ddH_2O, embedded in SlowFade® Gold antifade reagent (Invitrogen, Darmstadt, Germany; Cat. No. S36936) and kept at 4°C.

Both primary and secondary antibodies were diluted in PBS-based solution containing 10 % NGS, 1 % BSA and 0.5 % TX-100 in case of mice tissue and 1 % NGS and 0.5 % TX-100 in case of rat tissue. NGS was exchanged for fetal bovine serum in case of synapsin IIIa stain. All solutions were kept at 4 °C during the protocol and were applied cold to the brain sections.

2.7. Antibodies

Mouse monoclonal pan-synapsin I antibody, (1/1000), raised against electrophoretically purified rat synapsin I and recognizing the proline rich D-domain of synapsin I was acquired from Synaptic Systems (Göttingen, Germany) Rabbit monoclonal pan-synapsin II antibody, (1/1000), raised against synthetic peptide from human synapsin II was purchased from Abcam (Cambridge, UK). Rabbit polyclonal antibodies recognizing synapsin Ib (G-278), (1/1000), synapsin IIa (470 – 484 amino acids from domain H from synaspin IIa) (G-281), (1/500), synapsin IIb (G-466/467), (1/1000) and synapsin E-domain i.e. all synapsin a-isoforms (680 – 704 amino acids from E-domain), (G-304), (1/2500) (Giovedì et al., 2004b; Vaccaro et al., 1997; Zhai et al., 2001), were obtained from the Greengard laboratory (Rockefeller University, NYC, NY, USA). Goat polyclonal synapsin IIIa antibody, (1/50), produced against a peptide near the C-terminus of synapsin IIIa of human origin was purchased from Santa Cruz Biotechnology (Heidelberg, Germany). Guinea pig polyclonal vGluT1 antibody, (1/1000), developed against a synthetic peptide from rat vGluT1 protein without overlap with vGluT2 was obtained from Millipore (Billerica, MA, USA). Mouse monoclonal bassoon antibody (1/1000), raised against recombinant rat bassoon was purchased from Enzo® Life Sciences (Lörrach, Gemany). All synapsin antibodies reacted negatively in synapsin triple knock out mice (Gitler et al., 2004a) (Supplemenatary Figure 2). The used antibodies are listed in table 2.3.

2.8. Confocal imaging

Images were obtained on a Leica TCL SP5, using 63x glycerol immersion objective (NA 1.3). 476 nm, 488 nm, 514 nm, 561 nm and 633 nm laser lines to excite the different fluorophores used. mGFP was excited at 476 nm and EYFP – with 514 nm in case that both mGFP and EYFP were present in one specimen. To avoid cross talk between different fluorophores sequential scans were made, where applicable. Glycerol-based immersion medium with refractive index of 1.43 was used. No averaging algorithm was applied and the same laser

settings were used under all conditions. Images, oversampled to meet the Nyquist criterion, had a voxel size of 57.32 x 57.32 nm in axial and 150 nm in vertical dimensions in case of mice. Images had voxel size of 91.71 x 91.71 x 150 nm in case of rats. Images were deconvolved using Huygens software (Scientific Volume Imaging, Hilversum, The Netherlands). Overview images were acquired without digital magnification and are presented as a collapsed z-stack of 5 consecutive optical frames.

Primary Antibodies

Antigen	Species	Clone	Source (Cat. No.)
pan-Synapsin I	mouse	monoclonal	Synaptic Systems (106 001)
pan-Synapsin II	rabbit	monoclonal	Abcam (ab76494)
Synapsin Ib	rabbit	polyclonal	P. Greengard
Synapsin IIa	rabbit	polyclonal	P. Greengard
Synapsin IIb	rabbit	polyclonal	P. Greengard
Synapsin IIIa	goat	polyclonal	Santa Cruz (sc-8292)
pan-Synapsin E-domain	rabbit	polyclonal	P. Greengard
vGluT1	guinea pig	polyclonal	Millipore (AB5905)
Bassoon	mouse	monoclonal	Stressgen (VAM-PS003)

Secondary Antibodies

Against	Species	Fluorophore	Source (Cat. No.)
mouse	goat	Alexa - 488	Invitrogen (A11029)
rabbit	goat	Alexa - 488	Invitrogen (A11008)
goat	donkey	Alexa - 546	Invitrogen (A11056)
guinea pig	goat	Alexa - 633	Invitrogen (A21105)
mouse	goat	Alexa - 647	Invitrogen (A21235)
rabbit	goat	Alexa - 568	Invitrogen (A11011)
guinea pig	goat	Alexa - 546	Invitrogen (A11074)

Table 2.3: Antibodies used to visualize synapsin isoforms and other presynaptic proteins in the rodent calyx of Held.

2.8.1. Dye separation

In the experiments involving imaging of mGFP and EYFP-synapsin Ia/Ib in the same slice preparation, spectral unmixing of the acquired data was performed via the Channel Dye Separation Application of the Leica Application Software prior to deconvolution. For the purpose of defining reference regions we injected separate rats either with mGFP-coding rAAV or with EYFP-synapsin Ia/Ib-coding rAAV. Calyces from the non-infected ipsilateral MNTB of double infected animals were used as a reference for vGluT1-Alexa-633. The

reference regions were acquired as images containing the three channels but only one dye. Reference and real images were acquired with the same microscope settings

2.8.2. Excision of Calyx-specific immunosignals and visualization of 3D image data

Excision of calyx-specific immunosignals and 3D reconstruction of image data was performed with the visualization software AMIRA 5.3.1 (Visage Imaging). To describe the distribution of presynaptic proteins relative to the volume of the calyx, the calyx-specific immuno-labeled signal was excised from the confocal stack using the mGFP signal defining the plasma membrane of the terminal (Dondzillo et al., 2010). This was achieved by manually segmenting the mGFP channel to select only the voxels, which belong to the calyx.. Next, the channel representing the calyx structure was multiplied with the channel containing the immunosignal. The outcome of the procedure was a channel with immuno-labeled clusters of original intensity retained only within the calyx volume. The same procedure was applied to the mGFP and EYFP-synapsin Ia/synapsin Ib overexpressing calyces to excise the EYFP-synapsin Ia/synapsin Ib and vGluT1-immuno signals form the mGFP signal. The volume of the mGFP-defined structure and the total volume of the IHC positive structures were calculated based on the selected voxels and compared between the different treatments. Littermates injected only with rAAV-mGFP were used as controls.

2.9. ELISA

A sandwich enzyme-linked immunosorbent assay (ELISA) for quantification of synaptic proteins was preformed as described previously (Geumann et al., 2010). For this assay three WT and three TKO, p 28 mice were used.

2.10. Photooxidation and electron microscopy

After fixation with 4% PFA/PBS, 100 μm-thick coronal sections containing the MNTB were cut from p 20 rats infected with rAAV1/2, coding for either control EGFP or EGFP-synapsin Ia, or from naïve p 17 mice from both genotypes.

2.10.1. Photooxidation

Coronal sections of the MNTB containing EGFP or EGFP-synapsin Ia overexpressing calyces were washed for 10 min consecutively in PBS and in 50 mM Tris-HCl pH 7.6. Sections were

bubbled for 60 min with pure O_2 in 50 mM Tris-HCL pH 7.6 at 4 °C and stored over night in a closed system. On the following day the sections were again exposed to pure O_2 in 50 mM Tris-HCL pH 7.6 for 60 min at 4 °C, followed by 10 min incubation in 5 ml ice-cold 50 mM Tris-HCL pH 7.6 solution containing 5 mg Diaminobenzidene (DAB) and 40 µl 1 M NaOH. A Leica DM IRB microscope equipped with a 40x oil immersion objective (NA: 0.75 – 1.25) was used for the photooxidation. The light path aperture was closed to minimum and had a diameter of 150 µm. The region of interest was illuminated for 5 min with NA 0.75, followed by 5 min with NA 1.0 and then by 5 min with NA 1.25 and fine precipitates were observed in the exposed area.

2.10.2. Tissue preparation for EM

Coronal sections containing the MNTB were washed in 0.1 M cacodylic buffer pH 7.4, the MNTB area dissected out and post fixed in a mixture of 1.5 % potassium ferricyanide and 2 % osmiumtetroxide for 120 min. The sections were washed 3 times in distilled water and dehydrated in an ascending series of alcohol followed by propylenoxide and stored over night in a mixture consisting of propylenoxide and epoxy (Serva, Heidelberg, Germany) (1:1). The tissue was then transferred into fresh resin and polymerized at 60 °C for 36 hours.

2.10.3. Block preparation and serial sectioning

Once the resin was firm, the block was trimmed as previously described (Harris et al., 2006) using a 35° diamond trimmer (Diatome, Switzerland). We used an ultra microtome (Reichert Ultracut S, Vienna, Austria) to cut 20 – 30 serial sections/sample with a thickness of approximately 35 nm following the procedures described by (Harris et al., 2006).

2.10.4. Preparation of the silicon wafer strip

The ribbon was taken up with a custom made device attached to ultramicrotome (Horstmann et al., 2012). The silicon wafer (Si-Mat, Silicon Materials, Germany) was cleaned and made hydrophilic via incubation in sulfuoric acid and perhydrol (1:1) for 120 min followed by 3 rinses in distilled water. Once the ribbon was attached to the wafer, the wafer was slowly removed out and allowed to air dry. Sections were then counterstained in saturated solution of uranyl acetate in distilled H_2O for 17 min, washed 3x in H_2O and exposed for 7 min to Reynolds Lead citrate in CO_2 free medium. At the end the wafer was rinsed with distilled H_2O and air-dried.

2.10.5. SEM Imaging

A LEO Gemini 1530 with a FEG was used for SEM imaging (Horstmann et al., 2012). Inlens-detector with a working distance of 1.8 mm, a 60 µm aperture and 3 KeV acceleration voltage was used. The images were inverted to obtain images comparable to TEM. With a magnification of 10,000x, an area of 11.2 x 8.4 µm of the specimen was digitized by 3072 x 2304 pixels resulting in a pixel size of 3.87 x 1.8 nm. The pixel dwell time was 40 µs. Overview images of entire MNTB cells were acquired at 3,000x. Pre-alignment was done manually on the SEM through correlating the previous image with the next by stage rotation and shifting the electron beam.

2.10.6. Data Analysis

Three-dimensional reconstructions of the data were made by alignment of the serial sections using OpenCAR software, version 1.5.79 (Sätzler et al., 2002). Afterwards, structures such as presynaptic membrane, active zones (AZs) and synaptic vesicles (SVs) were contoured defined by visual landmarks. The three-dimensional geometry was reconstructed from the contours of the entire stack of images. Calculations of the volumes of the presynaptic segments, number and distribution of SVs were done with CARnEval, version 0.10, as previously described (Sätzler et al., 2002). The surface of the AZs was calculated by multiplying the summed length of the AZs by the thickness of the section (Taschenberger et al., 2002). Membrane regions that meet the following criteria were used for reconstruction of individual AZs: (1) the presynaptic and postsynaptic membranes are opposed to each other, forming the synaptic cleft with electron-dense material visible on both sides, (2) presence of SVs in close proximity to the presynaptic membrane, (3) the structure continues through at least three consecutive sections. SVs located within 400 nm from the AZ are defined as a SV cluster and included in the analysis. All SVs that were located at distances ≤ 10nm from the AZ were defined as docked SVs. The distance between the membrane specializations and SVs (SV-AZ distance) was calculated in 2D, separately for each section. It was calculated as the perpendicular line from the SV gravity center to the AZ outline and was corrected for the SV radius. The nearest neighbor distance was measured as the distance between the gravity centers of two neighboring objects (as an estimate of objects' density within the terminal correction for the SV radius was not required).

2.11. Electrophysiology

2.11.1 Rat experiments

Acute transverse slices 200 µm thick were made from p 16 – 18 rat brainstem, containing intact ventral stria and the MNTB. Slices were made on a vibratome (HM650V, Microm; Walldorf, Germany), at 4 ˚C in the slicing media, containing (in mM) 85 NaCl, 2.5 KCl, 25 glucose, 25 $NaHCO_3$, 1.25 NaH_2PO_4, 75 sucrose, 3 3-myo-inositol, 2 Na pyruvate, 0.4 Ascorbic Acid, 0.5 $CaCl_2$, and 7 $MgCl_2$. The pH was adjusted to 7.3 via constant aeration with carbogen (5% CO_2 in O_2), density was 315 – 320 mOsm. Slices were incubated for ~ 60 min at 35 ˚C in normal aCSF, containing (in mM) 125 NaCl, 2.5 KCl, 25 $NaHCO_3$, 1.25 NaH_2PO_4, 0.1 $CaCl_2$, 3 $MgCl_2$ and 25 glucose, freshly supplied, pH 7.3, density 315 – 320 mOs. Slices were used thereafter at room temperature (23 – 25 ˚C). Recordings were done in normal aCSF supplemented with strychnine (0.5 µM), SR9551 (10 µM), and APV (50 µM).

MNTB cells were visualized at 60x, using an EM CCD camera (Sensicam EM, PCO, Kelheim Germany), and gradient contrast optics on a Zeiss microscope (Axioskop 2 plus, Carl Zeiss, Oberkochen Germany). Infected calyx terminals were identified by strong fluorescence opposing intact principal cell somata. Intracellular recordings from the MNTB principal cell were made using 1.5 mm filamented borosilicate glass (WPI, Sarasota FL), pulled to tip resistances of 1.8 – 2.5 MΩ on a Sutter P-97 puller (Sutter, Novato CA). Pipette internal solution contained (in mM): 130 Cs-gluconate, 10 CsCl, 5 Na_2 phosphocreatine, 10 HEPES, 5 EGTA, 10 TEA-Cl, 4 Mg-ATP, 0.3 GTP, pH 7.2, 305 – 310 mOsm.

Cells were clamped at -70 mV, unless EPSC amplitude exceeded 18 nA, in which case holding potential was reduced to -30 mV to reduce the driving force and also eliminate AP spiking due to escape from voltage clamp. Spontaneous EPSCs were not evaluated at this reduced holding potential. Access resistance was in all cases ≤ 6 MΩ, and compensated 85 – 94 %, such that residual Rs < 0.5 MΩ. EPSCs were evoked via midline stimulation using parallel Pt-Ir bipolar electrodes (200 µm distance; FHC, Bowdoin ME). Leak current was usually less than 100 pA, and in no cases exceeded 200 pA. Stimuli were applied with an optically isolated bipolar stimulator (NPI Electronic GmbH, Tamm Germany), using 100 µs duration pulses. Stimulation amplitude was set to 1 V above threshold (1.0 – 3.5 V).

Stimulus trains were generally repeated 3 – 5 times per cell, with a 30 s interval between trains, and the mean initial EPSC size was normalized. The paired-pulse ratio, rate of depression, and steady-state level of the depressed synapse were then measured per cell, from the averaged traces (von Gersdorff and Borst, 2002).

Data was acquired with a HEKA EPC10 amplifier, driven by a PC running Pulse 8.80

software (HEKA, Lambrecht/Pfalz Germany). Data was filtered on-line at 2.9 kHz and corrected off-line for voltage errors due to uncompensated series resistance (Traynelis, 1998). Data analysis was performed in Igor 6.0 software (Wavemetrics, Lake Oswego Oregon USA). Detection of spEPSC was performed using a threshold-based detection algorithm in Igor (Wimmer et al, 2004), with detection threshold set to 14 pA. Detected events were excluded if they had decay times < 0 or > 5 ms, rise times < 0, charge < 0. Events larger than 500 pA were also excluded from analysis.

2.11.2 Mice experiments

Acute transverse slices, 200 µm thick, from p 14 – p 18 mice of both genotypes were prepared on a vibratome (Leica VT 1200S, Leica Microsystems) at 4°C in normal aCSF, supplemented with (in mM) 3 3-myo-inositol, 2 Na-pyruvate, 0.4 ascorbic acid, 0.1 $CaCl_2$, 3 $MgCl_2$ and 25 glucose, freshly supplied, pH 7.2, density 315 – 320 mOs. Slices were incubated at 37 °C in normal aSCF (pH 7.2, 315 – 320 mOs). Recordings were performed at RT in normal aSCF supplemented with 0.05 mM APV (Ascent Scientific).

MNTB cells were visualized with a 20x water immersion objective (HCX APO L 20x/1.0W) with 4x post-magnification, using a CCD camera (Leica DFC 350 FX) and DIC optics on a TCL SP5 Leica (Leica Microsystems). Whole-cell patch clamp recordings were performed similar to the experiments in the rats. MNTB principal cells were identified according to their morphology. Recordings were done using the same filamented borosilicate glass (WPI, Sarasota FL), but pulled to tip resistances of 2 – 3 MΩ on a Sutter P-97 puller (Sutter, Novato CA). The same Cs-gluconate internal solution was used as described above but with density of 300 – 310 mOs.

Cells were voltage-clamped at -70 mV, unless EPSC amplitude exceeded 20 nA, in which case holding potential was reduced to -30 mV similar to the experiments done in rats. In this case eEPSCs, recorded at V_h = -30mV were also extrapolated to currents at -70 mV on the basis of the IV relation. Spontaneous EPSCs were not evaluated at this reduced holding potential. Access resistance was in all cases ≤ 6 MΩ, and compensated 85 – 95%. Spontaneous activity was monitored for 2 min and after that stimuli were applied with an optically isolated bipolar stimulator (NPI Electronic GmbH, Tamm Germany), using 100 µs duration pulses. Stimulation amplitude was set to 0.5 V above threshold (1.0 – 10.0 V). EPSCs were evoked via midline stimulation using parallel Pt-Ir bipolar electrodes (200 µm distance; FHC, Bowdoin ME).

Data was acquired with a HEKA EPC10 plus amplifier (HEKA Elektronik, Lambrecht/Pfalz, Germany), operated by PatchMaster software and was online filtered

between 2.9 kHz and 10 kHz. Data analysis was performed in Igor Pro 6.0.2A software (WaveMetrics, Lake Oswego Oregon USA). Detection of spontaneous quantal events (spEPSC) was performed similar to the rat experiments, but with detection threshold set to 10 pA. Detected events were excluded if they had decay times <0 or >1 ms, rise times <0, amplitude >0. Events larger than 500 pA were also excluded from analysis.

All regents were purchased from Sigma-aldrich, unless stated otherwise. Desensitization is not present at stimulation frequencies < 300 Hz at the calyx of Held synapse at this age, so blockers of desesensitization (e.g. γ-DGG, Kyneurenic Acid, Cyclothiazde) were not needed (Renden et al., 2005).

2.12. Statistics

Statistical analysis and data presentation was done using Prism 5.0b (GraphPad Software, San Diego California USA). Data sets were corrected for outliers using Grubbs' test. One-way ANOVA, followed by Tukey-Kramer post-hoc test with significance level $p < 0.05$ in the experiments including more than two data sets. Otherwise, between-group comparisons were made using a two-tailed non-parametric test (Mann Whitney test) with 95% confidence interval for data sets, which do not follow normal Gaussian distribution. Data sets, which are normally distributed, were subjected to a two-tail unpaired t-test with Welch's correction, unless otherwise indicated. In the figures, * = $p < 0.05$, ** = $p < 0.01$, and *** = $p < 0.001$.

Photomicrographs were generated with Image J 1.41o, AMIRA 5.3.1 and Adobe Photoshop CS3, version 10.0. Final images were aligned and labelled in Adobe Illustrator CS3, version 13.0.0.

3. Results

3.1. Structural and functional consequences of the overexpression of synapsin I isoforms in the rat calyx of Held

3.1.1. Identification and distribution of endogenous synapsin isoforms in the rat calyx of Held

We examined the expression and distribution pattern of endogenous synapsins via immunohistochemistry to identify which synapsin isofroms contribute to synaptic transmission at the rat calyx of Held at p 16. At this stage the calyx has not yet reached its adult stage but it successfully mediates high-frequency synaptic transmission (Borst and Soria van Hoeve, 2012; Renden et al., 2005). Overview images (Fig. 3.1 A1 – E1) of slices stained with various synapsin antibodies show that multiple synapsin isoforms were present in the MNTB as well as outside the nucleus of p 16 rats. To study the exact localization of synapsin isoforms within the calyx of Held, we stereotaxicly delivered rAAV1/2 particles coding for membrane-bound GFP in the aVCN (Dondzillo et al., 2010; Schwenger and Kuner, 2010; Wimmer et al., 2004). Membrane labeling with mGFP allowed us to visualize the entire presynaptic volume and to exclude numerous non-calyceal terminals contacting the principal cells of the MNTB (Dondzillo et al., 2010). Staining with isoform-specific antibodies revealed the distribution of the endogenous synapsin isoforms within the lumen of the presynaptic terminal. The high-resolution images (Fig. 3.1 A2 – E2) represent separate presynaptic terminals where the synapsin immunosignal confound within the boundaries of the mGFP-labeled calyx is shown. The mGPF signal delineates the outer membrane of the calyx and is presented as a white outline in the merged images (Fig. 3.1 A2 – E2, right column). Synapsin-isoform staining revealed clusters of different sizes with large and bright clusters corresponding to regions with high SV density, while smaller and dimmer clusters reflect single active zone SV clusters or areas of low SV density. The overall immunostaining pattern was similar for the majority of the tested synapsin isoforms – pan-synapsin I (Fig. 3.1 A), synapsin Ib (Fig. 3.1 B), pan-synapsin II (Fig. 3.1 C), synapsin IIb (Fig. 3.1 D), synapsin IIIa (Fig.3.1 E). Three-dimensional reconstructions of the examined calyces (Supplementary Figure 1) revealed that the maximum intensity of the synapsin clusters was detected within the lumen of the presynaptic membrane and might represent clusters of SVs within the bulk

volume of the calyx localized distally from the active zones (AZ). Close to the presynaptic membrane facing the postsynaptic cell, where multiple AZs (Dondzillo et al., 2010; Sätzler et al., 2002) are located, the intensity of the detected immunofluorescent signal was lower, coinciding with a lower number of SVs or with the absence of synapsin isoforms from these regions.

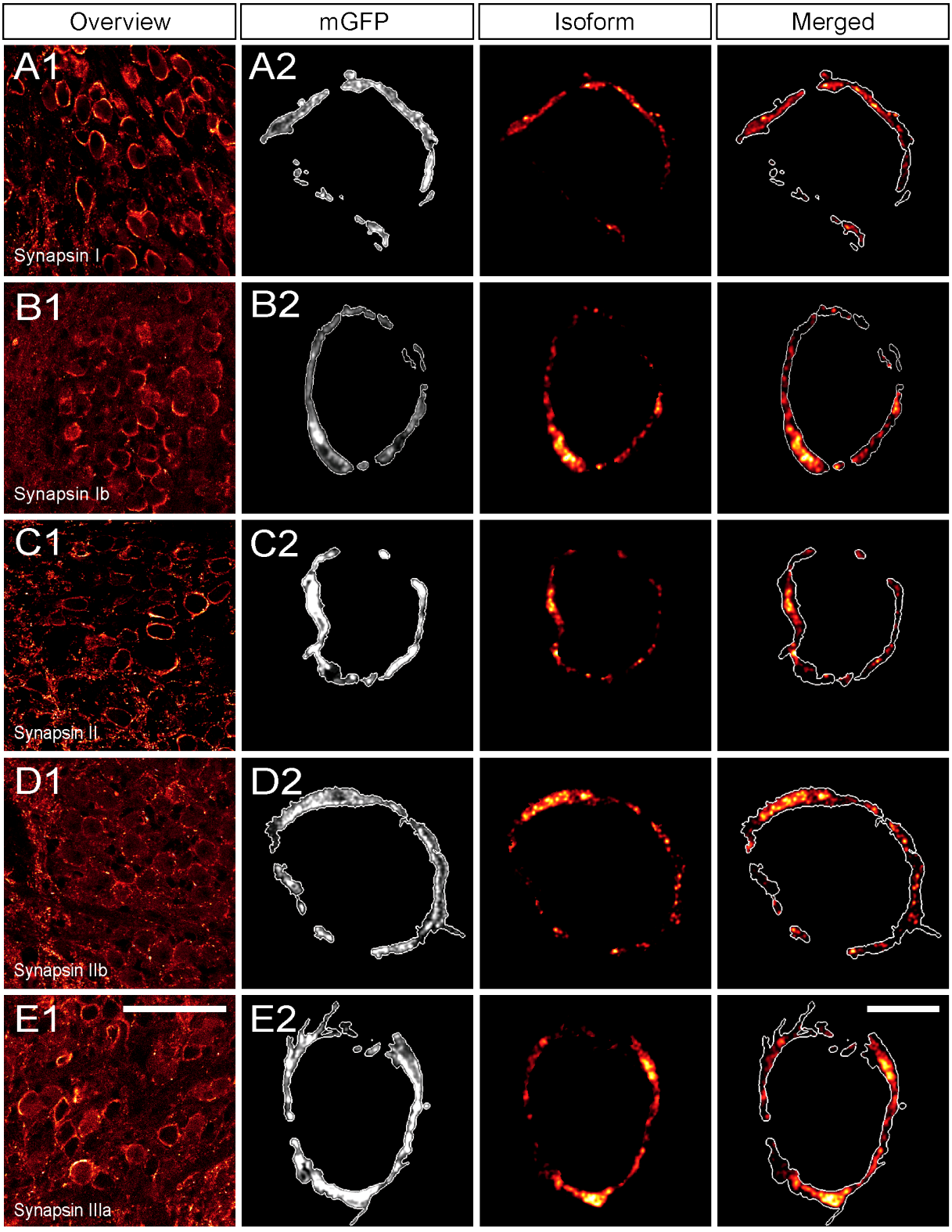

Figure 3.1: Products of all three synapsin genes are present in the rat calyx of Held at p 16. All tested isoforms were also present outside the MNTB. A1-E1: overview of the MNTB stained with isoform specific antibodies. A2-E2: mGFP labeling (left panel) allowed the visualization of synapsin isoforms (central panel) within the boundaries of the presynaptic terminal. Outer surface of the presynaptic membrane is delineated with white outline. In the merged images (right panel) the mGFP labeling is depicted only as white outline for clarity. A: pan-synapsin I; B: synapsin Ib; C: pan-synapsin II; D: synapsin IIb; E: synapsin IIIa. Images are presented in pseudo-colors. Scale bars: A1-E1: 100 μm; A2-E2: 10 μm.

Contrary to our expectations, synapsin IIa (Fig. 3.2 A) was not expressed in the calyx of Held, although it was present in the hippocampus at this maturational state (Fig. 3.2 B). In the hippocampus the immunosignal for synapsin IIa almost completely co-localized with vGluT1 – a marker for glutamatergic presynaptic terminals. The function of synapsin IIa at the calyx might be overtaken by the other synapsins and primarily by synapsin IIIa, which was broadly expressed in the MNTB. Synapsin IIIa was detected in p 16 calyces, in contrast to previous studies describing synapsin III as developmentally downregulated isoform, whose expression profile peaks at DIV 7 and declines to low levels after DIV 28 in cultured hippocampal neurons (Ferreira et al., 2000; Hosaka and Südhof, 1998a).

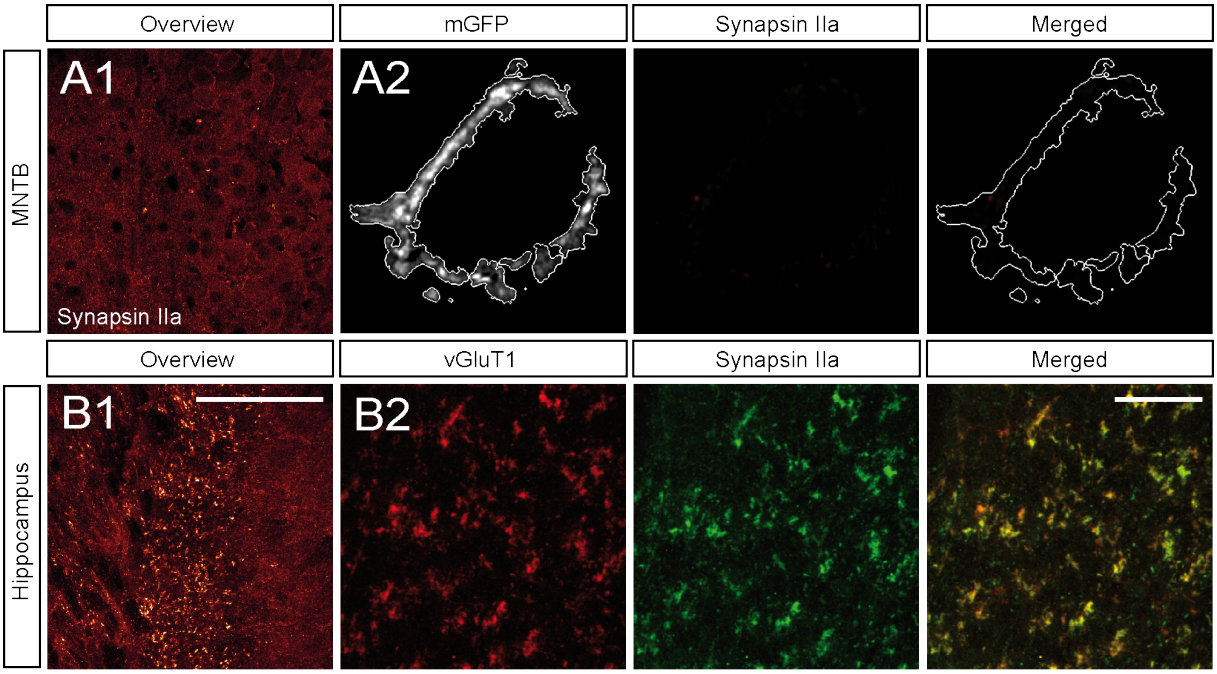

Figure 3.2: Synapsin IIa is not abundant in the juvenile calyx of Held. A: MNTB stained with an antibody against synapsin IIa. A-1: Overview image; A-2: Calyx overexpressing mGFP (left panel) negative for synapsin IIa (central panel), the mGFP labeling in the merged image (right panel) is presented as an outline of the outer presynaptic membrane. B: Hippocampus of the same rat stained for synapsin IIa: B-1: Overview of the pyramidal layer shows synapsin IIa-positive clusters along the dendrites of the pyramidal cells. B-2 Costaining with vGluT1 (left panel) certifies the presynaptic localization of the synapsin IIa (central panel) positive clusters. The merged image (right panel) proves the complete overlap of the two presynaptic proteins. Images are presented in pseudo-colors. Scale bars: A1-B1: 100 μm; A2-B2: 10 μm.

The hippocampus as part of the cerebral cortex might need synapsin IIa to maintain normal synaptic transmission in the mature animal. The specificity of the antibodies was additionally tested in tissue from triple knock out mice (TKO) (Gitler et al., 2004a) (Supplementary figure 2). Immunostaining for all tested synapsin antibodies was negative while that for vGluT1 resulted in the typical oval shape of the calyx of Held.

Next, we examined the localization of specific isoforms with respect to the distribution of synapsin I in order to elucidate if synapsin isoforms occupy the same volume or whether individual isoforms occupy distinct zones within the presynaptic compartment (Fig. 3.3).

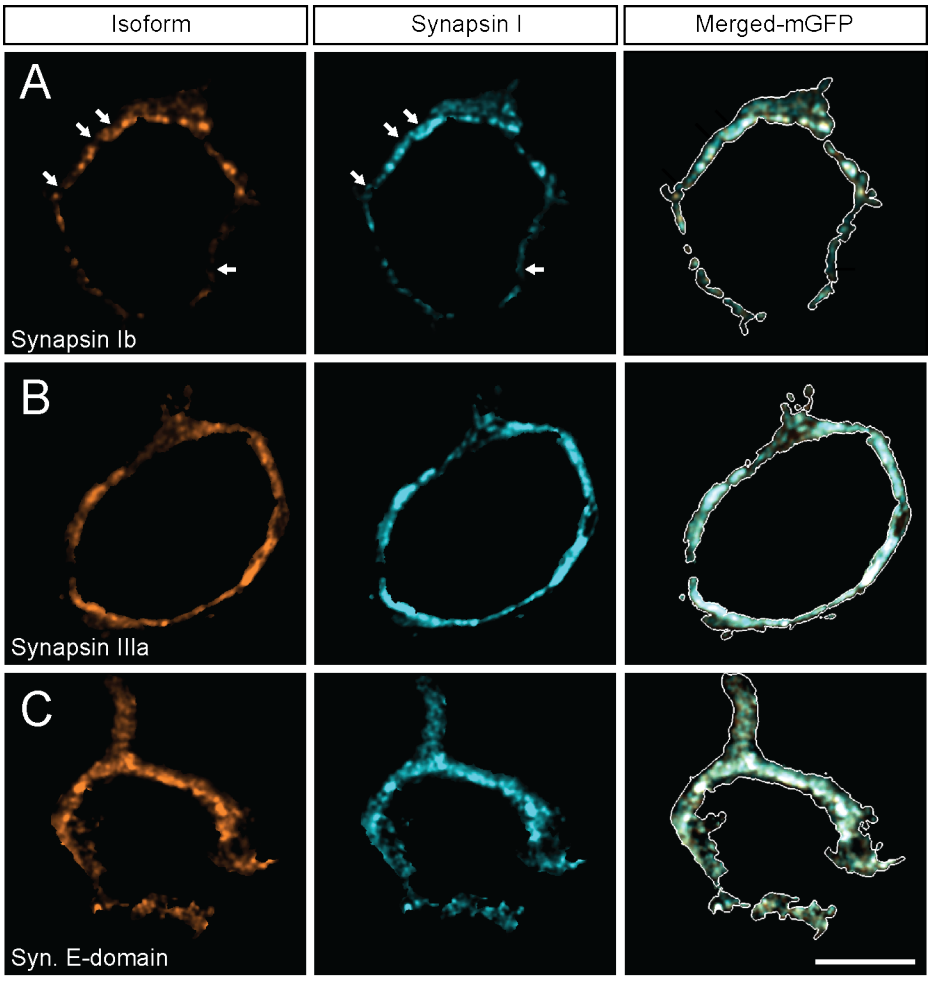

Figure 3.3: Different synapsin isoforms are localized within the same presynaptic volume. Isoform-specific staining pattern was compared to that of pan-synapsin I in mGFP-labeled calyces (white outline in the merged image (right panel)). A: Synapsin Ib (left panel) compared to pan-synapsin I (central panel), arrows indicate pan-synapsin I positive clusters that where synapsin Ib could not be detected. B: Synapsin IIIa (left panel) compared to pan-synapsin I (central panel). C: pan-synapsin E domain, recognizing all synapsin isoforms containing E domain, vs. pan-synapsin I. Images are presented in pseudo-colors. Scale bars: 10 μm.

Synapsin Ib (Fig. 3.3 A, left panel) immunofluorescence revealed more restricted, cluster-like patterns, while synapsin I (Fig. 3.3 A, middle panel) staining was widely distributed, filling

up a larger fraction of the presynaptic volume. There are spots that were positive only for synapsin I and were negative for synapsin Ib (Fig. 3.3 A arrows) and in 54% of all examined calyces (7 out of 13) we found differential expression pattern of synapsin Ib and synapsin I, thus we cannot exclude the presence of synapsin Ia in the calyx of Held at p 16. Synapsin IIIa signal co-localized completely with synapsin I, showing that these isoforms are located within the same presynaptic volume (Fig. 3.3 B). Immunofluorescence from a pan-synapsin antibody, recognizing the E-domain, specific for all a-isoforms, and hence recognizing both synapsin Ia and synapsin IIIa, also co-localized with the pan-synapsin I signal (Fig. 3.3 C), concluding that all a-synapsin isoforms expressed in the calyx did not show differential expression pattern within the presynaptic terminal.

We could determine via immunohistochemistry that synapsin Ia, Ib, synapsin IIb and synapsin IIIa are endogenously expressed in the calyx of Held at p 16 and that the different isoforms tend to be mostly localized within the same volume of the presynaptic terminal. Synapsin I isoforms might make an exception. Their expression patterns although largely overlapping, show some differences and it might be possible that they are associated with functionally different SVs (Rizzoli and Betz, 2005). Since synapsin IIa is not expressed in the calyx of Held, it is highly probable that its proposed function at hippocampal glutamatergic synapses (Gitler et al., 2008) does not hold true.

3.1.2. Colocalization of synapsin isoforms with synaptic vesicles within the calyx of Held

To obtain a more comprehensive description of the synapsin distribution within the calyx of Held we correlated synapsin localization with the overall distribution of SV clusters. For this purpose we visualized SVs using an antibody directed against vGluT1 within mGFP-labeled calyces. High degree of co-localization was examined between all synapsin isoforms expressed in the calyx of Held and vGluT1 within the boundaries of the presynaptic membrane (Fig. 3.4; Supplementary figure 3). Both synapsins and vGluT1 followed the general distribution of SVs within the terminal, showing that they are expressed on the same population of SVs. However, synapsin staining seemed to result in a broader distribution than vGluT1 (arrowheads). This signal might reflect synapsin molecules, which are found in a vesicle-unbound state at any given moment.

Synapsin positive clusters could be detected not only within the calyx of Held but also within putative extracalyceal terminals onto the principal cell of the MNTB. Interestingly, outside the presynaptic terminal synapsin positive puncta failed to contain vGluT1 (arrows). In 64 out of 75 examined synapses vGluT1 immunoreactivity was restricted to the presynaptic

volume outlined by mGFP, making this presynaptic protein a rather specific, but not exclusive, marker for SVs of the calyx of Held.

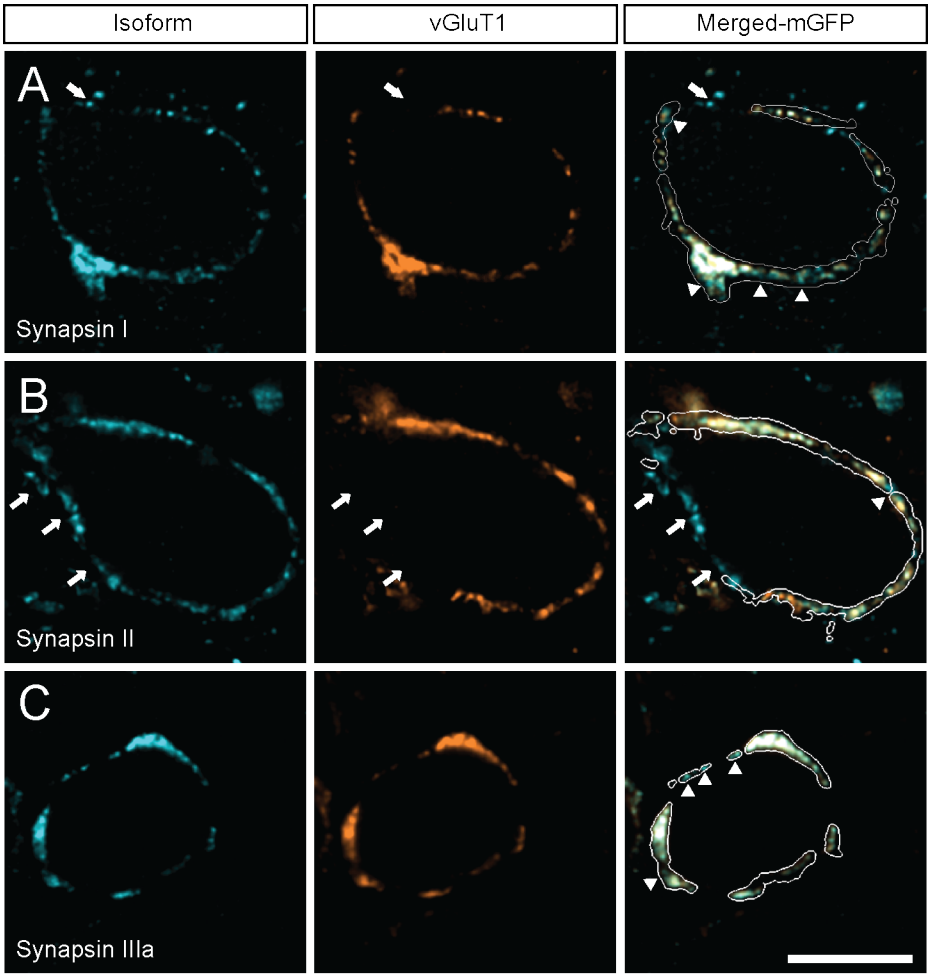

Figure 3.4: Synapsin isoforms colocalize with synaptic vesicles within the calyx of Held. The presynaptic membrane was labeled with mGFP (white outline in the merged images). Distribution of synapsin isoforms (left panel) compared to a SV marker – vGluT1 (central panel), overlay of the corresponding images within the calyx of Held (right panel). Arrowheads indicate synapsin signal outside the vesicle cluster. White arrows point out synapsin-positive clusters outside the mGFP-outlined presynaptic membrane, which do not show vGluT1 positve immunofluorescence. A: pan-synapsin I; B: pan-synapsin II; C: synapsin IIIa. Images are presented in pseudo-colors. Scale bars: 10 μm.

3.1.3. Proper targeting of acutely overexpressed synapsin Ia/Ib to the calyx of Held

To study how single isoforms maintain of synaptic transmission at the calyx of Held we used rAAV1/2 particles coding either for synapsin Ia or for synapsin Ib, N-terminally fused to enhanced yellow fluorescent proteins (EYFP) to perturb the molecular composition of the presynaptic terminal. In this way we wanted to test if dimerization of synapsin isoforms is important for the trafficking and localizing to the presynaptic terminal of the separate isoforms. Ten days after stereotaxic delivery into the aVCN of p 6 rats, both proteins were

successfully targeted to the MNTB where they localized to the calyces of Held (Fig. 3.5). Overview images of infected MNTBs show terminals together with their incoming axons, expressing the exogenous proteins. Overexpression of both proteins revealed the complex, highly fenestrated structure of the calyx. Synapsin Ia, as expected, was properly transported from the GBC cell body to the presynaptic terminal (Fig. 3.5 A). It seems that although synapsin Ib is lacking E-domain implicated in its proper binding to SVs and targeting to the presynaptic terminal, it is successfully localized to the calyx of Held (Fig. 3.5 B) most probably through formation of heteromers with the endogenous synapsin isoforms. This coincides with results obtained in hippocampal autaptic cultures (Gitler et al., 2004b). It is possible that the overexpressed synapsin Ib molecules outcompeted the endogenous isoforms and unbound synapsin Ib freely diffused to the presynaptic terminal.

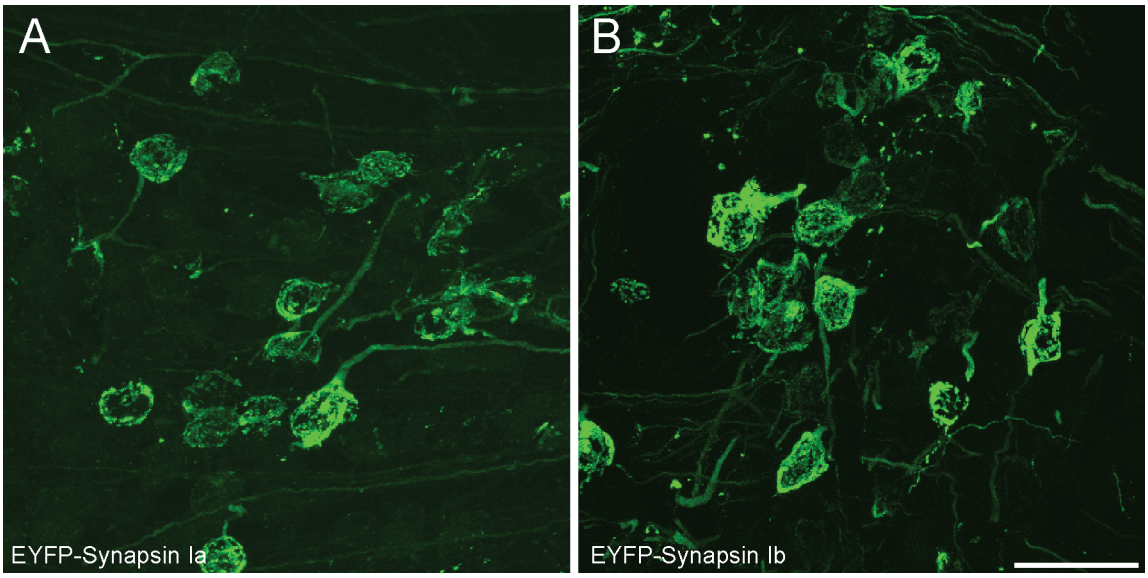

Figure 3.5: EYFP-fused synapsin I isoforms expression in the MNTB of p 16 rats. Both overexpressed isoforms are successfully targeted to the calyx of Held 10 days after rAAV injection into the aVCN. Multiple presynaptic terminals together with in the incoming axons are infected. A: EYFP-synapsin Ia; B: EYFP-syanspin Ib. Images represent a z-collapse of a confocal stack and are presented in pseudo colors. Scale bar: 50 μm.

Within the presynaptic terminals the overexpressed synapsin isoforms filled most of the presynaptic volume and colocalized with vGluT1, similar to endogenous isoforms. Single sections from confocal stacks (Fig. 3.6 A and C) revealed that synapsin I isoforms and vGluT1 occupy the same space within the calyx, pointing out that the overexpressed proteins are targeted to the SV clusters. When the entire presynaptic terminal was examined, it was obvious that both EYFP-synapsin Ia (Fig. 3.6 B) and EYFP-synapsin Ib (Fig. 3.6 D) could be visualized in the incoming axon, in the palm region of the calyx giving rise to individual stalks along the circumference of the postsynaptic cell and within structural specializations of

the synapse – donuts (arrows), which are composed of SVs organized around clusters of mitochondria (Wimmer et al., 2006).

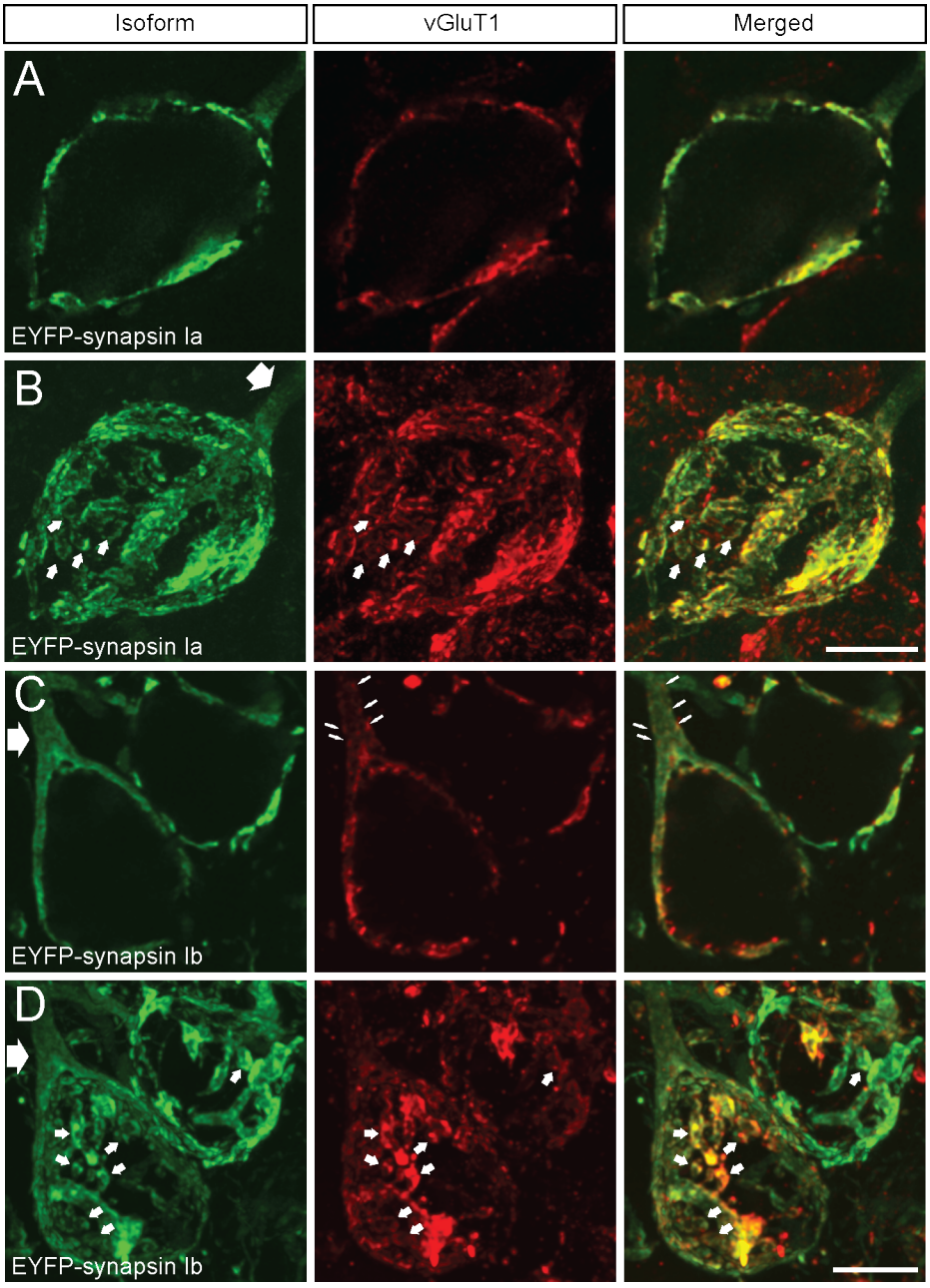

Figure 3.6: Overexpressed synapsin I isoforms co-localize with synaptic vesicles within the calyx of Held. Selected calyces positive for EYFP-synapsin Ia (A and B) and EYFP-syanspin Ib (C and D) (left panels) stained against vGluT1(central panels). The merged images (right panel) show the high degree of co-localization of the two proteins. Thick white arrows indicate the calyceal axon, white arrows point out donut-like formations within the infected terminals, thin white arrows indicate vGluT1 positive clusters in the axon of the calyx, putative SV precursors. A and C: single confocal images, B and D: z-collapse of a confocal stack. Images are presented in pseudo-colors. Scale bars: 10 μm.

The volume-fill pattern of the calyceal axon resulting from the overexpression of synapsin isoforms (thick arrows) contrasts with the discrete localization of small packages

containing SV precursor molecules along the axons (thin arrows), suggesting a different mode of transport for the overexpressed synapsin proteins than for the endogenous vGluT1. Additionally, vGluT1 immunofluorescence was a subset of the EYFP-synapsin signal, indicating an excess of synapsin molecules, which invade the presynaptic terminal upon overexpression. Although it has been shown that molecular perturbation with synapsins leads to alterations in the expression level of presynaptic proteins (Bogen et al., 2009; Gitler et al., 2004a; Rosahl et al., 1995), we did not see changes in the vGluT1 expression level, assessed by immunohistochemistry and the vGluT1 signal could be detected within the entire presynaptic terminal in both cases.

We could successfully show that 10 days post infection synapsin I isofroms are properly targeted to the presynaptic compartment, where they localize with SVs.

3.1.4. Redistribution of SVs within perturbed terminals upon overexpression of both synapsin I isoforms

The consequences of synapsins I isoforms overexpression on the general structure of the SV clusters at the calyx of Held were examined via 3D immunohistochemistry of infected terminals. For the purpose of obtaining the complete volume of the presynaptic terminal we labeled the presynaptic membrane with mGFP. We performed double infection with AAV1/2, coding for mGFP and rAAV1/2, coding for the synapsin isoform of interest. Control experiments, involving infection only with mGFP were conducted in parallel. SV distribution was examined via staining with vGluT1 antibody and 3D structural analysis of the entire presynaptic compartment was performed. The mGFP signal allowed us to examine the 3D distribution of SV clusters (Fig. 3.8 A and D) and the overexpressed proteins (Fig. 3.8 B and E) within the entire volume of genetically perturbed calyces. The overlay images (Fig. 3.8 C and F) revealed the distribution of SV clusters with respect to synapsin I isoforms and the mGFP-labeled calyx (green).

The 3D analysis revealed that the size and the architecture of the calyx of Held remained largely unaltered. The incoming axons are shown for clarity and were excluded from the volume calculation. The total volume the presynaptic terminal (Fig. 3.7 G) remained largely unaltered and had values of 960.6 ± 62.7 μm^3 for control calyces and 995.1 ± 55.2 μm^3 for synapsin Ib overexpressing calyces. Terminals positive for synapsin Ia, had smaller volume (803.2 ± 51.5μm^3) compared to synapsin Ib overexpressing calyces (one-way ANOVA, $p = 0.04$). This might be due to the variability between different animals and terminals. The volume occupied by SVs (Fig. 3.7 H), visualized via vGluT1

immunofluorescence was also not changed – 663.0 ± 54.0 µm^3 for control synapses, 760.1 ± 47.2 µm^3 for synapsin Ib and 596.2 ± 41.4 µm^3 for synapsin Ia overexpressing terminals. Consistent with the smaller volume of the calyx, synapsin Ia infected calyces had the tendency to show reduced vGluT1 volume (one-way ANOVA, p = 0.06).

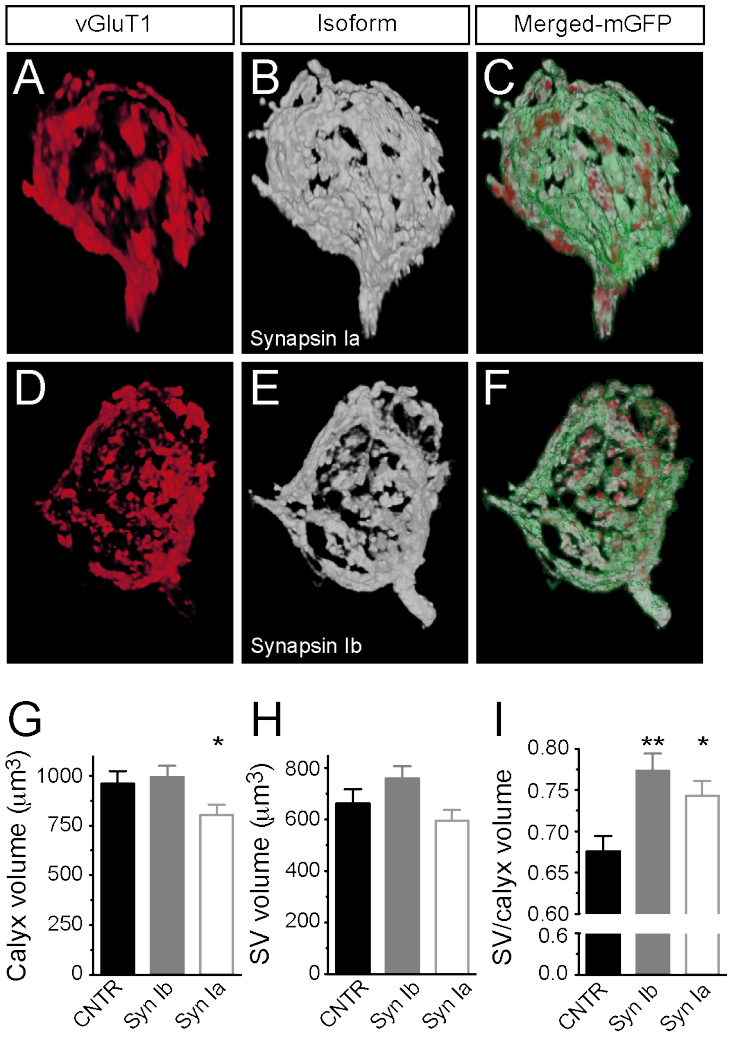

Figure 3.7: Overexepression of synapsin I isoforms at the calyx of Held leads to vesicle redistribution within the presynaptic terminal. 3D reconstructions of calyces overexpressing mGFP (green outline) and either EYFP-synapsin Ia or EYFP-synapsin Ib (white), stained for vGluT1 (red). A – C: overexpression of EYFP-synapsin Ia; D – F: overexpression of EYFP-synapsin Ib. Merged images (C and F) represent the overlay of the synapsin I isoforms with the vesicle stain within the boundaries of the calyx. G-I: Quantitative analyses for control, synapsin Ia and synapsin Ib overexpression. G: Volume of the space taken up by the mGFP-labeled presynaptic terminal (One Way ANOVA, p = 0.04). H: Volume taken up by SVs, stained for vGluT1. I: The Ratio of SV volume to calyx volume is increased by the overexpression of both synapsin I isoforms (One Way ANOVA, p = 0.002). N = 26 CNTR, 24 EYFP-synapsin Ib, 25 EYFP-synapsin Ia overexpressing calyces. Black – control, gray – EYFP-synaspin Ib, light gray – EYFP-synapsin Ia. (*) for p < 0.05, Scale bars 10 µm.

Since the size of the presynaptic terminals within the same preparation varied substantially, we calculated the ratio of the volume occupied by vGluT1 immunofluorescence to the volume of the entire calyx of Held (Fig. 3.7 I). Overexpression of either synapsin Ia or

Ib shifted this ratio to significantly higher values of 0.74 ± 0.02 for synapsin Ia and 0.77 ± 0.021 for synapsin Ib-overexpressing calyces versus 0.68 ± 0.02 for control calyces (one-way ANOVA, p = 0.002). This led us to the conclusion that synapsin I overexpression does not abolish the maturation of the presynaptic terminals. Their structure and size were comparable to that of control calyces overexpressing only mGFP. However, structural alterations of the vesicle cluster take place and the same total amount of SVs occupied a larger part of the presynaptic volume in perturbed calyces than in WT calyces. The redistribution of SVs within the entire volume of the calyx upon overexpression of either synapsin Ia or synapsin Ib implies that vesicle immobilization and clustering within the perturbed terminals is impaired.

3.1.5. Basal transmission at the calyx of Held is independent of synapsin I isoforms

After having shown that acute overexpression of synapsin I isoforms in the calyx of Held leads to redistribution of vesicles within the presynaptic terminal, we assessed the electrophysiological properties of these terminals. We did whole cell patch clamp recordings form the MNTB principal cells making connections with genetically manipulated calyces. Infected terminals were selected on the basis of strong fluorescent signal, whereas control measurements were done from cells showing no fluorescence in the same preparation. Spontaneous activity was recorded in MNTB principal cells for 2 – 4 min after whole cell configuration was made, and prior to any high-frequency stimulation (Fig. 3.8). Spontaneous quantal excitatory postsynaptic events (spEPSCs) were detected in all three conditions tested – control, synapsin Ia- and synapsin Ib-overexpression (Fig. 3.8 A) and analyzed using a threshold algorithm and their size, frequency and time were calculated. Overall, spEPSC size and frequency were not significantly affected by overexpression of synapsin Ia, or synapsin Ib. The frequency of events was 1.67 ± 0.21 Hz in control cells, and showed no significant change due to overexpression of either of the synapsin isoforms (one-way ANOVA, p = 0.69) (Fig. 3.8 B). Quantal size was determined as the charge integral of individual events. Medians of single cells were similar between the control and overexpression conditions: 31.83 ± 1.52 fC in control (3238 events), 31.86 ± 1.91 fC in terminals overexpressing synapsin Ib (3478 events), and 29.05 ± 1.23 fC in terminals overexpressing synapsin Ia (7943 events) (one-way ANOVA, p = 0.32) (Fig. 3.8 C). Hence, quantal size was unaffected by overexpression of either of the synapsin isofoms tested. Kinetic analysis of spontaneous events showed that neither synapsin Ia nor Ib overexpression affected rise or decay times. Median rise times (20 – 80 % of amplitude) were 110.3 ± 4.7 µs in control, 109.2 ± 2.9 µs in terminals overexpressing synapsin Ib, and 113.9 ± 2.4 µs in terminals overexpressing synapsin Ia (one-way ANOVA, p

= 0.56) (Fig. 3.8 D). Median decay time constants for quantal events were 352 ± 24 µs in control calyces, 349 ± 17 µs in terminals overexpressing synapsin Ib, and 356 ± 14 µs in terminals overexpressing synapsin Ia (one-way ANOVA, p = 0.96) (Fig. 3.8 E). Thus, overexpression of neither synapsin Ia nor -Ib changed the quantal content versus the uninfected control.

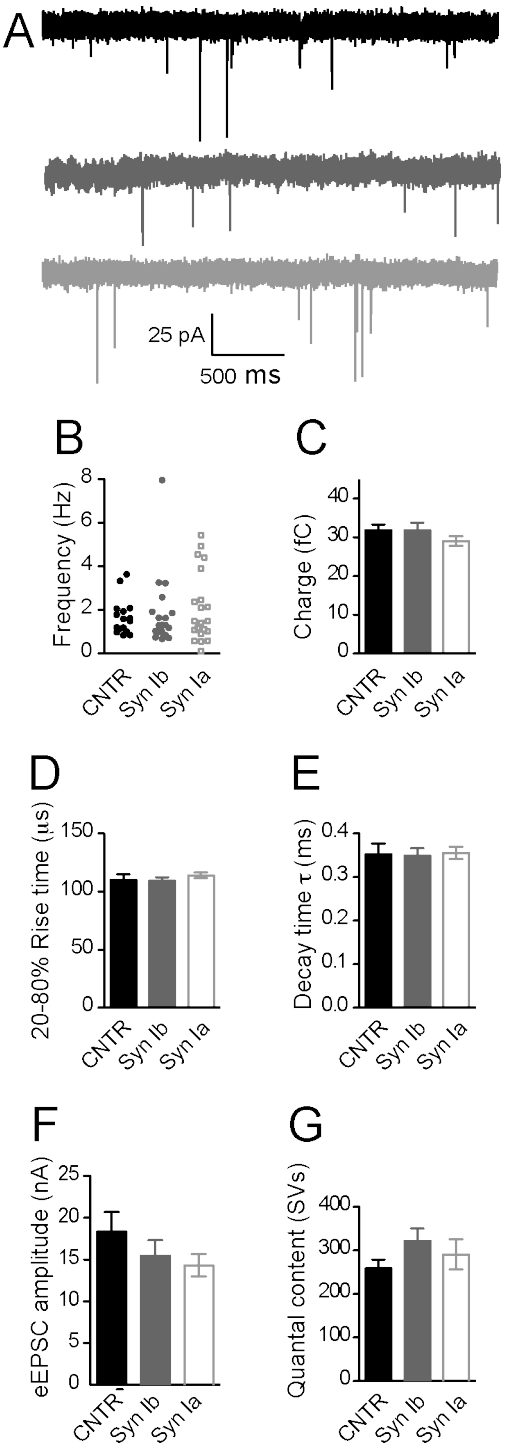

Figure 3.8: Basal synaptic transmission remains intact upon overexpression of synapsin I isoforms at the calyx of Held. A-E: parameters of spEPSCs. A: example traces from spEPSC recording from CNTR (black), synapsin Ib (gray) and synapsin Ia (light gray) overexpressing terminals. spEPSC frequency (B) and charge (C) remained intact upon overexpression of synapsin I isoforms. Kinetics of the spontaneous evens: rise time (D) and decay time (E) were also not altered. F: The normalized eEPSC amplitude was comparable between synapsin I isoforms overexpressing and CNTR terminals. G: Intact quantal content, the quantal content, calculated as the ratio between the charge of an eEPSC and the charge of a single quantal event. N is provided in table 3.1. Black – control, gray – EYFP-synaspin Ib, light gray – EYFP-synapsin Ia.

The calyx displays wide variance in the size of the EPSC at basal stimulation frequencies (Taschenberger and von Gersdorff, 2000), and at the age investigated here many EPSCs saturated our recording conditions. As a result, recordings of evoked EPSCs were made at various holding potentials, and are thus not directly comparable, without biased selection. We recorded several cells at both -70 and -30 mV holding potential and were able to scale the EPSCs post-hoc to normalize against holding potential. The results from this manipulation gave a predicted mean EPSC size of 18.35 ± 2.33 nA in control recordings at -70 mV holding potential, and did not significantly differ between control and experimental conditions (one-way ANOVA, $p = 0.37$) (Fig. 3.8 F). Quantal content, which is a measure of the number of synaptic vesicles released per evoked response was estimated as the quotient of the charge integral of a single excitatory postsynaptic current (EPSC) taken at low frequency (0.1Hz) over the median quantal charge, per cell. Quantal content was found to be 259 ± 20 SV in control, 322 ± 29 SV in synapsin Ib overexpression, and 291 ± 35 SV due to synapsin Ia overexpression. These results were similar between control and the experimental conditions (one-way ANOVA, $p = 0.25$) (Fig. 3.8 G). All analyzed parameters of evoked EPSCs were comparable between the three tested conditions. Table 3.1 gives a summary of the basal synaptic transmission. Thus we can conclude that although overexpression of synapsin I isoforms led to pronounced structural modifications of the synaptic vesicle cluster, it did not alter the basal synaptic transmission at the calyx of Held. Synapsin I isoforms might not be necessary for maintaining single quantal events and responses to isolated APs. The effect of the overexpression, however, might be made milder and even occluded by the presence of endogenous synapsins.

spESPC properties

	Frequency (Hz)	Charge (pC)	Rise time (ms)	Decay time (ms)
CNTR	1.76 ± 0.20 (16)	31.83 ± 1.52 (16)	110.3 ± 4.7	352 ± 24
EYFP-synIb	1.85 ± 0.38 (19)	31.86 ± 1.91(18)	109.2 ± 3.3	349 ± 17
EYFP-synIa	2.09 ± 0.35 (21)	29.05 ± 1.23 (20)	113.9 ± 2.4	356 ± 14

eESPC properties

	Estimated EPSC size (nA)	Quantal Content (SVs)	Estimated RRP size (SVs)	Estimated Pr (EPSC/RRP)
CNTR	18.35 ± 2.33 (36)	259 ± 20 (16)	1015 ± 52 (13)	0.27 ± 0.01
EYFP-synIb	15.48 ± 1.86 (27)	322 ± 29 (15)	1273 ± 74 (13)	0.32 ± 0.02
EYFP-synIa	14.31 ± 1.32 (21)	291 ± 35 (12)	1125 ± 142 (12)	0.34 ± 0.03

Table 3.1: Properties of basal neurotransmission at calyces overexpressing synapsin I isoforms compared to uninfected control presynaptic terminals.

3.1.6. Synapsin I isoforms control the use-dependent synaptic plasticity at the calyx of Held without changing the size of the readily releasable pool

At the calyx, trains of repetitive stimuli reduce the synaptic response mostly due to a depletion of the RRP (von Gersdorff and Borst, 2002) and at this age desensitization of AMPA receptors is not present at stimulation frequencies < 300 Hz due to fast glutamate clearance (Renden et al., 2005; von Gersdorff and Borst, 2002). Towards the end of the stimulus train a steady-state is achieved which reflects the balance between the rate of depletion of the RRP and its replenishment. Synapsins are thought to mediate the mobilization of SVs within the presynaptic terminal and hence to be involved in the trafficking of SVs between different pools (Gitler et al., 2004a; Rosahl et al., 1993). Therefore we analyzed the properties of synaptic depression at the calyx of Held through application of trains of repetitive stimuli upon overexpression of synapsin I isoforms and compared it to that in control terminals. Stimulation with 10 Hz frequency (Fig. 3.9 A) resulted in all three conditions to similar depression extent. Synapses depressed to about 35 – 40 % of the initial EPSC size after approximately 10 stimuli (Fig. 3.9 B). Onset of depression was fit by a monoexponential function for each cell and had an average time constant (τ) of 304 ± 33 ms in control cells. The decay constant was significantly faster in synapses overexpressing synapsin Ib (191 ± 16 ms), ($p < 0.01$), or synapsin Ia (170 ± 19 ms), (one-way ANOVA, $p < 0.01$) (Fig. 3.9 C). The steady state level of depression was estimated as the average of 10^{th} – 20^{th} stimuli and was determined individually for each replicate. It was similar between all three conditions (Fig. 3.9 D) – control terminals showed steady-state depression of 43.9 ± 2.2 % of initial EPSC size, whereas synapsin Ib overexpression depressed to 39.1 ± 2.3 %, and terminals with synapsin Ia overexpression resulted in depression to 37.9 ± 1.7 % of the initial EPSC size (one-way ANOVA, $p = 0.12$).

Stimulation at higher frequency (100 Hz) resulted in all three examined cases to very pronounced short-term depression (Fig. 3.9 E), which was fit by an exponential function of responses in individual cells for the 2^{nd} – 50^{th} stimuli (Fig. 3.9 F). The first response was excluded because there was occasional facilitation of the postsynaptic response. Control synapses depressed to 25.4 ± 1.9 % of the initial state with a time constant of 44.2 ± 3.7 ms. Overexpression of either synapsin I isoforms led to faster time course of depression and lower steady state level of transmission during the stimulation train (Fig. 3.9 E – H). Synapsin Ib overexpression resulted in depression with a time constant of 32.6 ± 2.1 ms, and a steady state of 18.2 ± 1.4 % (one-way ANOVA, $p < 0.05$ for both indices, relative to control). Synapsin Ia overexpression sped depression even more than synapsin Ia, leading to a time constant of 25.8

± 3.1 ms and steady state level of 15.4 ± 1.2 % (one-way ANOVA, $p < 0.001$ for both indices, relative to control). Thus, overexpression of either of the synapsin Ia or synapsin Ib at the calyx of Held resulted in accelerated and more severe depression at 100 Hz than in non-infected terminal.

We stimulated control and infected terminals at 300 Hz (Fig. 3.9 I), which can be regarded as the upper bound on stimulation frequency at room temperature (Renden et al., 2005; Taschenberger and von Gersdorff, 2000), and monitored synaptic responses from stimuli 2^{nd} – 50^{th}, again to avoid early facilitation at some synapses (Fig. 3.9 J). Notably, at this frequency synaptic depression was not monoexponential, but consisted of an additional fast (< 10 ms) phase in both control and genetically manipulated synapses. The average time constants (and relative weight for τ_{fast}) for depression in control synapses for this protocol were τ_{fast} = 7.4 ± 1.0 ms (70.0 ± 1.3 %), and τ_{slow} = 33.5 ± 2.8 ms. In terminals overexpressing synapsin Ib, both τ_{fast} was 6.01 ± 0.66 ms with relative weight of the fast component 73.3 ± 1.7%, and τ_{slow} of 31.1 ± 3.0 ms were similar to control. However, overexpression of the synapsin Ia isoform in these synapses resulted in significantly faster τ_{fast} (4.0 ± 0.5 ms), (one-way ANOVA, $p < 0.05$) and τ_{slow} (21.64 ± 2.54 ms), ($p < 0.05$) but with a similar relative weight (68.0 ± 2.3%). Accordingly, when the mean depression time constant is calculated (τ_{mean} [$\tau_m = \tau_{fast}*(\%\tau_{fast}) + \tau_{slow}*(1-\%\tau_{fast})$]), the effect on the time constants was increased and synapsin Ia overexpression resulted in a significantly faster mean depression time constant, relative to control (one-way ANOVA, $p < 0.01$) (Fig.3.9 K). Control synapses depressed to 8.4 ± 1.0 % of the initial EPSC size by the end of the 50 x 300 Hz train. Although the steady state at 300 Hz was not affected by synapsin Ib overexpression (5.6 ± 0.8 %), synapsin Ia overexpression reduced the steady state significantly (3.3 ± 0.6 %,) ($p < 0.01$, relative to control) (Fig.3.9 L). The time constants of depression and the steady state of depression for all examined cases are summarized in table 3.2.

Using the same data presented above, we examined the paired-pulse ratio (PPR) for potential differences in facilitation or depression early in the stimulus train, due to synapsin I overexpression. Overlay of the first two responses from a 300 Hz stimulation train is presented in (Fig. 3.10 A). Overexpression of synapsin Ia significantly affected the PPR at all tested inter-stimulus intervals (one-way ANOVA, $p < 0.01$ for ISI 3.33 ms, 10 ms and $p < 0.05$ for ISI 100 ms). There was no effect of synapsin Ib overexpression on the PPR at any inter-stimulus interval (Fig. 3.10 B).

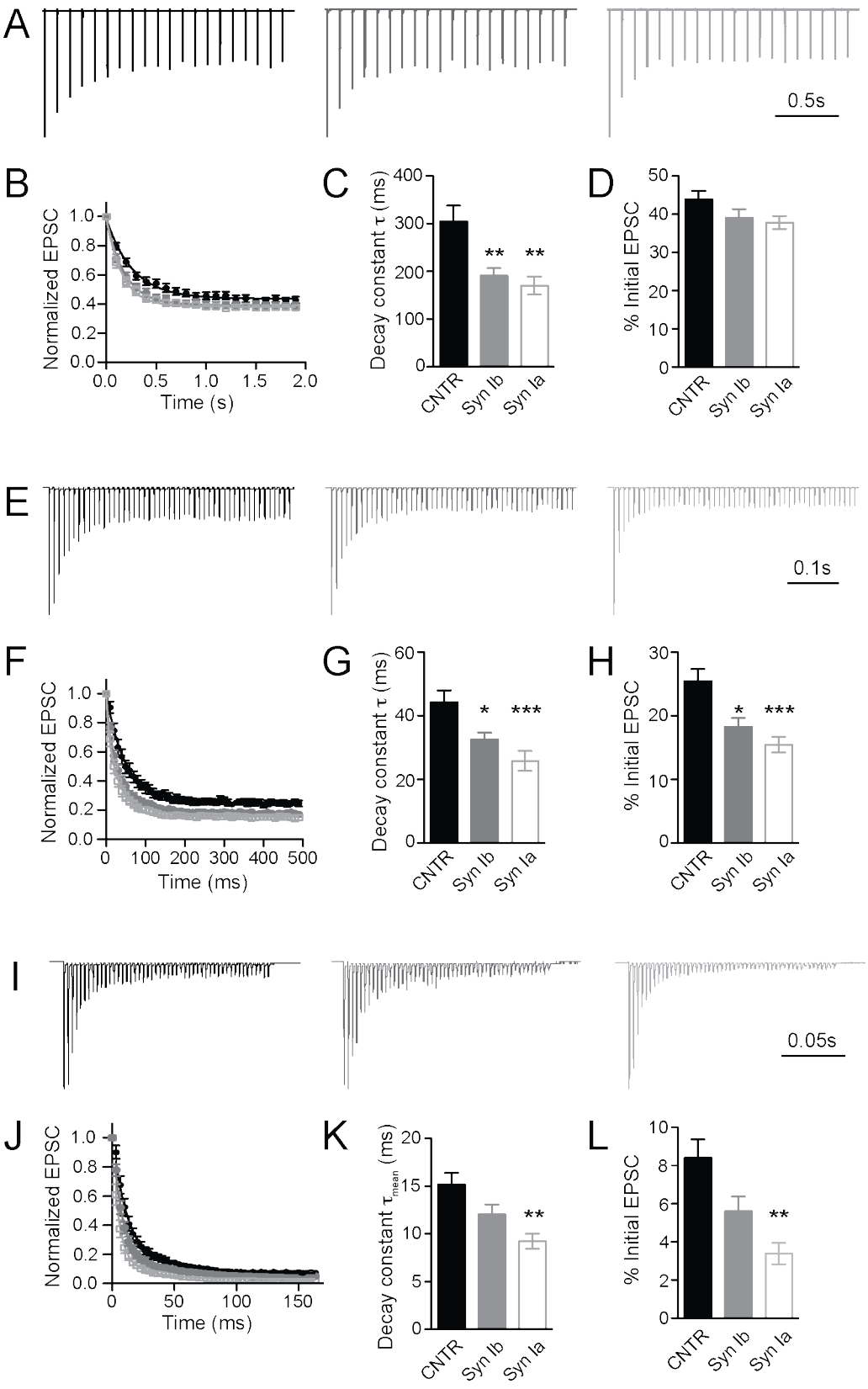

Figure 3.9: Overexpression of synapsin Ia or synapsin Ib increases depression during repetitive stimulation. Synapses were challenged with repetitive stimulation (20 – 50 pulses) at varying frequencies. A, E and I: representative traces from the STD recordings. A-D: Stimulation at 10 Hz. N = 20 CNTR, 16 EYFP-synapsin Ib, 13 EYFP-synapsin Ia overexpressing calyces. E-H: Depression at 100 Hz. N = 20 CNTR, 19 EYFP-synapsin Ib, 21 EYFP-synapsin Ia overexpressing calyces. I-L: Depression at 300 Hz. N = 14 CNTR, 15 EYFP-synapsin Ib, 11 EYFP-synapsin Ia overexpressing calyces. N is provided in table 3.2. Black – control, gray – EYFP-synaspin Ib, light gray – EYFP-synapsin Ia. (*) for $p < 0.05$, (**) for $p < 0.01$, (***) for $p < 0.001$.

10Hz x 20 pulses

	Decay constant t (ms)	% initial EPSC
CNTR	304 ± 33 (20)	43.9 ± 2.2
EYFP-synIb	191 ± 15.8 (16) **	39.1 ± 2.3
EYFP-synIa	170 ± 19 (13) **	37.9 ± 6.8

100Hz x 50 pulses

	Decay constant t (ms)	% initial EPSC
CNTR	44.23 ± 3.74 (20)	25.4 ± 1.9
EYFP-synIb	32.6 ± 2.1 (19) *	18.2 ± 1.4 *
EYFP-synIa	25.8 ± 3.1 (21) ***	15.4 ± 1.2 ***

300Hz x 50 pulses

	Decay constant t_{fast} (ms)	Decay constant t_{slow} (ms)	% initial EPSC
CNTR	7.4 ± 1.0 (17)	33.5 ± 2.8	8.4 ± 1.0
EYFP-synIb	6.01 ± 0.66 (15)	31.1 ± 3.0	5.6 ± 0.8
EYFP-synIa	4.0 ± 0.5 (11) *	21.64 ± 2.5 *	3.3 ± 0.6 **

Table 3.2 Properties of short-term synaptic depression at calyces overexpressing synapsin I isoforms compared to uninfected control presynaptic terminals.

An extrapolation of the data provided by depression trains at 100 Hz allows an estimation of the size of the releasable pool of vesicles (Schneggenburger et al., 1999; Stevens and Williams, 2007). When EPSC areas are plotted as a cumulative charge function, the Y-intercept yields the size of the releasable pool, whereas the slope is proportional to the steady state. The number of SVs in the releasable pool was then calculated as the ratio between the intercept value and the median quantal size, estimated from recordings in the same cell. This analysis resulted in pool size estimates of 1015 ± 52.3 SV in control terminals, similar to what has been previously reported (Iwasaki and Takahashi, 2001; Kushmerick et al., 2006). Overexpression of neither synapsin I isoform significantly differed from control. We found the RRP to be approximately 1273 ± 74 SVs in terminals overexpressing synapsin Ib, and 1125 ± 142 SVs in terminals overexpressing synapsin Ia (Table 3.1). Using this estimation of the total releasable pool size, we then determined the probability of release (Pr), by dividing the relative size of the first EPSC to the estimated size of the total RRP. There was no significant difference between the Pr of control and synapses overexpressing synapsin Ia or synapsin Ib (Fig. 3.10 C). Thus overexpression of synapsin I isofroms accelerated short-term depression at all tested frequencies at the calyx of Held without altering the size and release probability of readily releasable pool of vesicles. Contrary to our expectations, based on the synapsin dimerization theory, the overexpression of synapsin Ia resulted in a more

pronounced phenotype than the overexpression of synapsin Ib and led to altered paired pulse ratio.

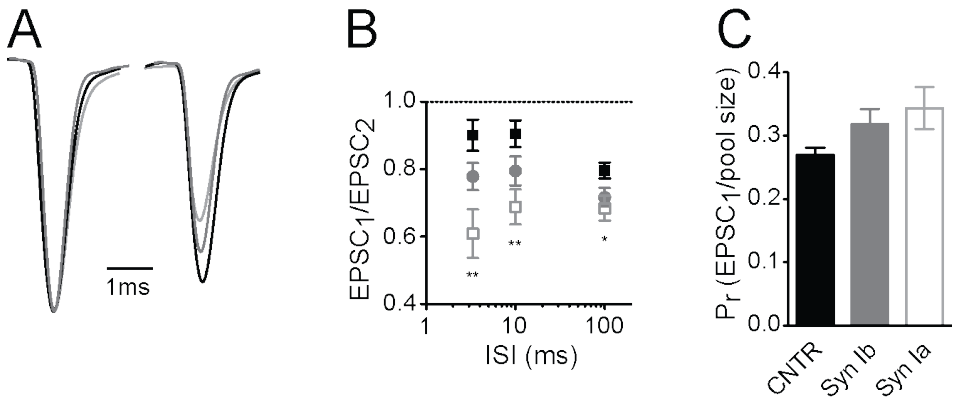

Figure 3.10: Paired-pulse ratio of the first two stimuli in a train. A: Traces show an ensemble of recordings from calyces of the three genotypes studied. Sweeps were taken at -30 mV holding potential, and normalized and aligned to the first peak. Stimulation artifacts have been removed for clarity. B: Plot shows the paired-pulse ratio (PPR) for the three genotypes, across the range of frequencies studied. C: Release probability was calculated from the RRP estimation (table 3.1). N is provided in table 3.1. Black – control, gray – EYFP-synaspin Ib, light gray – EYFP-synapsin Ia. (*) for $p < 0.05$, (**) for $p < 0.01$.

3.1.7. Accelerated recovery from depression in calyces overexpressing synapsin I isoforms

Following short trains at 100 Hz, recovery of the partially depleted pool of release-competent vesicles was assayed, using single test pulses at different intervals (64 ms to 12 s) after the end of the stimulus train (Fig. 3.11 A). Recovery at the calyx of Held should be complete within 10 – 12 s at similar ages (Kushmerick et al., 2006). Recovery was measured as ($A-A_{ss}/A_0-A_{ss}$), where A is equal to the response to the test pulse, A_0 is the first response from the stimulation train and A_{ss} represents the steady-state EPSC integral, to account for different levels of depression between the control and infected terminals.

For a short 6 x 100 Hz train (Fig.3.11 B), transmission was depressed to ~ 50% in control synapses, and recovered in all conditions with a monoexponential time course. Control synapses needed 4.8 ± 0.6 s to recover to the level of the initial EPSC. Overexpression of either synapsin Ia or synapsin Ib did not significantly affect the time course of recovery following moderate depression in this protocol, with synapses overexpressing synapsin Ia recovering after 4.4 ± 0.4 s, and synapsin Ib overexpressing synapses recovering after 4.7 ± 0.7 s (Fig.3.11 C).

For a longer depleting train at 20x100 Hz (Fig. 3.11 D), recovery also followed a monoexponential time course in control terminals (τ = 4.59 ± 0.66 s); however, overexpression of either synapsin I isoforms resulted in significantly faster recovery to the

initial EPSC size. The faster recovery proved to be the result of the introduction of an additional fast kinetic component in the infected synapses. Therefore, recovery data in synapsin Ia and synapsin Ib overexpressing synapses was better fit by a biexponential function ($p < 0.001$; extra sum of squares F test; $r^2 > 0.997$). Recovery from this depression protocol in synapsin Ib infected terminals resulted in τ_{fast} = 215.0 ± 92.9 ms (contributing 27.8 ± 3.4 % of total recovery) and τ_{slow} = 5.1 ± 1.04 s.

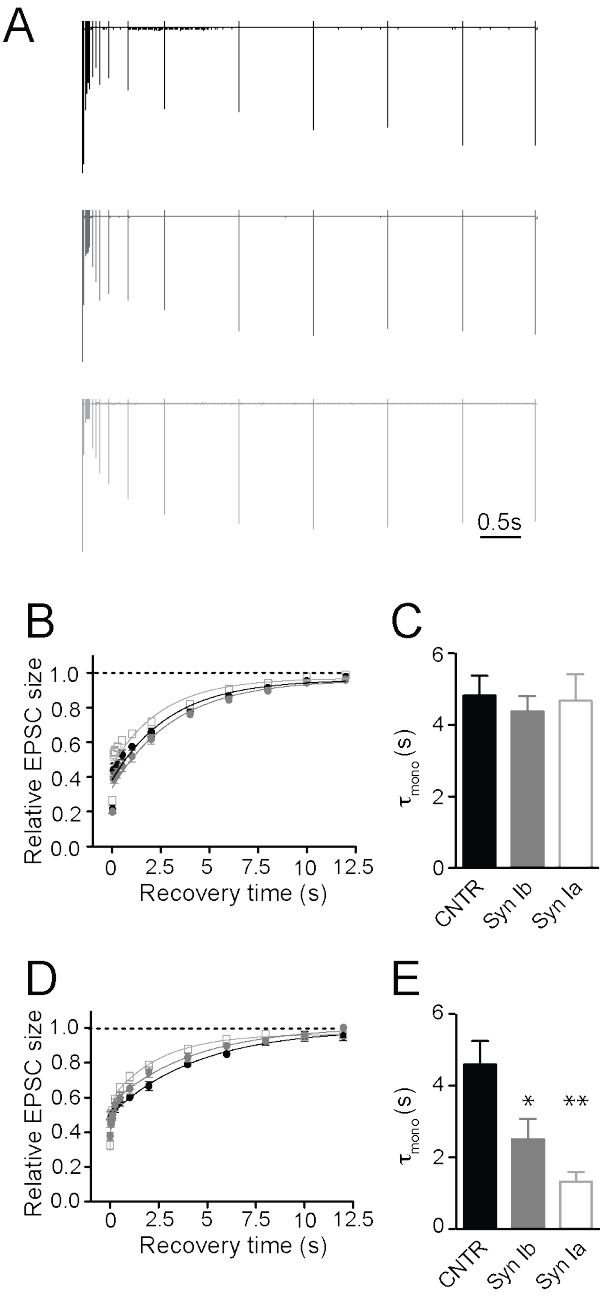

Figure 3.11: Synapsin I isoforms accelerate recovery from depression after strong stimulus trains. A. Sample traces, illustrating the recovery from depression stimulation protocol in a CNTR (black), synapsin Ib (gray) and synapsin Ia (light gray) positive synapse. Synapses were depressed with a stimulation train and recovery of EPSC amplitudes measured at varying intervals. B – C: Recovery from a 20x100Hz depression train. B: Peak amplitudes are shown relative to the initial EPSC amplitude. C: Due to the variance in depression between genotypes (see Fig. 3.9), depression was normalized to zero, and recovery kinetics measured from the resulting curves. Normalization of the depressed state revealed significantly faster recovery in synapses overexpressing Synapsin Ib, and to a stronger extent in Synapsin Ia. For simplicity monoexponential rates of recovery were plotted. N and significance level are provided in table 3.3. Black – control, gray – EYFP-synaspin Ib, light gray – EYFP-synapsin Ia. (*) for $p < 0.05$, (**) for $p < 0.01$.

Synapsin Ia overexpression additionally sped recovery due to an increase in the weight of the fast component to 38.3 ± 3.5 % of recovery, and had a τ_{fast} = 88.9 ± 10.9 ms and a τ_{slow} = 2.68 ± 0.3 s. To be able to make a direct comparison with the control we fitted the data from

the synapsin overexpressing terminals monoexponentially with recovery time constant τ_{mono} = 2.51 ± 0.57 s for synapsin Ib and τ_{mono} = 1.32 ± 0.28 s for synapsin Ia overexpressing calyces (one-way ANOVA, p = 0.003) (Fig.3.11 E). The results from the recovery from depression experiments are summarized in table 3.3.

Single exponential

	100Hz x 6 pulses	100Hz x 20 pulses
	Recovery time constant τ (s)	Recovery time constant τ_{mono} (s)
CNTR	4.8 ± 0.6 (11)	4.59 ± 0.66 (11)
EYFP-synIb	4.4 ± 0.4 (9)	2.51 ± 0.57 (11) *
EYFP-synIa	4.7 ± 0.7 (8)	1.32 ± 0.28 (7) **

Double exponential

	100Hz x 20 pulses		
	Recovery time constant τ_{slow} (s)	Recovery time constant τ_{fast} (ms)	Weight of the fast component (%)
CNTR	-	-	-
EYFP-synIb	5.1 ± 1.04 (10)	215.0 ± 92.9 (10)	27.8 ± 3.4 (10)
EYFP-synIa	2.68 ± 0.3 (7)	88.9 ± 10.9 (7)	38.3 ± 3.5 (7)

Table 3.3 Recovery from STD after overexpression of synapsin I isoforms.

From these results, we conclude that overexpression of both synapsin I isoforms slowed down the refilling of the RRP during trains of intense stimulation most probably through depletion of the vesicle pool. Furthermore, at rest the two isoforms accelerated recovery kinetics following partial depression of the readily releasable vesicle pool, due to the addition of a rapid recovery component.

3.1.9. Ultrastructural alterations at the calyx of Held upon overexpression of synapsin Ia

Photooxidation of the EGFP allowed us to visualize infected cells and to study their ultrastructure using electron microscopy. Low magnification images (Fig. 3.12) show MNTB principal cells innervated by an EGFP (Fig. 3.12 A) and EGFP-synapsin Ia (Fig. 3.12 B) terminals. In both cases photooxidation of the fluorophore resulted in the formation of dark precipitate of electron dense material within the lumen of the infected presynaptic terminals (denoted by *). We selected calyceal segments according to the intensity of the electron dense material and performed serial section EM (Horstmann et al., 2012), which allowed us to do 3D reconstructions and examine the SV distribution within the infected terminals (Fig. 3.13). The darker regions (Fig. 3.13 A and B) correspond to presynaptic terminals infected with EGFP and EGFP-synapsin Ia, whose 3D reconstruction is presented in (Fig. 3.13 C and D). Four EGFP-positive segments from two animals and four EGFP-synapsin Ia positive

terminals from two animals were analyzed and the SV distribution was determined. Serial ultrathin (approximately 35 nm) sections, each containing a single layer of SVs allowed unbiased, precise characterization of the location of the complete vesicle population within the segments of the presynaptic compartment. Reconstructions were generated from 20 – 30 consecutive sections mainly from regions where the calyx morphology was highly fenestrated and single calyceal protrusions on the surface of the principal cell could be analyzed. Total volume of 53.16 μm^3 from EGFP positive calyces and 25.44 μm^3 from EGFP-synapsin Ia containing terminals was reconstructed.

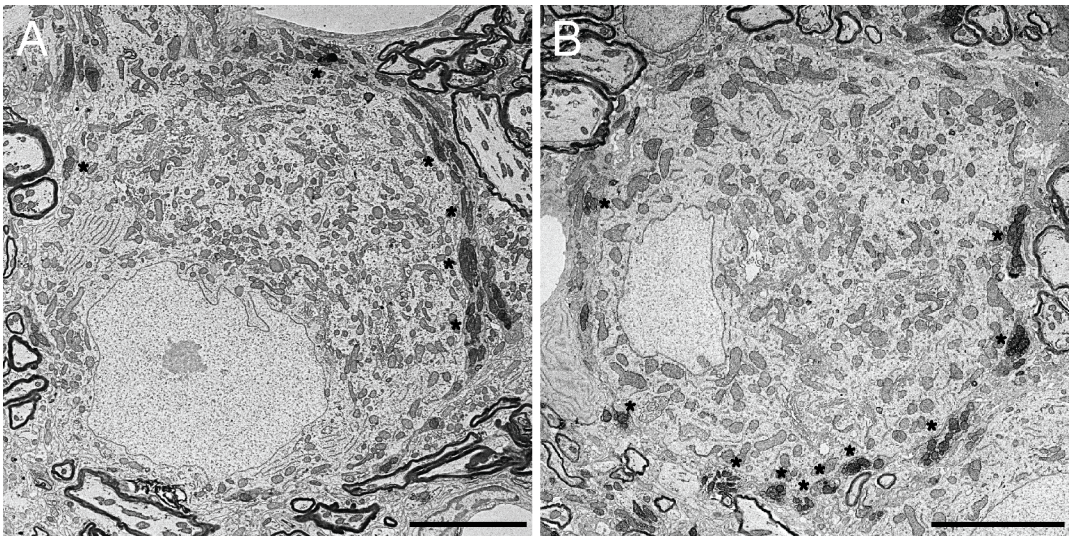

Figure 3.12: Photooxidation of overexpressed EGFP (A) or EGFP-synapsin Ia (B) allowed the ultrastructural analysis of genetically perturbed calyces. Low magnification images showing characteristic electron dense material along the perimeter of the MNTB principal cell allowed the identification of infected terminals. Scale bars: 5 μm.

The overall ultrastructure was not grossly impaired by the overexpression of synapsin Ia. The average volume of an EGFP segment was 13.29 ± 4.22 μm^3 and contained 767.91 ± 150.62 SV/μm^3. The average volume of an EGFP-synapsin Ia segment was 6.36 ± 1.63 μm^3 and contained 572.8 ± 70.89 SV/μm^3 ($p = 0.49$, Mann Whitney test) (Fig. 3.13 E and Table 3.4). From this calculation we could extrapolate the total SV number to the entire volume of calyx of Held, measured (Fig. 3.7). From this estimation we obtained 509,184 ± 8,154 SVs in control calyx and 326,152 ± 2,939 SVs in synapsin Ia overexpressing calyx. This difference might arise from the decreased volume of synapsin Ia overexpressing calyces calculated from the 3D reconstructions of entire presynaptic terminals. These values are much larger than what has been already reported (de Lange et al., 2003). The discrepancy might result from the different age of the animals used (p 6 – 10 vs. p 20) and from the fact that the volume of the presynaptic compartment increases with age (Dondzillo et al., 2010). Additionally, (de Lange

et al., 2003) used the volume estimated from a single p 9 terminal (Sätzler et al., 2002) and thicker sections (85 nm vs. 35 nm), which might highly underestimate the SV number.

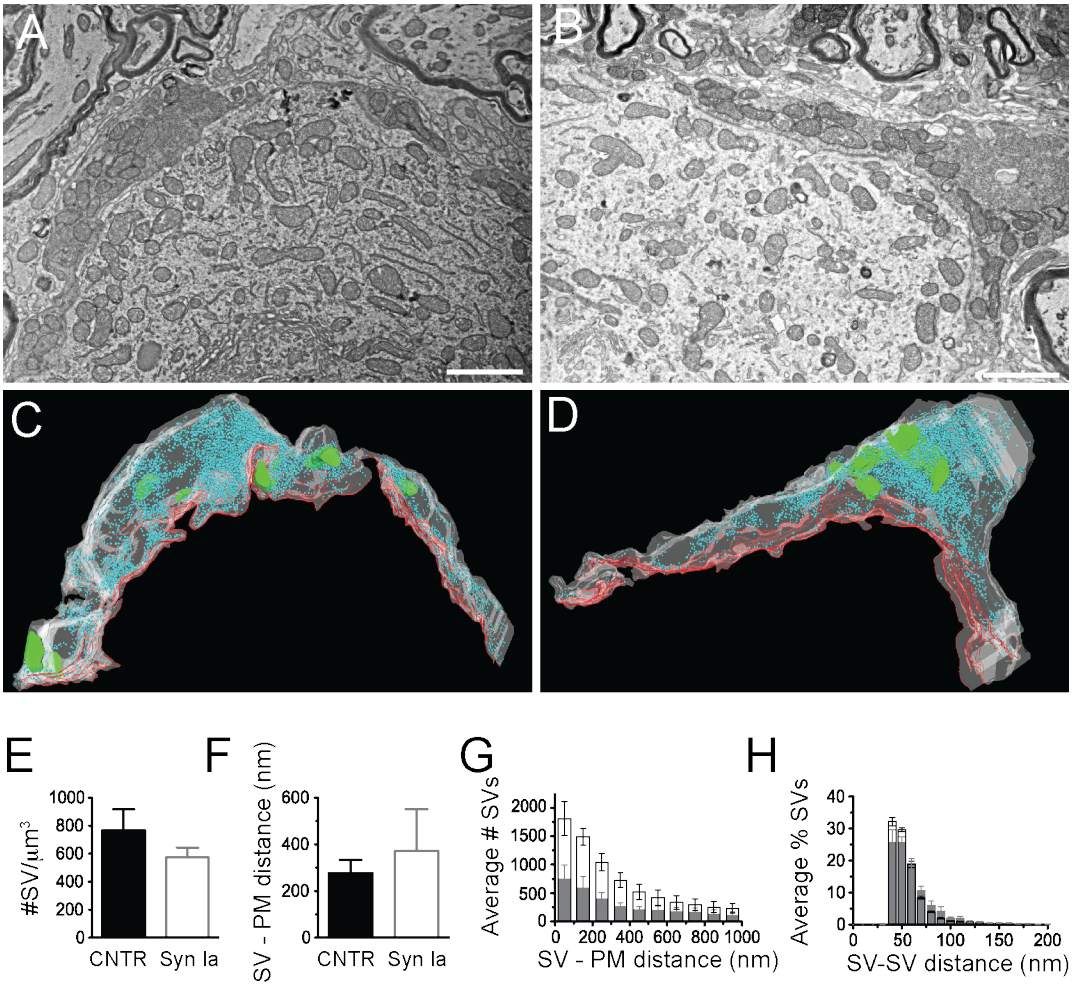

Figure 3.13: Overexpression of synapsin Ia did not lead to vesicle redistribution within the entire volume of selected calyceal segments. High magnification (10,000x) images of EGFP (A) and EGFP-synaspin Ia (B). C: 3D reconstructions of the calyceal segment shown in B. D: 3D reconstruction of the segment shown in A. SVs were presented as cyan spheres, the presynaptic membrane opposing the MNTB principal cell was shown as red line, the volume of the reconstructed segments is presented in white and was rendered transparent for clarity, parts of the postsynaptic cell engulfed by the presynaptic element were presented in green. E: SV density in the reconstructed segments. F: Median distance of SVs to the membrane. G: Histogram of the SV distribution from the presynaptic membrane opposing the principal cell. H: Histogram of the distribution of the nearest distance between neighboring SVs. Black – CNTR, gray – EGFP-synapsin Ia. N = 4 CNTR and N = 4 EGFP-synapsin Ia segments. Scale bars: 1 µm.

To assess alteration in the SV distribution pattern within the lumen of the terminal we measured the distance between the SVs and the presynaptic membrane (PM), opposing the MNTB principal cell. The average median distance was comparable between the EGFP-synapsin Ia overexpressing (371.1 ± 180.4 nm) and control (276.5 ± 57.0 nm) synapses (p = 0.9, Mann Whitney test) (Fig. 3.13 F and Table 3.4). The number of SVs decreased with increasing distance to the PM, however the overall vesicle distribution within the first 1000

nm from the PM was comparable between EGFP and EGFP-synapsin Ia overexpressing terminals (Fig. 3.13 G). Accordingly, synapsin Ia overexpression did not change the distance between two neighboring vesicles. The nearest distance between the centers of two neighboring SVs was 50.8 ± 0.5 nm in EGFP positive terminals and 54.9 ± 2.4 nm in EGFP-synapsin Ia terminals (Fig. 3.13 H and Table 3.4).

EGFP	Volume (μm^3)	SV #	SV/μm^3	PM-SV distance (nm)	SV-SV distance (nm)
Calyx-1	4.08	4171	1022.30	168.20	50.38
Calyx-2	22.73	12236	538.32	420.56	51.51
Calyx-3	17.64	8426	477.66	204.75	51.58
Calyx-4	8.71	9001	1033.41	312.43	49.49
Average	13.29	8458.50	767.92	276.49	50.74

EGFP-syn Ia	Volume (μm^3)	SV #	SV/μm^3	PM-SV distance (nm)	SV-SV distance (nm)
Calyx-1	8.95	6547	731.51	910.25	53.73
Calyx-2	1.66	817	492.17	177.51	60.25
Calyx-3	6.70	4330	646.27	162.38	48.98
Calyx-4	8.13	3425	421.28	234.15	56.42
Average	6.36	3779.75	572.81	371.07	54.85

Table 3.4 Ultrastructural analysis of EGPF and EGFP-synapsin Ia overexpressing calyces. The data is based on the 3D reconstruction of calyceal segments.

We next examined the SV distribution in close proximity to the active zones. We identified 33 AZs in EGFP overexpressing calyces and 32 AZs in EGFP-synapsin Ia terminals and analyzed the SV distribution within an arbitrarily distance of 400 nm from the AZ selected to include most of the vesicles that are potentially associated with the AZ. Representative AZs are shown in (Fig. 3.14 A and B). We did 3D reconstructions of the AZs (Fig. 3.14 C and D) and characterized the vesicle population associated with each AZ (Fig. 3.14 E – M). The SVs in synapsin Ia overexpressing terminals were smaller in size than SVs from control terminals, thus SVs had an average diameter of 37.57 ± 0.33 nm, while the SVs in control terminals – 40.2 ± 0.38 nm ($p < 0.0001$, unpaired t-test with Welch's correction) (Fig. 3.14 E). Overexpression of synapsin Ia did not only led to decreased average size of clear core vesicles, but reduced their number as well. The clusters in control terminals contained 101.3 ± 9.2 SVs per AZ, whereas we counted only 41.7 ± 3.9 SVs per AZ after overexpresssion of synapsin Ia ($p < 0.0001$, Mann Whitney test) (Fig. 3.14 F). Alongside with the decrease in the total number of SVs, the number of docked vesicles, physically attached to the AZ, was also significantly altered. Although the coefficients of variation were large, $C_{vEGFP} = 0.96$ and $C_{vEGFP\text{-}synapsinIa} = 1.86$, we counted 1.7 ± 0.3 docked SVs per AZ in control terminals and only 0.6 ± 0.2 docked SVs per AZ in synapsin Ia overexpressing calyces (p =

0.0004, Mann Whitney test) (Fig. 3.14 G). We next estimated the surface area of the AZ by multiplying their total length by the thickness of the slice. AZs from synapsin Ia overexpressing calyces had smaller surface area compared to controls – 0.069 ± 0.006 μm^2 versus 0.124 ± 0.012 μm^2 ($p < 0.0001$, Mann Whitney test) (Fig. 3.14 H). Overexpression of synapsin Ia led to a 33 % reduction in the density of SVs in the cluster. The average SV density was 884.4 ± 60.7 SVs/μm^2 in EGFP and 596.3 ± 45.1 SVs/μm^2 in synapsin Ia case ($p = 0.0009$, Mann Whitney test) (Fig. 3.14 I). However, the average density of docked SVs remained unaltered and had values of 14.1 ± 2.3 docked SVs/μm^2 in EGFP and 9.8 ± 3.8 docked SVs/μm^2 in synapsin Ia overexpressing calyces ($p = 0.33$). In control terminals we found larger AZs with bigger SV clusters than smaller AZs, while the size of the AZ did not influence much the number of SVs in case of synapsin Ia overexpression (Fig. 3.14 J). Additionally, the distance between two neighboring SVs was shifted from 53.16 ± 0.87 nm in EGFP overexpressing synapses to 59.98 ± 1.56 nm in synapsin Ia positive terminals ($p = 0.0002$, Mann Whitney test) (Fig. 3.14 K), reflecting the decreased vesicle density induced by synapsin Ia overexpression.

When the SV distribution within the cluster was examined, SVs were found at all distances from the AZ, albeit less in number ($p < 0.0001$, two-way ANOVA) (Fig. 3.14 L and M), reflecting a decreased SV density within the clusters of synapsin Ia overexpressing calyces. The cumulative distribution was fitted in both cases by an exponential function (Fig.3.14 M), showing that the total number of SVs grew with increasing distances from the AZ.

The EM analysis showed that overexpression of synapsin Ia in the calyx of Held led to structural reorganization of the SV clusters associated with AZs. Both the size of AZs and the SV density in close proximity to the release sites were significantly decreased and the remaining SVs had smaller diameter. Therefore, synapsin Ia might control both the number and size of SVs at the active zone. However, the total SV number within the entire bulk volume of the presynaptic terminal remained the same as in control terminals.

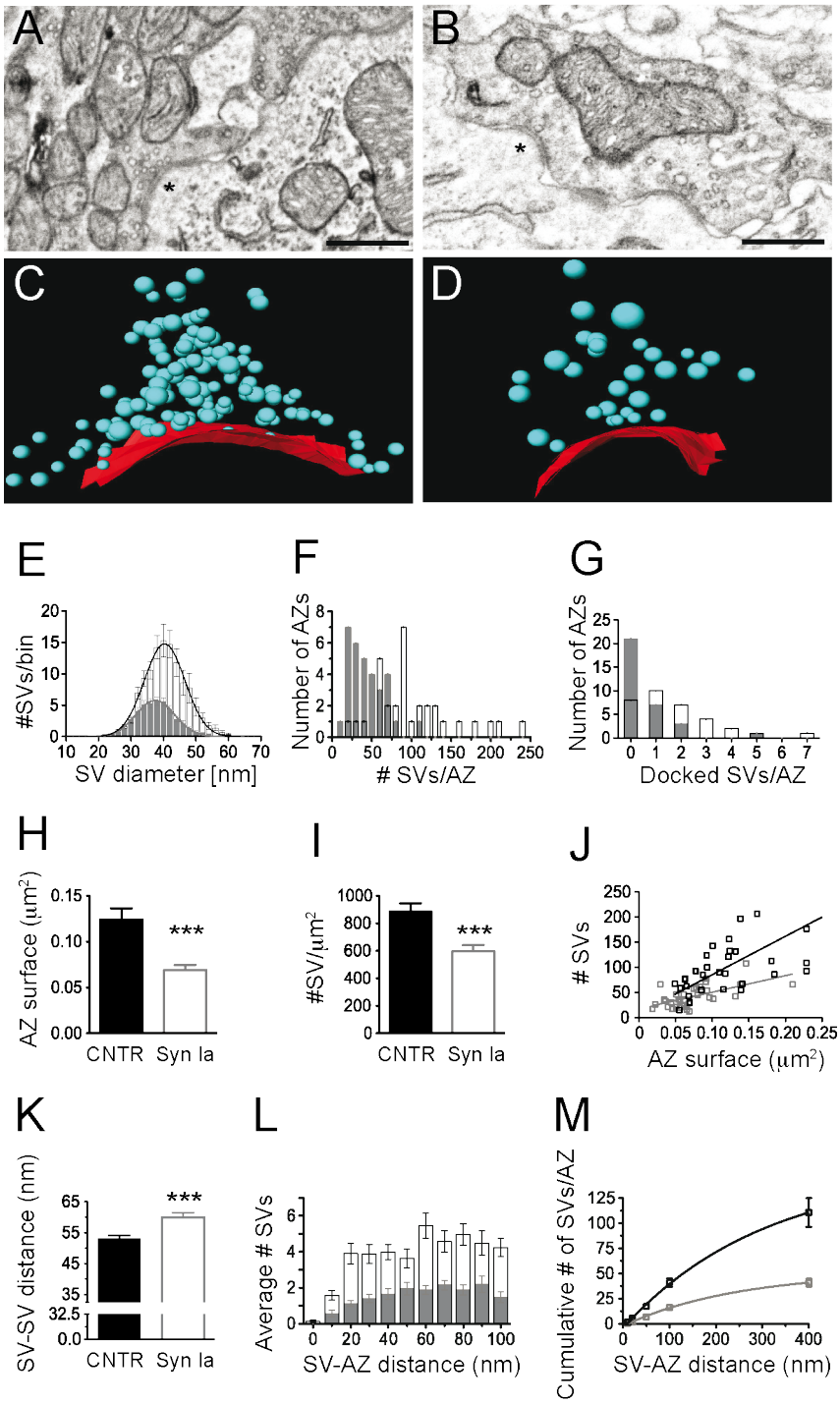

Figure 3.14: Overexpression of synapsin Ia resulted in decreased vesicle number in close proximity to the active zone – analysis of the proximal SV cluster. A: Two AZs from a calyx overexpressing EGFP. B: Two AZs from a calyx overexpressing EGFP-synapsin Ia. C: 3D reconstruction of the AZ, pointed out with * in A. D: 3D reconstruction of the AZ pointed out with * in B. SVs were presented as cyan spheres, the surface of the AZ was presented in red. E: Histogram of the distribution of the SV diameter. F: Number of SVs per AZ. G: Number of docked SVs per AZ. H: AZ surface area was decreased by the overexpression of synapsin Ia. I: Density of the SVs within the cluster associated with AZs is reduced upon overexpression of synapsin Ia. J: Number of SVs plotted versus the surface area of the AZ. K: Increased median distance between neighboring SVs upon synapsin Ia overexpression. L: Histogram of the SV distribution within the first 100 nm from the AZ. M: Cumulative distribution of SVs within 400 nm from the AZ. Black – GFP, gray – EGFP-synapsin Ia. Scale bars: 200 nm. (***) for $p < 0.001$.

3.1.10. Summary – overexpression of synapsin I isoforms leads to structural redistribution at the active zone, which underlies increased short-term depression at the calyx of Held synapse

At p 16, shortly after the hearing onset, synapsins Ia, Ib, IIb and IIIa were present in the calyx of Held, while the IIa isoform was not detectable via immunohistochemistry. We overexpressed either synapsin Ia or synapsin Ib in the calyx of Held via recombinant adeno-associated virus – mediated gene transfer in order to study isoform-specific functions. Both isoforms were properly targeted to the presynaptic terminal and co-localized with SVs regardless of their structural differences and differential dimerization properties (Gitler et al., 2004b). Although, the size and the overall morphology of the perturbed calyces remained unaltered, overexpression of synapsin I isoforms resulted in a redistribution of SV within the presynaptic terminal as shown by 3D immunohistochemistry and volume analysis. Ultrastructural analysis of synapsin Ia overexpressing calyces revealed that the total number of SV within the synapse remained unchanged, while the vesicle density in close proximity to the active zones was decreased. Additionally, the size of the AZs was decreased and they harbored vesicles with smaller diameter.

The SVs that remained in the cluster proximal to the AZ proved to be sufficient to maintain intact basal synaptic transmission. Therefore, synapsin I isoforms do not control the properties of spontaneous and evoked EPSCs. The redistribution of SVs underpins impaired SV recruitment to the AZs and hence affects transmission during high-frequency stimulation trains. Overexpression of both synapsin Ia and Ib resulted in accelerated short-term depression at stimulation frequencies exceeding 10 Hz and faster recovery from depression after strong depressing stimuli. Both synapsin I isoforms introduced a fast component of recovery, which was absent from the control terminals. We could show that synapsin I isoforms function on two different time scales to maintain the refilling of the RRP. During a high-frequency train SVs are fed into the RRP at slower rate upon overexpression of synapsin Ia/Ib, whereas at rest overexpression aided recovery. Although both isoforms showed impact on the analyzed forms of synaptic plasticity, the effect of overexpression of synapsin Ia was be stronger than that of synapsin Ib. However, the overexpression of synapsin I isoforms resulted in a mild functional phenotype, not occluding basal release process. Our data strongly indicates that the amount of synapsin I expressed in the calyx does not regulate neurotransmission *per se* but fine tunes the rate and extent of short-term synaptic plasticity via maintaining the size of the SV cluster.

3.2. Structure – function relationship at the calyx of Held in TKO mice

After having established the phenotype of synapsin I isoforms overexpression in the rat calyx of Held, we analyzed the structural and functional consequences of deleting all three synapsin genes. For the purpose we used triple knock-out mice (TKO), previously generated by crossing single knock-outs (Gitler et al., 2004a).

3.2.1. Distribution of endogenous synapsin isoforms in the mouse MNTB

To exclude differences between rats and mice in the expression pattern of synapsin genes, we analyzed the distribution of synapsin isoforms in the MNTB of p 17 mice (Fig. 3.15). We used antibodies against pan-synapsin I (Fig. 3.15 A and B), pan-synapsin II (Fig. 3.15 C and D) and synapsin IIIa (Fig. 3.15 E and F) to probe which genes are expressed in WT mice. We could show that all three genes are expressed in and outside the MNTB (overview images). As expected, synapsin stain colocalized with vGluT1 signal within the MNTB. The immunosignal was distributed in the typical for the calyx of Held oval shape (magnified images) and was similar to the already described staining pattern of synapsins in the rat. Within the presynaptic terminal the two SV markers also co-localized. Similar to the rat MNTB, synapsin positive spots were found on the surface of the principal cell, which did not contain vGluT1, representing non-calyceal synapses on the esurface of the MNTB principal cell. As shown in the rat calyx of Held (Fig. 3.1 E), synapsin IIIa was also present in the mouse (Fig. 3.15 F). It might be possible that synapsin IIIa is expressed only within the boundaries of the calyx of Held, because we did not detect any deviations from the vGluT1 pattern, in contrast to the synapsin I and II positive synapses outside the calyx. Therefore, we could conclude that all the major synapsin isoforms present in the rat are also expressed in the mouse calyx and that their deletion has the potential to cause severe impairments in synapse formation and neurotransmission.

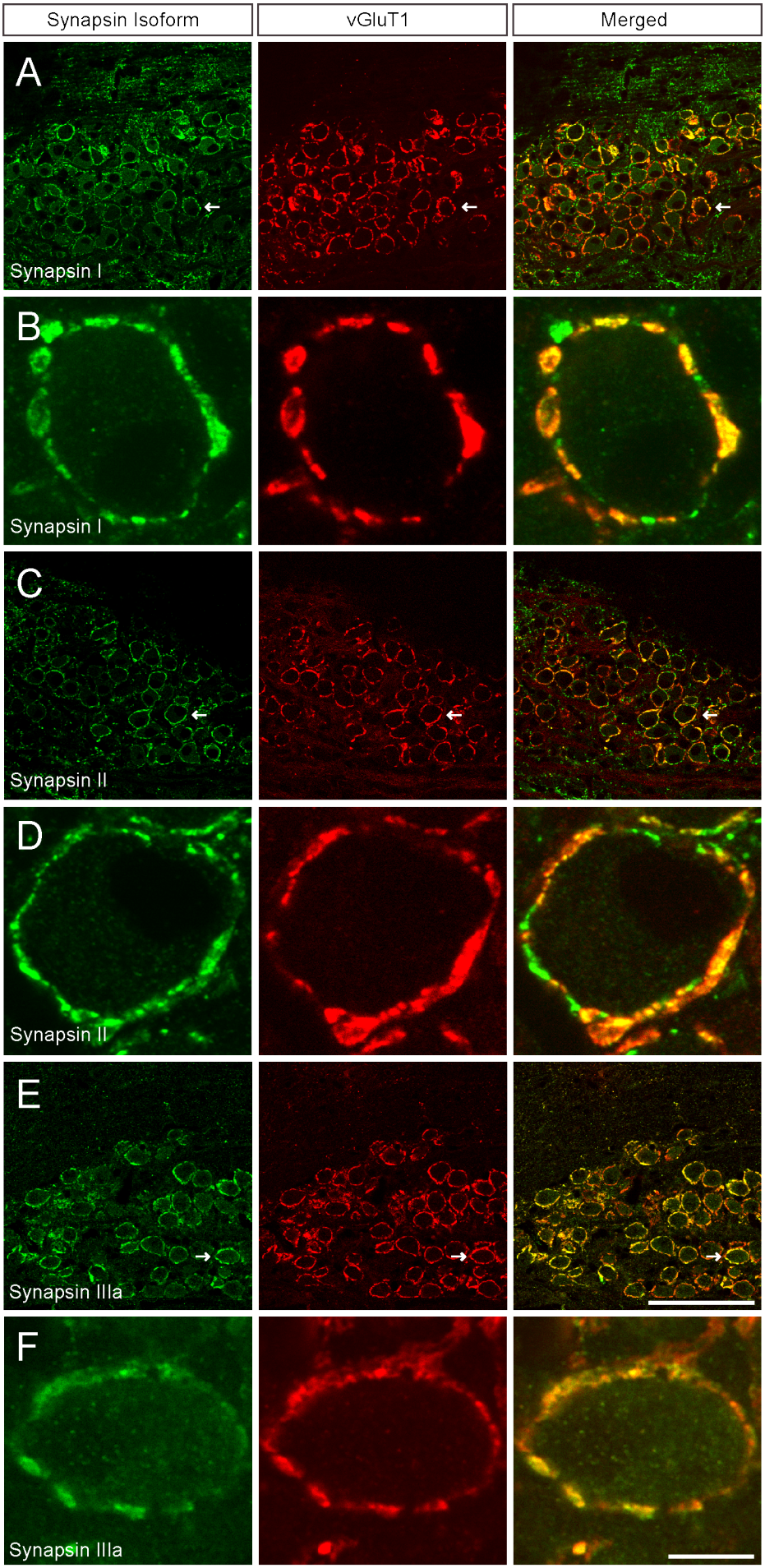
Synapsin Isoform
vGluT1
Merged
A
Synapsin I
B
Synapsin I
C
Synapsin II
D
Synapsin II
E
Synapsin IIIa
F
Synapsin IIIa

Figure 3.15: Products of all three synapsin genes are present in the mouse MNTB at p 17. MNTB of a WT mouse stained with pan-synapsin I (A), pan-synapsin II (C), synapsin IIIa (E) (left panel) and vGluT1 (central panel) antibodies. High-resolution confocal images showing single optical sections of the calyces pointed out by white arrows are presented in B (pan-synapsin I), D (pan-synapsin II) and F (synapsin IIIa) (left panel). These images illustrate the high degree of co-localization of synapsins and vGluT1 (right panel) within the calyx of Held. Scale bars: A, C and E: 100 μm, B, D and F: 10 μm.

3.2.2. Deletion of synapsin genes results in downregulation of SV associated proteins

The classical hypothesis of synapsin function at nervous terminals argues that synapsins immobilize SVs within the presynaptic terminals and hence a dramatic decrease in the level of SV proteins in preparations from diverse synapsin knockout mice was found (Gitler et al., 2004a; Rosahl et al., 1995). Here we performed ELISA from whole brain lysates from TKO mice in order to measure the level of synapse-associated proteins (Table 3.5). We analyzed three different groups of proteins: (1) SV-associated proteins, (2) other presynaptic proteins, which are mostly localized to the AZ and (3) postsynaptic components and compared their levels between TKO and WT mice. Synapsin concentration was probed with a pan antibody detecting both synapsin I and II. As expected, synapsin I and II were not detectable in the lysates from TKO brains. The levels of all SV proteins were reduced (on average to 61 ± 11 %) while non-vesicular presynaptic proteins and postsynaptic proteins remained unchanged (101 ± 10 % and 95 ± 10 %, respectively, Table 3.5), in agreement with (Gitler et al., 2004a; Rosahl et al., 1995). Synaptophysin was the most downregulated protein in the TKO lysates, remaining only 38.4 ± 20.3 % after gene deletion. The level of glutamate transporters was also significantly reduced in TKO relative to WT. The vGluT1 concentration in lysates of TKO mice was reduced to 53.4 ± 10.3 % and that of vGluT2 – to 60.7 ± 4.0%. Other SV associated proteins included in the analysis were the vSNARE synaptobrevin 2, the Ca^{2+} sensor synaptotagmin 1 and GTP-binding protein Rab3a (Table 3.5). The level of t-SNAREs (SNAP-25, syntaxin 1B) and AZ components (Bassoon and Munc 13-1) remained unaltered in TKOs compared to WTs. The levels of postsynaptic proteins such as neuroligin 2, NMDAR1, gephyrin and arc also remained intact in TKO lysates. The observation that both pre- and postsynaptic membrane proteins were unchanged is consistent with an unaltered total number of synapses. The selective reduction of SV proteins may have two, not necessarily mutually exclusive, explanations: neurons lacking synapsins produce either a reduced amount of SV proteins while maintaining the number of SVs or they generate fewer SVs each containing a normal complement of SV proteins. In the former case SVs would contain less copies of the respective proteins, leading to improper SV cycles. In the latter case, the

presynaptic terminals would contain decreased number of vesicles, which have a normal protein set (Takamori et al., 2006).

Protein	Category	WT	TKO
Synapsin 1/2	SV	100.0 ± 4.3%	-0.8 ± 2.4%
vGluT1	SV	100.0 ± 11.9%	53.4 ± 10.3%
vGluT2	SV	100.0 ± 6.7%	60.7 ± 4.0%
Synaptobrevin 2	SV	100.0 ± 7.9%	57.3 ± 8.3%
Synaptophysin	SV	100.0 ± 4.7%	38.4 ± 20.3%
Synaptotagmin 1	SV	100.0 ± 7.2%	78.3 ± 2.6%
Rab 3a	SV	100.0 ± 11.9%	76.1 ± 5.1%
Average	SV	100.0 ± 9.8%	60.7 ± 11.3%
SNAP-25	Presynaptic	100.0 ± 11.9%	105.0 ± 0.9%
Syntaxin 1B	Presynaptic	100.0 ± 3.8%	104.1 ± 6.9%
Bassoon	Presynaptic	100.0 ± 12.1 %	107.7 ± 17.7%
Munc13-1	Presynaptic	100.0 ± 7.5%	88.2 ± 4.1%
Average	Presynaptic	100.0 ± 9.5%	101.3 ± 9.7%
Neuroligin 2	Postsynaptic	100.0 ± 15.4%	92.3 ± 13.3%
NMDA R1	Postsynaptic	100.0 ± 3.4%	94.1 ± 14.4%
Gephyrin	Postsynaptic	100.0 ± 7.2%	103 ± 6.6%
Arc	Postsynaptic	100.0 ± 6.9%	91.7 ± 5.1%
Average	Postsynaptic	100 ± 9.3%	95.3 ± 10.7%

Table 3.5 ELISA measurements showed a selective reduction in the level of vesicle-associated presynaptic proteins in TKO relative to WT.

3.2.3. Deletion of synapsin results in decreased levels of vGluT1 immunofluorescence within the calyx of Held

After showing that the deletion of synapsin genes leads to a global downregulation of SV-associated proteins, we assessed the level of two presynaptic proteins within the calyx of Held via immunohistochemistry. We stained mGFP-labeled terminals with vGluT1 and bassoon (Fig. 3.16) and studied their localization pattern within the boundaries of the presynaptic terminal. Calyces within the entire MNTB and their incoming axons were labeled by the expression of mGFP (Fig. 3.16 A and C, right panels). The axons cross the midline and innervate principal cells in the contralateral MNTB in both WT and TKO animals. Overview images taken from coronal brain stem sections (Fig. 3.16 A and C) show dense expression of vGluT1 and bassoon as well a large number of calyces labeled with mGFP in both WT and TKO mice. Single optical frames of the calyces highlighted in the overview panels, obtained at maximal confocal resolution (Fig. 3.16 B and D), suggest that vGluT1 and bassoon co-localize within the presynaptic terminals of both WT and TKO mice. For clarity the mGFP is

presented as an outline of the membrane in the merged images. Similar to what has been reported in the rat calyx of Held (Dondzillo et al., 2010), the bassoon immunosignal was preferentially restricted to areas closer to the membrane apposed to the postsynaptic principal cell while vGluT1 showed a more wide spread distribution within the calyx volume including regions with differential SV density (Fig.3.16 B and D).

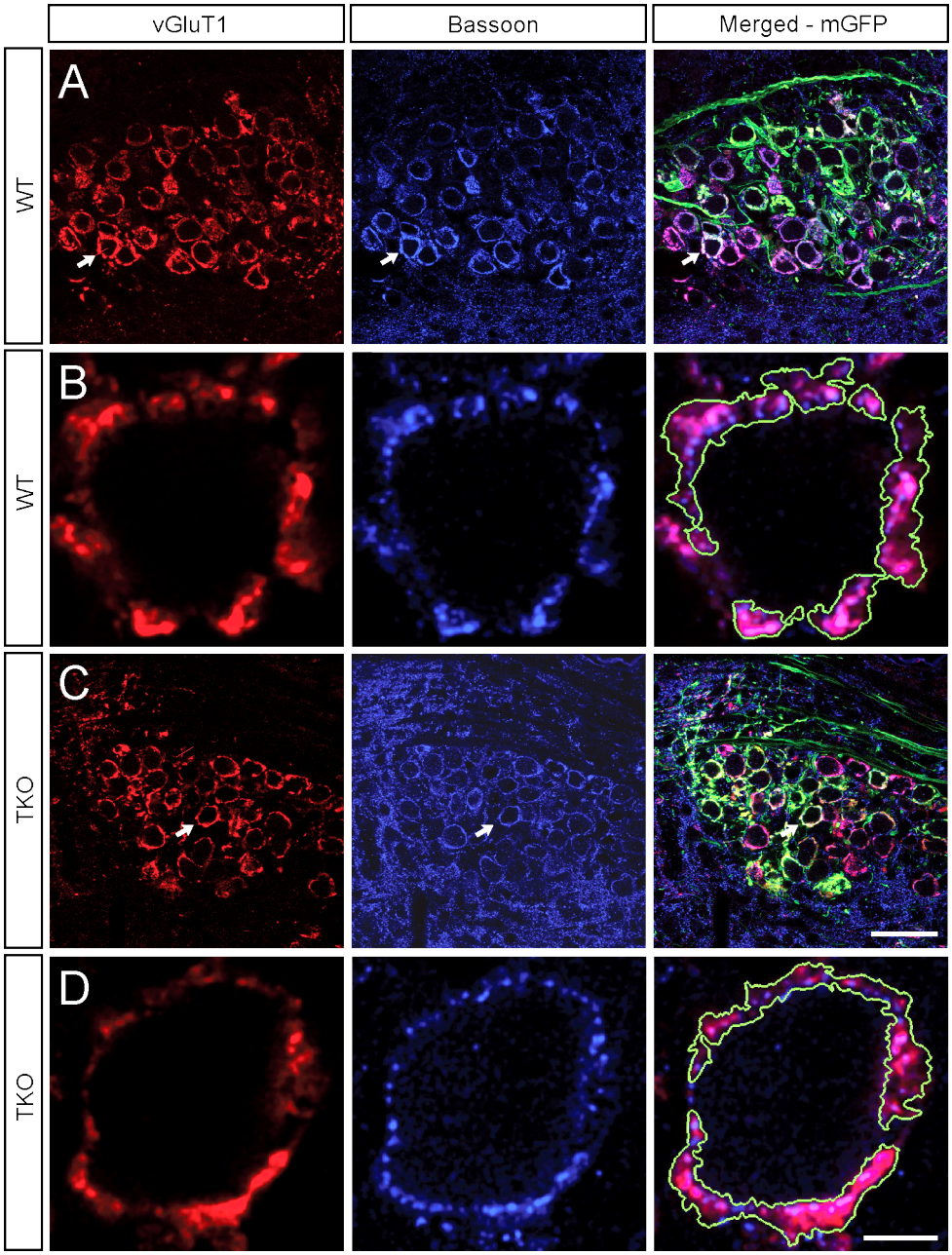

Figure 3.16: vGluT1 and Bassoon are expressed in both WT and TKO calyces, pre-labeled with mGFP. A: MNTB of a WT mouse stained against vGluT1 (left panel) and bassoon (central panel). Merged image (right panel) represents an overlay of overexpressed mGFP (green) and the two antibody stains. Images represent a projection of z-stacks consisting of 5 optical frames. B: Single optical section of the mGFP prelabeled calyx, pointed out in A (white arrow). The mGFP is depicted as the green outline of the calyx in the merged image. The vGluT1 stain resulted in extensive but inhomogeneous staining of SVs within the calyx. Bassoon staining resulted in multiple puncta close to the presynaptic membrane, which overlap with the vGluT signal. C: MNTB of a TKO mouse. D: single optical section of the calyx pointed out in C. Scale bars: A and C 50 µm; B and D 5 µm.

To quantify the expression level of the vGluT1 (Fig. 3.17 A and B, left panels) and bassoon (central panels) we did 3D reconstructions of confocal data stacks acquired at maximal resolution with the same parameters. The volume of the presynaptic compartment was reconstructed from the mGFP-signal (green outline, right panels), allowing us to consider only those immunosignals, which are part of the identified calyx (Dondzillo et al., 2010). A cross section through an arbitrary plane together with the remaining structure behind the plane is shown to provide a better visibility of the 3D protein localization within the presynaptic terminal. The overall structure of the calyx remained unchanged in mice lacking synapsins. The mean volume of a calyx was 706 ± 49 μm^3 in WT and 657 ± 47 μm^3 in TKO ($p = 0.49$, unpaired t-test with Welch's correction), suggesting that deletion of synapsins did not affect calyx size (Fig. 3.17 C). We then determined the volume occupied by vGluT1 and bassoon within the mGFP volume. Although the vGluT1 signal was widely distributed within the volume of the reconstructed calyces its volume was significantly reduced from 514 ± 48 μm^3 in WT terminals to 388 ± 30 μm^3 in TKO synapses ($p = 0.03$, unpaired t-test with Welch's correction) (Fig. 3.17 D). The volume occupied by bassoon was similar in both genotypes, 56 ± 4.7 μm^3 in WT versus 67 ± 8.4 μm^3 in TKO ($p = 0.29$, unpaired t-test, with Welch's correction) (Fig. 3.17 E). We counted 192 ± 15 bassoon-positive clusters per calyx in control terminals and 207 ± 19 clusters per terminal in TKOs ($p = 0.53$, unpaired t-test with Welch's corerction) (Fig. 3.17 F). Due to the variability in the size of calyceal terminals we calculated the fraction of the presynaptic volume occupied by the two proteins. The presynaptic volume occupied by vGluT1, i.e. by SVs (Fig. 3.17 G), was significantly decreased by approximately 17%, from 0.72 ± 0.03 in WT to 0.6 ± 0.04 in TKO ($p = 0.02$, unpaired t-test with Welch's correction). The volume taken up by the bassoon clusters was smaller than the volume occupied by vGlutT1, consistent with the more restricted distribution of bassoon. Additionally, the fraction of the presynaptic volume occupied by bassoon was unchanged in TKOs (0.1 ± 0.01 in WT and 0.09 ± 0.01 in TKO, $p = 0.58$, unpaired t-test with Welch's correction) (Fig. 3.17 H). These results demonstrate that the deletion of all three synapsin genes does not lead to alterations in the size of the calyx and number of bassoon-positive active zones. The genetic deletion selectively led to lower level of vGluT1 immunofluorescence within the calyx of Held, suggesting a reduction in the total number of SVs or in the number of vGluT1 molecules per SV. Although we did not observe change in the vGluT1 level within the innervating axons in the TKO mice, we cannot exclude that the SVs redistribute from the terminal back into the axon as reported in hippocampal cultures (Orenbuch et al., 2012a).

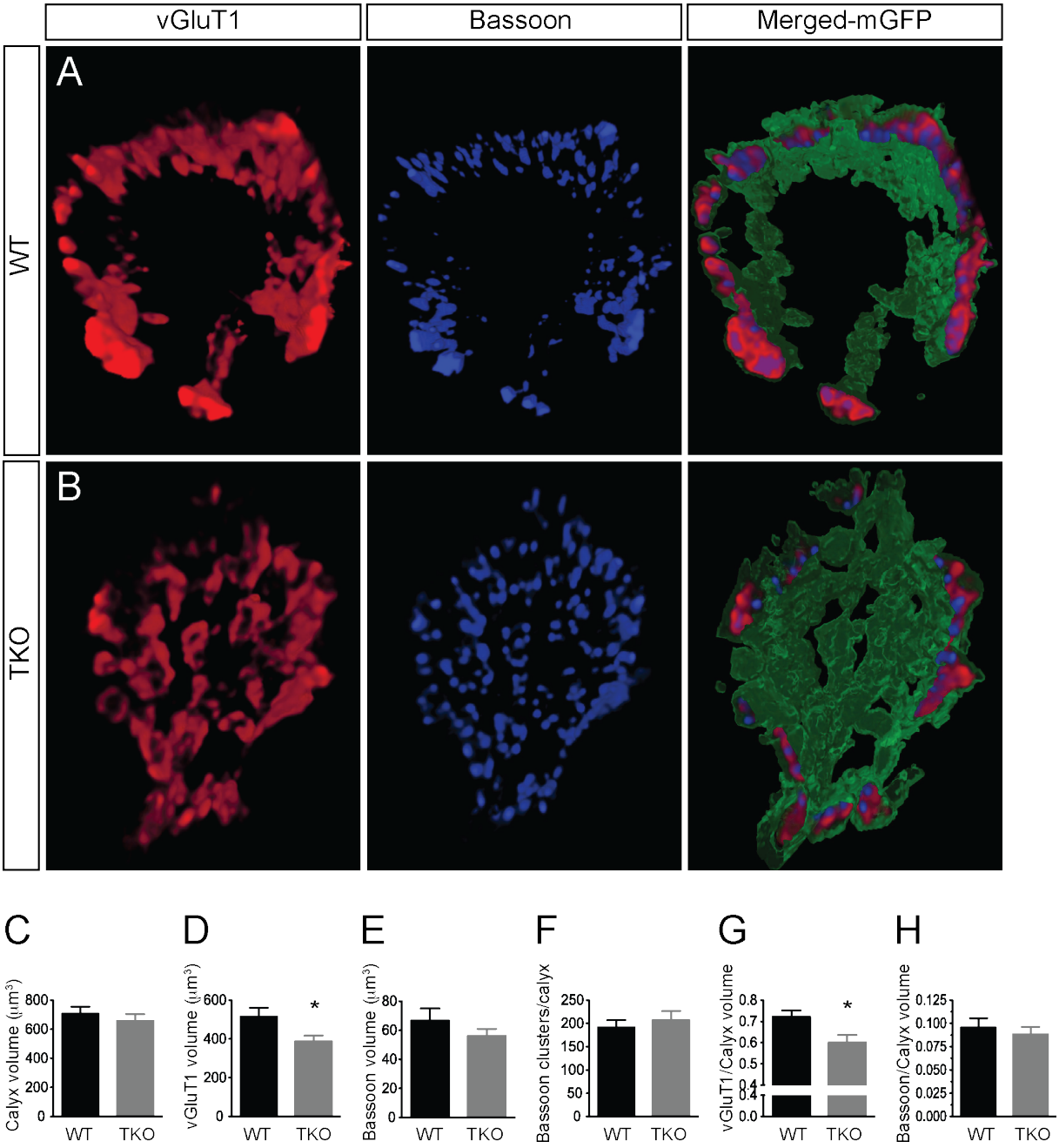

Figure 3.17: Synapsin deletion led to a decrease in the level of the vesicle associated protein vGluT1, but spared the levels of AZ marker bassoon. 3D reconstruction of WT (A) and TKO (B) calyx, stained for vGluT1 (left panel), bassoon (central panel) and labeled with mGFP (green outline in the right panel). An arbitrary plane was selected and a cross-section through the 3D structure at this plane is presented together with the remaining structure behind the plane. C: Calyx volume extracted from the mGFP pre-labeling. Presynaptic volume occupied by vGluT1 (D) and bassoon (E) signal. F: Number of bassoon positive clusters per presynaptic terminal. G: Ratio between the volume occupied by vGluT1 stain (red) and the calyceal volume (green). H: Ratio between the volume occupied by the bassoon stain (blue) and volume of the presynaptic protein (green). N = 14 WT and 14 TKO synapses. WT – black, TKO – gray, data is presented as mean ± s.e.m., (*) for $p < 0.05$.

3.2.4. Electron microscopy revealed decreased number of SVs within the bulk volume of the TKO calyx of Held

The huge size of the calyx of Held allows precise examination of the structural organization and localization of SVs within the terminal. We performed serial sectioning scanning electron microscopy on selected terminals at p 17 from TKO and control mice to reveal the distribution of SVs and their spatial relationship to other structural components of the presynaptic apparatus (Figure 3.18). At this age the calyx is close to its adult morphology, characterized by extended digits and numerous bouton-like swellings, containing multiple AZs with associated SVs clusters and mitochondria (Grande and Wang, 2011; Kandler and Friauf, 1993; Wimmer et al., 2006).

We analyzed five segments randomly chosen from calyces of three WT mice and five segments taken from two TKO mice. In total we reconstructed a volume of 35.9 μm^3 from 5 control calyces and 33.4 μm^3 from 5 TKO calyces. Representative sections of WT and TKO calyceal segments containing elongated presynaptic fenestrations are shown in Figure 3.18 A and C, respectively (presynaptic elements shown in yellow) and quantitative results of all analyzed segments are listed in Table 3.6. Similarly to the synapsin Ia overexpression experiment, the calyceal segments here were manually reconstructed via segmenting the presynaptic compartment in each section and three-dimensional models were generated through 3D alignment of the consecutive sections (c.f. Materials and Methods) and the number of synaptic vesicles (cyan spheres) within the presynaptic compartments was counted (Fig. 3.18 B and D). The average median thickness of the reconstructed segments, i.e. the distance between the presynaptic membrane opposing the principal cell and the backside of the terminals, was 746.2 ± 132.6 nm in WT and 619.8 ± 60.8 nm in TKO with maximum of 1703 ± 231 nm in WT and 1861 ± 505 nm in TKO. The average volume of a segment was 7.2 ± 1.1 μm^3 in WT and 6.7 ± 1.3 μm^3 in TKO. A significant reduction in the number of SVs within the reconstructed segments was detected in the knock out terminals. The average vesicle number per calyceal segment in WT mice was 6517 ± 447 SVs, while in TKO mice we could count only 3260 ± 877 SVs per segment. This resulted in an average density of 981 ± 148 SV/μm^3 in WT calyces, but only of 476 ± 94 SV/μm^3 in TKO calyces ($p = 0.03$, Mann Whitney test), suggesting that the mean SV density in TKO calyces was reduced to half of that found in WT calyces (Fig. 3.18 E). This allowed us to make an extrapolation of the total number of SVs within the entire presynaptic terminal. We showed via mGFP labeling of the presynaptic membrane (Fig. 3.17 C) that a WT type calyx has a volume of 706 ± 49 μm^3, resulting in 692,586 ± 7,252 SVs, while a TKO terminal with volume of 657 ± 47 μm^3

contains 312,732 ± 4,418 SVs, similar to what we showed above for the rat calyx of Held. To assess if also the geometrical distribution of SVs differed in the two genotypes we determined the median distance between SVs and the presynaptic plasma membrane facing the principal cell (red line in Fig. 3.18 B and D). We could locate SVs within the entire presynaptic compartment and the measured median distance to the front membrane was 220.8 ± 37.4 nm in WT and 158.1 ± 16.2 nm in TKO terminals ($p = 0.2$, Mann Whitney test) (Fig. 3.18 F). When the SV distribution within 1000 nm from the presynaptic membrane opposing the MNTB principal cell was analyzed in detail (Fig. 3.18 G and H) we could show that the number of SVs away from the presynaptic membrane was selectively reduced ($p < 0.0001$, two way ANOVA). As expected, there was a strong reduction of SV number within 100 nm from the contact surface in TKO calyces ($p < 0.0001$, two-way ANOVA). However, no difference was found within the first 30 nm (Fig. 3.18 I). We could conclude that although vesicles are located within the entire volume of the presynaptic terminal, their total number decreases dramatically upon deletion of synapsins.

We next measured the 3D nearest neighbor distances between all counted SVs (Fig. 3.18 J). The median distance between two SVs in WT terminals was 48.8 ± 1.7 nm and 60.2 ± 3.2 nm in TKO calyces, corresponding to a net increase of approximately 20 % ($p = 0.03$, Mann Whitney test). The distribution of the SV-SV distances was wider and had a lower and right-shifted peak in TKO, arguing for a reduction in the number of SVs and/or a spread in the SV distribution back into the innervating axon (Orenbuch et al., 2012a). To determine the more precise localization of the SV population within the terminals we measured the distance between the SVs and the backside of the segment and calculated a ratio between the vesicle distance to the membrane opposing the principal cell and the SV distance to the backside (Fig. 3.18 K and L). SVs which are situated closer to the membrane opposing the postsynaptic side had ratio < 1.0 and SVs closer to the backside – had ratio > 1.0. Although, the general distribution did not vary between genotypes (two-way ANOVA, n.s.), there was significantly larger number of SVs with ratio ≤ 0.25 in TKO terminals (two-way ANOVA, $p < 0.001$) (Fig. 3.18 K). In WT terminals 54.3 ± 3.5% of all SVs were localized closer to the front membrane, while in TKO terminals these SVs were 63.1 ± 2.8% of all SVs (Fig. 3.18 L) ($p = 0.2$, Mann Whitney test). These results are consistent with a reduced number of synaptic vesicles (Gaffield and Betz, 2007; Gitler et al., 2004a; Orenbuch et al., 2012a; Siksou et al., 2007) but not with the dispersion of SVs back into the axon (Orenbuch et al., 2012a) observed in other synapses from TKO mice.

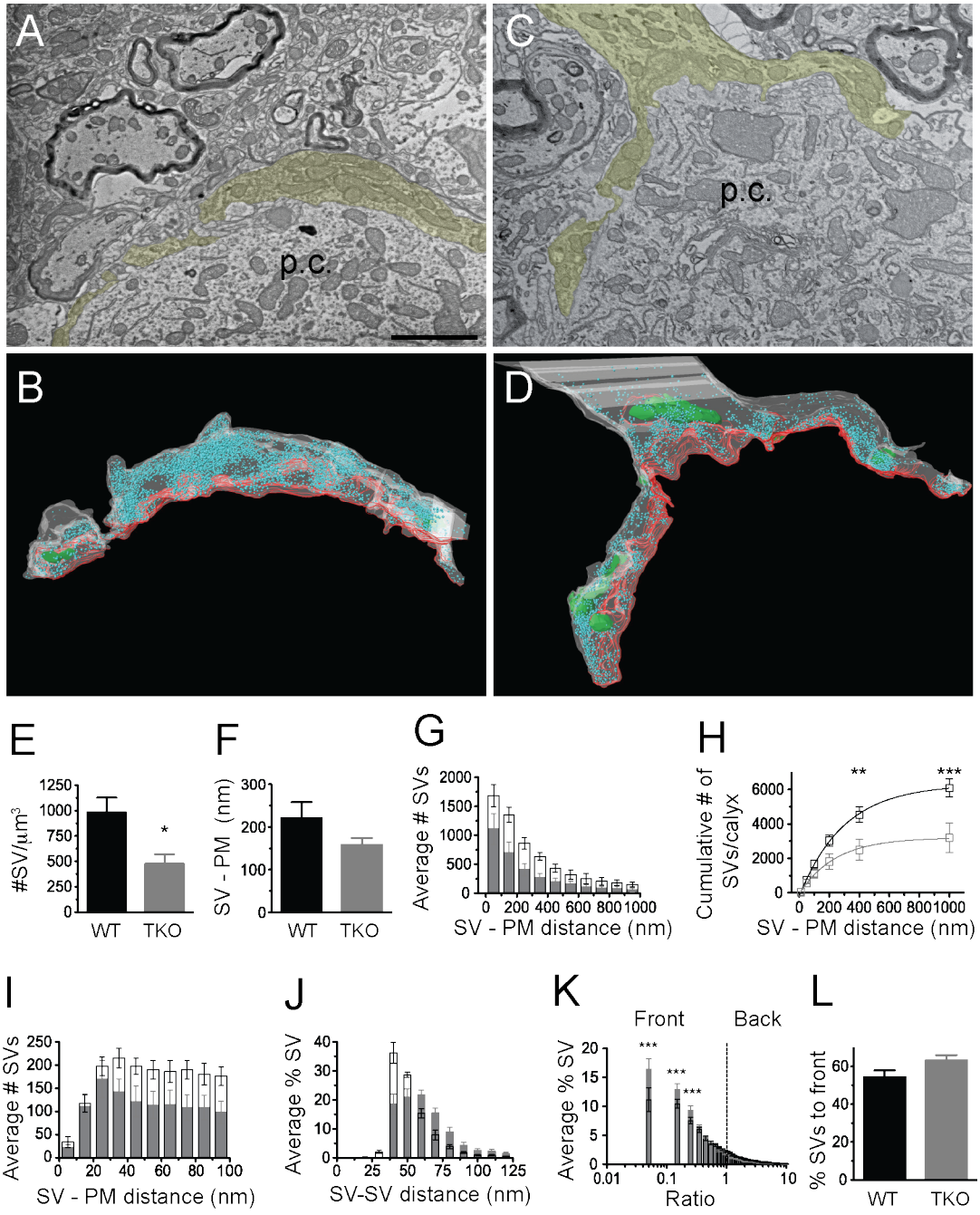

Figure 3.18: Synapsins control the vesicle number within the volume of the calyx of Held. Ultrastructural analysis of calyces of Held from WT (A-B) and TKO (C-D) mice revealed reduced number of SVs within the lumen of the presynaptic terminal. The presynaptic parts are presented in yellow for clarity. The principal cell is denoted as p.c. (A and C). B: 3D reconstruction from 26 serial sections of the WT calyceal segment shown in A. The volume of the presynaptic compartment was reconstructed from the serial sections and is presented in white and rendered transparent for clarity. SVs are shown as cyan spheres, the presynaptic membrane opposing the principal cell is outlined in red, somatic appendages of the principal cell which were engulfed within the presynaptic terminal are shown as green objects and were subtracted from the volume calculation. D: Same as B but a 3D reconstruction from 20 serial sections of the TKO calyceal segment shown in C. E: SV density calculated from the volume measurement. F: Median distance between SVs and the presynaptic membrane. G-L: Characterization of SV distribution within the entire examined segments: G: Histogram of the SV distribution within 1000 nm from the presynaptic membrane opposing the MNTB principal cell, bin size 100 nm. H: Cumulative number of SVs per calyx within 1000 nm. I: Histogram of SV distribution within the first 100 nm from the opposition membrane, bin size: 10 nm. J: Histogram of the nearest neighbor distance between two vesicles, number of SVs/bin is presented as % of the total SV number. K: Histogram of the ratio of the SV distance to the presynaptic membrane opposing the MNTB principal cell and the SV distance to the backside of

the calyx. This SV position ratio describes the position of SVs relative to the local diameter of the calyx. L: Derived from panel K, "% SVs to front" describes the percentage of total SVs located in the front half of the calyx normalized to the local diameter of the calyx. N = 5 WT calyceal segments and N = 5 TKO segments containing 40289 SVs and 16303 SVs respectively. Data is presented as mean ± s.e.m., (*) for $p < 0.05$, (**) for $p < 0.01$, (***) for $p < 0.001$. WT – black, TKO – gray. Scale bar: 2 μm.

WT	Volume (mm^3)	SV #	SV/mm^3	PM-SV distance (nm)	SV-SV distance (nm)
Calyx-1	11.16	5761	516	513.5	55.6
Calyx-2	7.28	7571	1040	320.7	46.3
Calyx-3	6.37	5746	902	329.4	47.6
Calyx-4	5.80	5855	1009	188.5	46.3
Calyx-5	5.32	7652	1439	362.8	48.1
Average	7.19	6517	981.1	343.0	48.78
s.e.m.	1.05	447	147.7	52.0	1.74

TKO	Volume (mm^3)	SV #	SV/mm^3	PM-SV distance (nm)	SV-SV distance (nm)
Calyx-1	8.27	2947	356	299.7	63.2
Calyx-2	9.49	3650	385	274.2	57.6
Calyx-3	3.10	774	250	194.0	71.3
Calyx-4	4.27	2727	638	185.4	55.6
Calyx-5	8.28	6205	749	300.3	53.1
Average	6.68	3261	475.5	250.7	60.16
s.e.m.	1.26	877	93.5	25.4	3.24

Table 3.6 Ultrastructural analysis of WT and TKO calyces of Held. The PM-SV distance and SV-SV distance are presented as mean values of the WT and TKO populations.

3.2.5. Increased AZ areas and SV diameters in calyces lacking synapsins

After having confirmed that the total number of SVs in the presynaptic terminal was decreased in TKO calyces, we examined the distribution of SVs within the clusters associated with active zones. For this purpose we identified separate AZs again based on the criteria defined in Materials and Methods. The cluster of SVs belonging to the respective AZ was marked within close proximity of the AZs. Single sections from a WT and a TKO segment, containing multiple AZs and associated mitochondria (Rowland et al., 2000) are presented in Figure 3.19 A and B respectively. Presynaptic segments are highlighted in yellow. Representative examples of single AZs together with the belonging SV clusters (boxed regions in Fig. 3.19 A and B) are shown in Fig. 3.19 C (WT) and D (TKO). In both cases a rather compact cluster containing clear core vesicles could be detected in association with the AZs. In total 71 AZ in the WT segments and 41 AZs in the TKO segments were analyzed and 3D reconstructions of each AZ and its associated SVs were generated (Fig. 3.20 A and B). SVs in TKO calyces seemed to be larger in size, so we quantified their outer diameter. The vesicle diameter distributions, containing 2849 WT SVs and 1748 TKO SVs, showed a high

variability and could be fitted by a Gaussian function (Fig. 3.20 C). The average SV diameter in WT was 38.8 ± 0.36 nm, somewhat lower than reported previously (Perkins et al., 2010; Sätzler et al., 2002; Taschenberger et al., 2002). This could potentially be due to the different experimental conditions and species used. The peak of the SV diameter distribution was shifted to the right in TKO calyces yielding an average SV diameter of 43.2 ± 0.41 nm. This diameter was significantly larger ($p < 0.001$, unpaired t-test with Welch's correction), demonstrating that calyces lacking synapsins contain larger SVs.

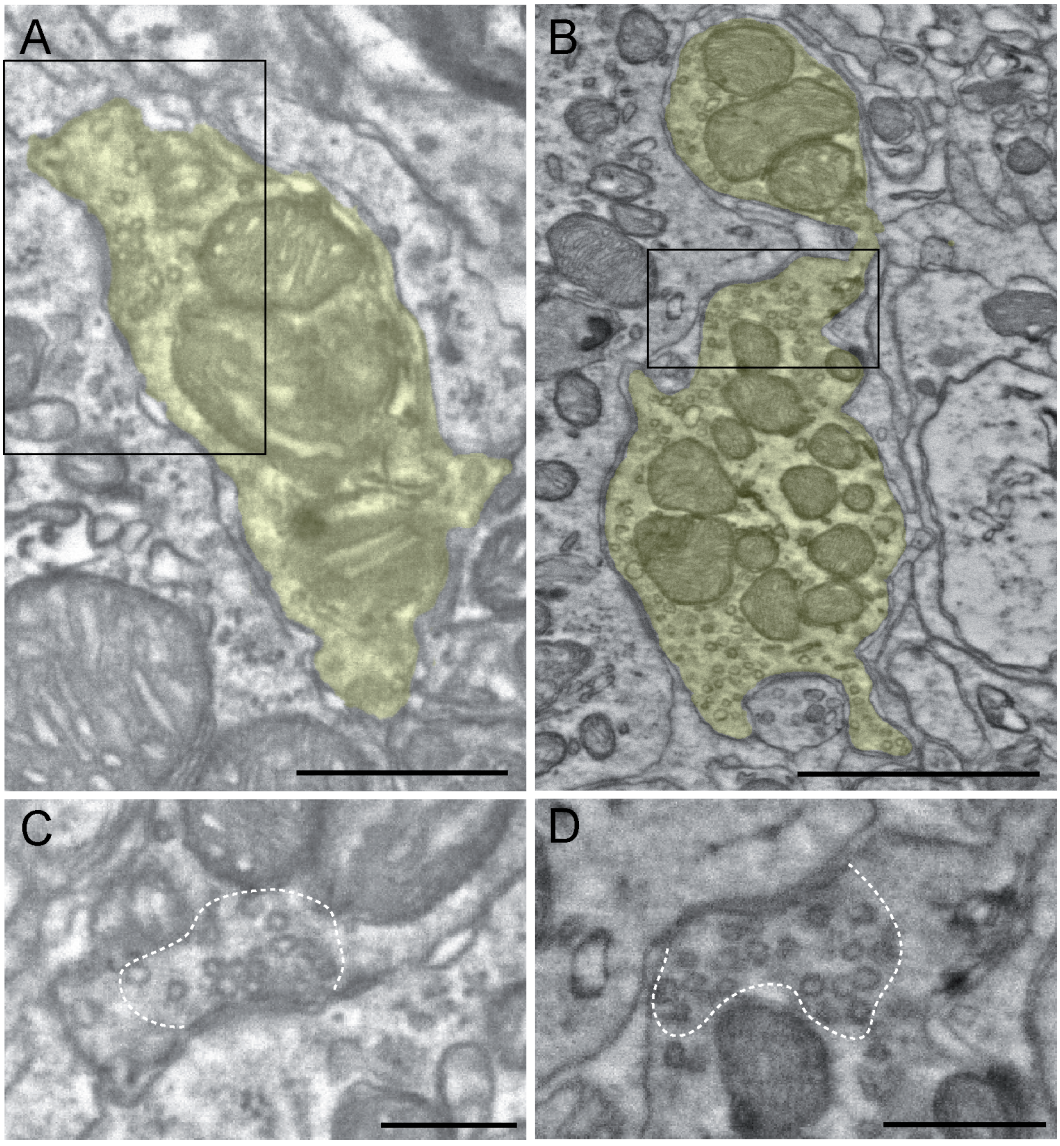

Figure 3.19: EM analysis of single active zones did not reveal any structural difference between WT and TKO calyces. A-B: Segments containing AZs and mitochondria from WT (A) and TKO (B) calyces. The presynaptic elements are shown in yellow. C-D: Magnification of the boxed regions in A and B presenting active zones with SV clusters from WT (A) and TKO (B). The SV cluster is delineated with white dotted line. Scale bars: A: 250 nm; B: 500 nm; C and D 100 nm.

We next determined the distribution pattern of SVs within a distance of 400 nm shell surrounding an AZ. We counted within this distance 38.8 ± 2.4 SVs/AZ in WT terminals and 40.4 ± 3.1 SVs/AZ in TKO calyces (Fig. 3.20 D). The number of docked SVs localized at a distance ≤ 10 nm from the AZ membrane was 0.75 ± 0.13 SVs in WT and 0.98 ± 0.19 SVs in TKO calyces with large coefficients of variation (C_{vWT} = 1.2 and C_{vTKO} = 2.1) (Fig. 3.20 E). Hence, AZs of WT and TKO calyces contain the same number of docked SVs. Because the large C_v may reflect differences in AZ size, we determined the average AZ surface area (Fig. 3.20 F). Surprisingly, the area was increased from 0.06 ± 0.004 μm^2 in WT to 0.09 ± 0.007 μm^2 in TKO, reflecting an enlargement of 50 % ($p < 0.0001$, Mann Whitney test). In calyces from both genotypes the number of SV associated with an AZ correlated with its size, with smaller AZs containing fewer SVs and larger AZ containing more SVs (Fig. 3.20 G). Due to the increase in the surface area of the AZs, the number of SVs per unit area (SVs/μm^2) was decreased by 22% in TKO terminals (Fig. 3.20 H). Thus, the density of SV within the cluster was 673 ± 37 SVs/μm^2 in WT and only 522 ± 38 SVs/μm^2 in TKO calyces ($p = 0.01$, Mann Whitney test). The reduced SV density was also reflected in the nearest neighbor distance between SVs (Fig. 3.20 I). The averaged median measured SV-SV distance was 54 ± 0.94 nm in WT and 59 ±1.41 nm in TKO ($p = 0.001$, Mann Whitney test), consistent with a lower density of SVs in TKO calyces. Hence, the absence of synapsins resulted in enlarged AZs and decreased density of associated SVs.

Based on these findings the question arises if the decreased SV density at AZs goes along with a different geometrical arrangement of the SVs. The cumulative vesicle distribution within the entire 400 nm overlapped for WT and TKOs (Fig. 3.20 J) showing that there was a similar number of SVs at all distances from the AZs in both genotypes. Within a shell of 100 nm from the AZ, SVs were also evenly distributed within the SV clusters in both WT and TKO calyces (Fig. 3.20 K). There was no reduction in the number of SVs at any distance from the AZ membrane. The average median distance between SVs and the respective AZs was similar for both genotypes and was measured to be 100.8 ± 3.3 nm in WT terminals and 105.2 ± 5.8 nm in TKO synapses.

Since synapsins are supposed to interact with SVs that are localized distally to the AZs, we analyzed the SV distribution beyond the boundaries of the vesicle cluster. For this purpose, we measured the distance between all SVs counted within the terminal and the nearest AZ (Fig. 3.20 L). There was a selective decrease in the number of SVs located distally to the AZs in TKO calyces ($p = 0.003$, two-way ANOVA). The vesicles that remain in the TKO presynaptic terminals showed very high tendency to be localzed closer to the AZ with

median distance of 1445 ± 452 nm. The determined median distance in WT controls was determined to be 2681 ± 405 nm (p = 0.06, Mann Whitney test). Hence, SVs located distally from the AZs form a synapsin-dependent pool. The integrity of the vesicle cluster proximal to the AZ is, however, not disrupted in synapsin-lacking terminals.

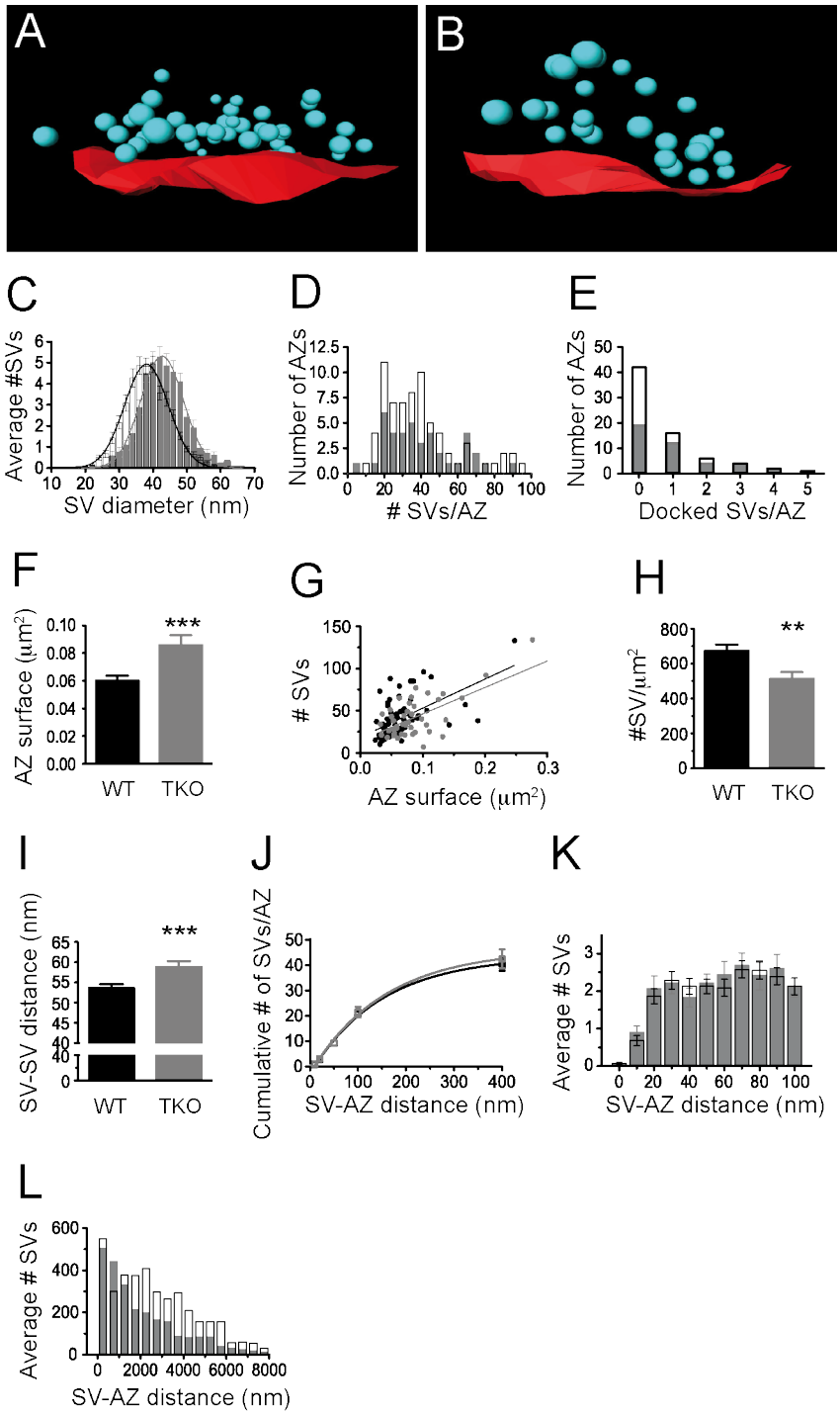

Figure 3.20: The architecture of the active zone and the associated SV cluster remains unaltered upon synapsin deletion. Three-dimensional reconstructions of the active zones and the SV cluster shown in Fig. 3.19, presenting the distances of SVs (cyan) from the active zone surface (red). A: WT active zone. B: TKO active zone. C: Gaussian distribution of the diameter of SV labeled in close proximity to the active zone. D-I: Distribution of SVs per AZ in WT and TKO calyces. D: Number of AZs plotted versus the total number of SVs in the associated cluster in WT and TKO terminals. E: Number of AZs plotted versus the number of docked SVs associated with the respective AZ. F: Increased active zone surface in TKO terminals in comparison to WT ($p < 0.0001$, Mann Whitney test). G: Correlation between AZ surface and number of associated SVs. H: Decreased

number of SVs per area of the active zone in decreased in TKO synapses (p = 0.01, Mann Whitney test). I: Increased nearest neighbor distance in TKO calyces (p = 0.001, Mann Whitney test). J-K: Vesicle distribution within 400nm from the AZ. J: Cumulative vesicle distribution within the entire 400 nm. K: Histogram of SV distribution within the first 100 nm from the AZ, bin size: 10 nm. Data is presented as mean ± s.e.m., N = 2873 WT SVs from N = 71 WT AZs, N = 1748 TKO SVs from N = 41 TKO AZs. M: Histogram of the distribution of the SVs from the nearest AZ, beyond the boundaries of the associated cluster, bin size 500 nm. Data is presented as mean for the N = 5 WT terminals containing 19072 SVs and N = 5 TKO terminals with 12322 SVs, error bars are omitted for clarity. WT – black, TKO – gray, (**) for $p < 0.01$ and (***) for $p < 0.001$.

In summary, our electronmicroscopic analysis revealed that lack of synapsins reduced the total number of SVs within the bulk volume of the presynaptic compartment without affecting the SV population in close proximity to the AZs. The distal vesicle cluster is typically associated with the resting and parts of the recycling pools of SVs and is thought to be synapsin-dependent. Although synapsin depletion did not affect SV number and distribution of the SVs associated with an AZ, an increase in AZ size resulted in a lower density of SVs associated with it. The increase in AZ size as well as in SV diameter may reflect compensatory changes that ensue to keep the synapse functional in response to synapsin depletion.

3.2.6. Synapsin deletion spares basal synaptic transmission at the calyx of Held

After showing a dramatically reduced number of SVs in TKO calyces, we examined whether the physiological properties of the mutant terminals were altered. We aimed at proving if the SVs distant to the release sites, which are reduced in number in TKO terminals, actively participate in neurotransmitter release at the calyx of Held. For this purpose we performed whole cell voltage clamp recordings from the MNTB principal cells at p 14 – p 18. Spontaneous excitatory postsynaptic currents (spEPSC) were measured for 2 min immediately after breaking in the cell (Fig. 3.21). Spontaneous fusion events could be detected in both WT and TKO terminals (Fig. 3.21 A). The spEPSC amplitude was not altered and had mean values of 50.7 ± 2.3 pA in WT and 50.9 ± 1.5 pA in TKO synapses (p = 0.77, Mann Whitney test) (Fig. 3.21 B). There was a small but significant decrease in the frequency of spEPSCs in TKO synapses (Fig. 3.21 C), which was underlined by the presence of more cells firing at low frequency in TKO than in WT. We measured 4.52 ± 0.46 Hz in WT and 3.50 ± 0.34 Hz in TKO calyces (p = 0.04, Mann Whitney test). The lower SV density at AZ from TKO calyces might underline the decreased spEPSC frequency. The kinetics of spontaneous vesicle fusion remained unchanged in TKOs, thus the distributions of the time constants in WT and TKO terminals were overlapping. The 20 – 80% rise time of spEPSC was comparable in calyces from WT and TKO mice: 161 ± 7 μs and 163 ± 8 μs, respectively (p = 0.61, Mann Whitney

test) (Fig. 3.21 D) and the decay time constants were 0.51 ± 0.01 ms and 0.52 ± 0.01 ms respectively (p = 0.08, Mann Whitney test) (Fig. 3.21 E). This led to the conclusion that synapsins do not control the size and the kinetics of quantal release.

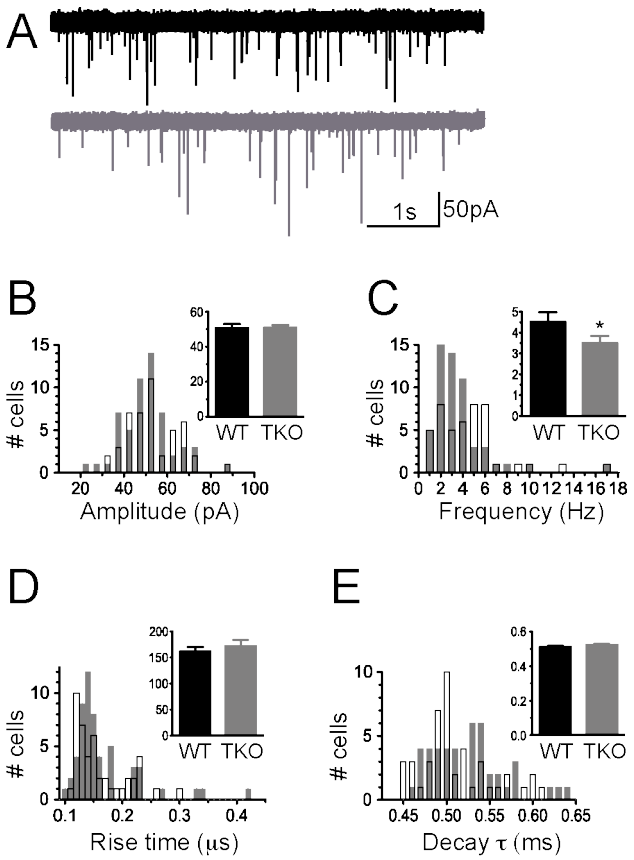

Figure 3.21: Spontaneous synaptic activity was largely unchanged in TKO mice. A: Example traces from spEPSC recordings in WT (black) and TKO (gray). B: The spEPSC amplitude was similar in WT and TKO cells. C: The frequency of spEPSCs (number of events per second) was significantly decreased in TKO terminals. Significant difference was detected neither in the decay-time constant (D), nor in the rise time (20 – 80% of peak amplitude) of spEPSCs (E). N = 45 WT and 55 TKO cells. Histograms represent the distribution of the entire data set. The insets depict mean ± s.e.m. of the distribution, (*) for p < 0.05. WT – black, TKO – gray.

Isolated stimuli were applied at the midline to evoke an action potential in the calyx of Held. The response of the postsynaptic cell was measured and analyzed. The shape of the evoked excitatory postsynaptic currents (eEPSCs) was not altered by deletion of synapsin genes (Fig. 3.22 A). To compensate for the saturation of the amplifier at large current amplitudes in some cells, evoked responses of 9 WT and 12 TKO cells were recorded at various holding potentials between -80 mV and +60 mV (Fig. 3.22 B). Due to the linear current-voltage relation the eEPSC amplitudes could be scaled when necessary to a reference holding potential of -70 mV, yielding mean eEPSC sizes of 18.6 ± 1.2 nA in WT and 20.2 ± 1.4 nA in TKO synapses (p = 0.93, Mann Whitney test) (Fig. 3.22 C). The quantal content, calculated as the number of quanta released per AP, was not altered and had values of 339 ± 30 and 406 ± 32 SVs in WT and TKO synapses (p = 0.21, Mann Whitney test), respectively (Fig. 3.22 D). Hence, evoked amplitudes and quantal content are not affected by synapsin deletion.

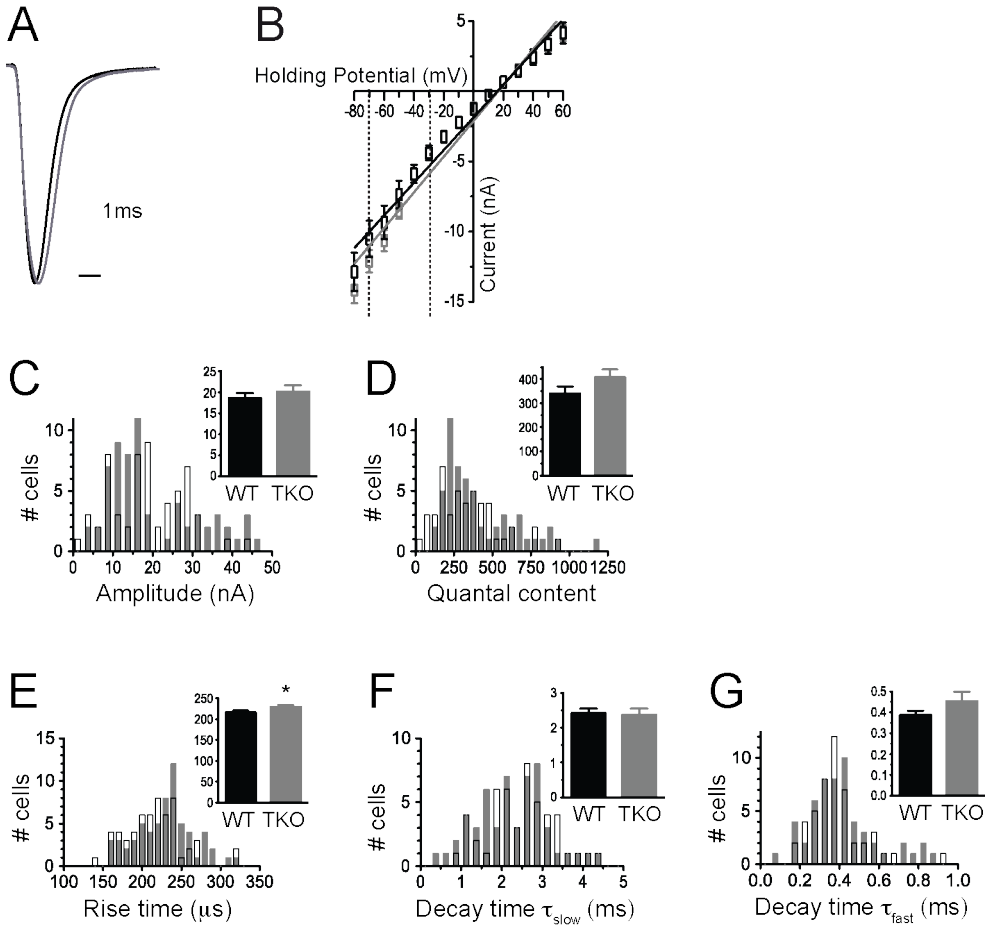

Figure 3.22: Synapsin deletion slows down the rise time of evoked EPSCs, leaving the other EPSC properties intact. A: Excitatory postsynaptic events (eEPSCs) were evoked in response to presynaptic action potentials. B: Linear I/V relationship for WT and TKO terminals, used to calculate the size of eEPSC recorded at V_h = -30 mV. The reference range is between the dotted lines. C: Difference in the size of eEPSCs was not detected (N = 59 WT and 64 TKO synapses). D: Quantal content was determined per cell by dividing the sEPSC amplitude by the amplitude of the average eEPSC (V_h = -70 mV, where the EPSC at this potential was nonsaturating), (N = 46 WT and 56 TKO synapses). E: A small but statistically significant increase in the rise time of eEPSCs was detected in TKO mice, (N = 58 WT and 63 TKO synapses). Decay kinetics of eEPSCs was characterized with two components – a fast (F) and a slow (G) time constant, which did not vary between genotypes. (N = 48 WT and 56 TKO synapses). WT – black, TKO – gray. Histograms represent the distribution of the entire data set. The insets depict mean ± s.e.m., (*) for $p < 0.05$.

Analysis of the eEPSC kinetics revealed a slower rise time of the response in TKO synapses (Fig. 3.22 D). The distribution of the rise time was slightly shifted to the right in TKO compared to WT terminals. WT calyces required 216 ± 4.8 μs to reach 80% of their maximum amplitude, while TKO terminals required 229 ± 4.5 μs ($p = 0.03$, Mann Whitney test). The decay time kinetics was not altered in TKO mice (Fig. 3.22 E and F). In both genotypes the eESPCs were fitted by a biexponential decay curve, splitting the response into a slow and a fast component. The mean slow decay time component (τ_{slow}) was 2.5 ± 0.12 ms in WT terminals and 2.4 ± 0.17 ms in TKO calyces ($p = 0.26$, Mann Whitney test). The fast

decay time component (τ_{fast}) was 0.4 ± 0.02 ms in WT and 0.45 ± 0.05 ms in TKO (p = 0.40, Mann Whitney test).

Deletion of synapsin genes did not lead to alteration in the size of neither spontaneous nor evoked release at the close-to-mature mouse calyx of Held. The decay time kinetics of the events remained unchanged. However, we could provide evidence that synapsins control the frequency of spontaneous SV fusion and the rise time of evoked events.

3.2.7. Synapsins control short-term depression at the calyx of Held

We investigated synaptic pool size and refilling rates at TKO calyces using trains of action potential-evoked EPSCs at frequencies between 10 – 300 Hz at RT. Synapses of both genotypes fired reliably and showed pronounced short-term depression for all tested stimulation frequencies (Fig. 3.23 A and B, Fig. 3.24 A). Both WT and TKO calyx synapses showed a comparable extent of synaptic depression, when stimulated at low frequencies. After 10 stimuli at 10 Hz both WT and TKO synapses depressed to 42.2 ± 2.8 % in WT and 36.4 ± 2.2 % in TKO of the initial EPSC size (p = 0.12, Mann Whitney test) (Fig. 3.23 C and D). The depression was best described with a monoexponential function for each cell and had similar average time constants in both genotypes. The steady state level in WT calyces was reached after 195.0 ± 9.8 ms and in TKO terminals – after 209.2 ± 14.3 ms, which was not significantly different (p = 0.77, Mann Whitney test) (Fig. 3.23 E). When stimulated at higher frequency (20 Hz and 50 Hz for 1 s) both WT and TKO calyces depressed even more but to a similar extent (Fig. 3.24, Table 3.7).

Synapsins are implied to control sustained release during the late phase of a high-frequency stimulation train (Sun et al., 2006). Therefore, WT and TKO calyces of Held were challenged with a 100-Hz stimulation train for 1 s (Fig. 3.23 B). A constant steady-state level was achieved in both WT and TKO terminals after approximately 20 stimuli (Fig. 3.23 F). This stimulation paradigm resulted in a strong depression to 17.5 ± 1.8 %of the initial EPSC amplitude in WT synapses, while TKO mice had steady state level of 12.0 ± 0.8 % (p = 0.01, Mann Whitney test) (Fig. 3.23 G). The time course of depression, calculated from a monoexponential fit of the responses during the stimulation train, (Fig. 3.23 H) was significantly accelerated in TKO mice and had a time constant of 26.0 ± 1.7 ms, compared to 36.3 ± 3.4 ms in WT calyces (p = 0.04, Mann Whitney test).

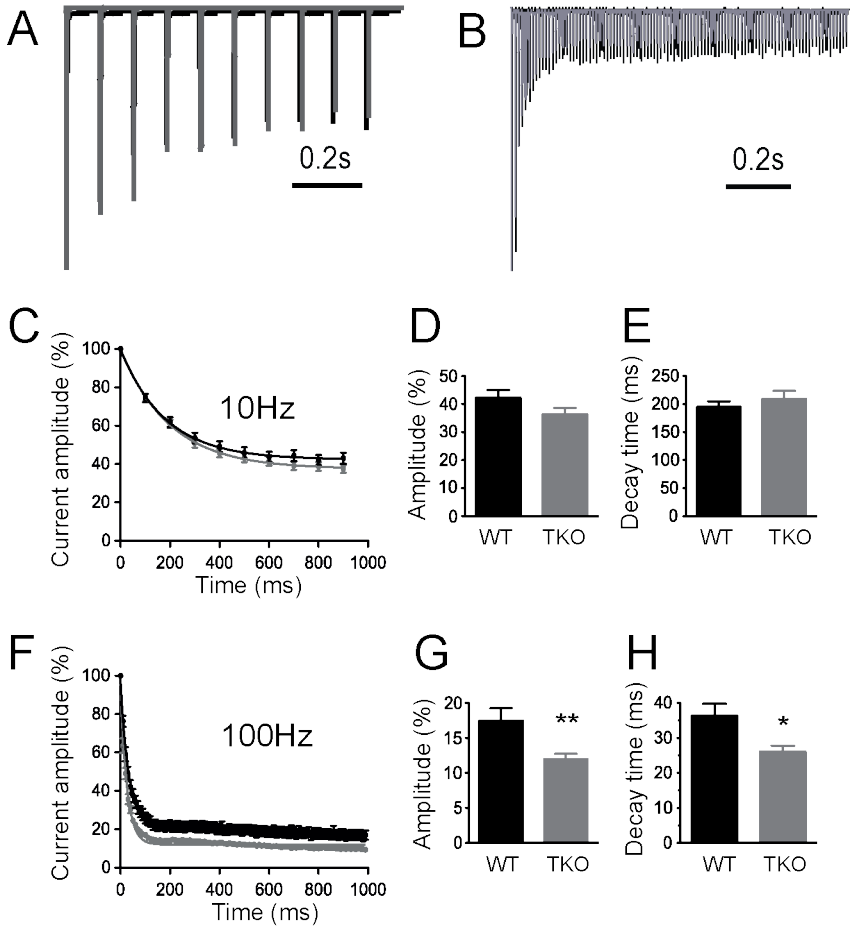

Figure 3.23: Short-term depression upon high-frequency stimulation is increased and accelerated in calyces from TKO mice. Synaptic responses were elicited through a 10 Hz (A) and 100 Hz (B) stimulation train for 1 s. Peak amplitudes were normalized for better comparison. C: The amplitude of EPSC in the train was normalized to the size of the first EPSC ($EPSC_1$) to assess the steady state level of depression when stimulated at 10 Hz. D: Amplitude of the steady-state level of the depression presented as % of the first EPSC. E: Time necessary for the steady-state level to be established. F: The amplitude of EPSC in the train was normalized to the size of $EPSC_1$ to assess the steady state level of depression when stimulated at 100 Hz. G: same as D but for a 100 Hz stimulation train. H: same as E but for a 100 HZ stimulation train. Black – WT, gray – TKO, N and level of significance is given in table 3.7. (*) for $p < 0.05$, (**) for $p < 0.01$.

Summary of the data obtained at all tested stimulation frequencies is presented in Fig. 3.24 and in table 3.7. There was a strong, frequency dependent effect on the properties of STD. Deletion of all synapsins led to a faster and more pronounced extent of depression at all tested frequencies higher than 100 Hz. In conclusion, deletion of synapsins resulted in an increased and accelerated presynaptic depression at high stimulation frequencies.

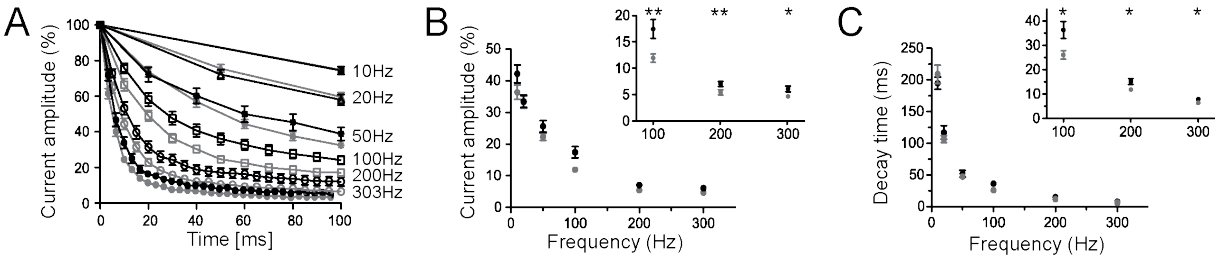

Figure 3.24: Summary of the short-term depression at all tested frequencies (10 – 300 Hz). Calyces from both genotypes showed pronounced STD. A: Current amplitude normalized to the size of the $EPSC_1$ in the train during the first 100 ms of the recording. B: Plot of the amplitude of the steady state, presented as % of the $EPSC_1$. C: Plot of the decay time constants. Insets present the data points for high-frequency stimulation trains (100 – 300 Hz). Black – WT, gray – TKO, N and level of significance is given in table 3.7. (*) for $p < 0.05$, (**) for $p < 0.01$.

Stimulation frequency (Hz)	Steady-state level TWT	TKO	p-value
10	42.2 ± 2.8 % (39)	36.4 ± 2.2 % (41)	0.160
20	33.5 ± 2.0 % (30)	33.3 ± 2.0 % (34)	0.877
50	25.6 ± 1.8 % (20)	22.3 ± 1.2 % (30)	0.138
100	17.5 ± 1.8 % (39)	12.0 ± 0.8 % (47)	0.010
200	7.0 ± 0.5 % (30)	5.4 ± 0.5 % (41)	0.009
300	6.1 ± 0.5 % (29)	4.7 ± 0.3 % (35)	0.023

Stimulation frequency (Hz)	Decay time (ms) TWT	TKO	p-value
10	195.0 ± 9.79 (39)	209.2 ± 14.26 (41)	0.773
20	117.1 ± 5.50 (30)	106.6 ± 10.63 (34)	0.909
50	51.86 ± 5.24 (21)	47.35 ± 2.87 (31)	0.456
100	36.28 ± 3.44 (39)	26.04 ± 1.74 (47)	0.040
200	15.18 ± 1.02 (31)	11.39 ± 0.66 (39)	0.036
300	7.88 ± 0.54 (29)	6.4 ± 0.34 (35)	0.025

Table 3.7 Properties of STD in TKO compared to WT presynaptic terminals.

3.2.8. Synapsins contribute to replenishment of the readily releasable pool

To test if the absence of synapsins led to alterations in the pool of release-competent SVs at the calyx of Held we analyzed synaptic vesicle pool size and replenishment properties from cumulative amplitude analysis of the EPSCs obtained during the protocols used to measure the rate and time-course of STD, which are sufficient to empty the RRP (Fig. 3.25). An extrapolation of the data provided by depression trains at 100 Hz (Fig. 3.24 B) allowed an estimation of the size of the releasable pool (RRP) of vesicles, similar to (Grande and Wang, 2011; Schneggenburger et al., 1999; Stevens and Williams, 2007) but using the entire train. When EPSC amplitudes were plotted as a cumulative function, a line function was fit tangentially to the curve at 20th stimulus and was back-extrapolated (Fig. 3.25 A). The Y-

intercept yielded the size of the releasable pool, whereas the slope was proportional to the replenishment rate.

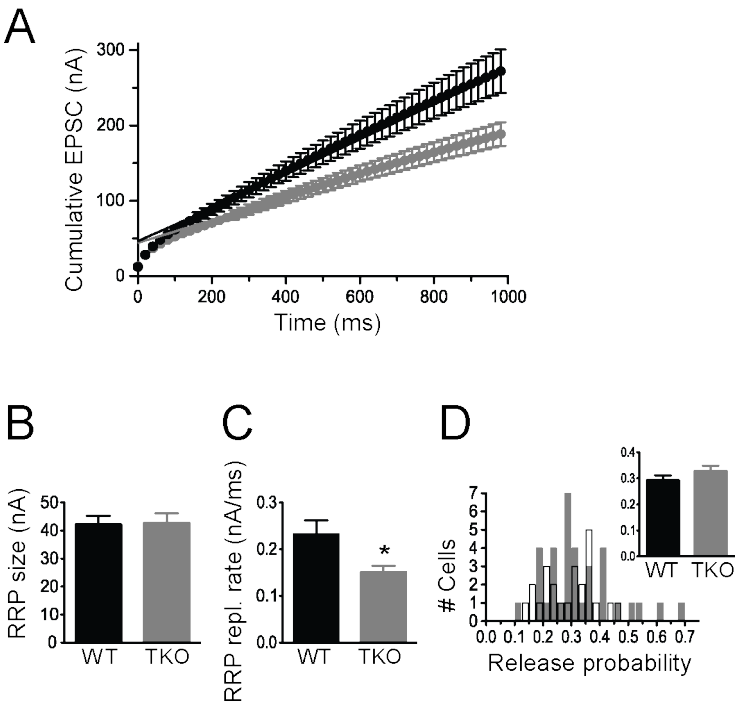

Figure 3.25: Synapsin deletion slows down the RRP replenishment rate. Properties of the RRP of SVs were estimated from 100 Hz stimulation trains in cells recorded at V_h = -70 mV. A: Cumulative EPSC was calculated via summing up the amplitude of the consecutive events in a 100 Hz train and a linear extrapolation was done. B: The size of the RRP was not altered in TKO terminals. C: The rate of RRP replenishment was significantly decreased in TKO animals. D: The release probability, calculated as the ratio between the size of eEPSC and the y-intercept of the line fit also remained similar in WT and TKO terminals. The histogram shows the heterogeneous release probability across different calyces. (N = 24 WT and 35 TKO synapses). WT – black, TKO – gray. Data points are presented as mean ± s.e.m., (*) for $p < 0.05$.

The size of the RRP was 45.42 ± 4.44 nA in WT and 44.3 ± 3.7 nA in TKO terminals (p = 0.73, Mann Whitney test) (Fig. 3.25 B). The number of SVs in the releasable pool was then calculated from this estimation as the ratio of the RRP size to the quantal size, estimated from recordings in the same cell at V_h = -70 mV. The RRP was estimated to contain 905 ± 139 SVs in WT calyces, consistent with previous reports (Grande and Wang, 2011; Iwasaki and Takahashi, 2001; Kushmerick et al., 2006). RRP in TKO terminals comprised of 891 ± 57 SVs (p = 0.6, Mann Whitney test). The RRP replenishment rate, the rate at which SVs are recruited, was significantly decreased in terminals from TKO animals and had a value of 0.15 ± 0.01 nA/ms in TKO compared to 0.23 ± 0.03 nA/ms estimated in WT terminals (p = 0.03, Mann Whitney test) (Fig. 3.25 C). Using the estimation of the total RRP size we then determined the probability of release by dividing the size of the eEPSC by the intercept value (Fig. 3.25 D). The histogram shows that the release probability of single cells was quite hetrogeneous and some TKO cells exhibited extraordinarily high release probability. The mean values were: P_{rWT} = 0.29 ± 0.02 and P_{rTKO} = 0.33 ± 0.02 without statistical difference (p = 0.51, Mann Whitney test) (Fig. 3.25 D inset), suggesting that control and knockout synapses had the same release probability. In summary, deletion of synapsins slowed the rate of

replenishment of the RRP during high-frequency activity while leaving the RRP size and P_r intact.

3.2.9. Synapsins control the fast component of recovery from depression

Short-term depression at the calyx of Held is largely accounted by the depletion of the pool of release competent vesicles. To ensure synaptic fidelity and precision at high frequencies of synaptic transmission, the synapse needs to quickly refill this pool after depletion. After having shown that short-term depression is accelerated in synapsin-lacking calyces, we probed the speed of recovery from depression in TKO calyces. The differences between STD properties in WT and TKO were most evident after a 100 Hz stimulus train and reached steady-state level after approximately 200 ms (Fig. 3.23 F). Therefore, we induced depression with 20 stimuli at 100 Hz and measured recovery from depression by subsequent application of single stimuli at various time intervals ranging from 0.01 s to 14.8 s relative to the depleting stimulus train. (Fig. 3.26). Representative recordings form WT and TKO terminals are shown in Fig. 3.26 A and B respectively. To make an estimate of the extent and time profile of the recovery process, the resulting EPSC was normalized to the first EPSC of the 100-Hz stimulation train (Fig. 3.26 C). When stimulated by a 20x100 Hz train both WT and TKO synapses depressed to less than 20% of the initial EPSC. The resulting recovery curves were best described by a bi-exponential function, thus two kinetic components (τ_{fast} and τ_{slow}) were assigned to the recovery time (Gabriel et al., 2011; Wang and Kaczmarek, 1998). After approximately 10 s the postsynaptic response recovered to the value of the initial EPSC. The relative weights of the two components were comparable between WT and TKO with fast component being responsible for 31.0 ± 3 % in WT and 30.4 ± 3 % in TKO of the recovery ($p = 0.76$, Mann Whitney test). The recovery process, however, took longer in TKO synapses and had τ_{fast} = 0.14 ± 0.02 s while in WT calyces τ_{fast} = 0.11 ± 0.02 s ($p = 0.03$, Mann Whitney test) (Fig. 3.26 D). There was a tendency towards increased slow component of recovery but this did not reach significance (Fig. 3.26 E). The calculated values for τ_{slow} were 3.0 ± 0.3 s in WT and 3.5 ± 0.3 s in TKO terminals ($p = 0.1$, Mann Whitney test).

Deletion of synapsins did not affect the extent of recovery after short-term depression but led to a prolongation of this process, similar to results obtained from the hippocampus of synapsin I and II double knock out mice (Gabriel et al., 2011). We could detect a rapid phase of refilling in both WT and TKO. This process was, however, slowed down in the knock out terminals. Although mutant synapses needed slightly longer time, they successfully recovered to the size of the initial EPSC. Synapsins might control the rate of vesicle recovery at rest

from depleted state but not the recovery process *per se*, thus concluding that lack of synapsins does not abolish but only slightly impairs normal physiological processes at a CNS synapse.

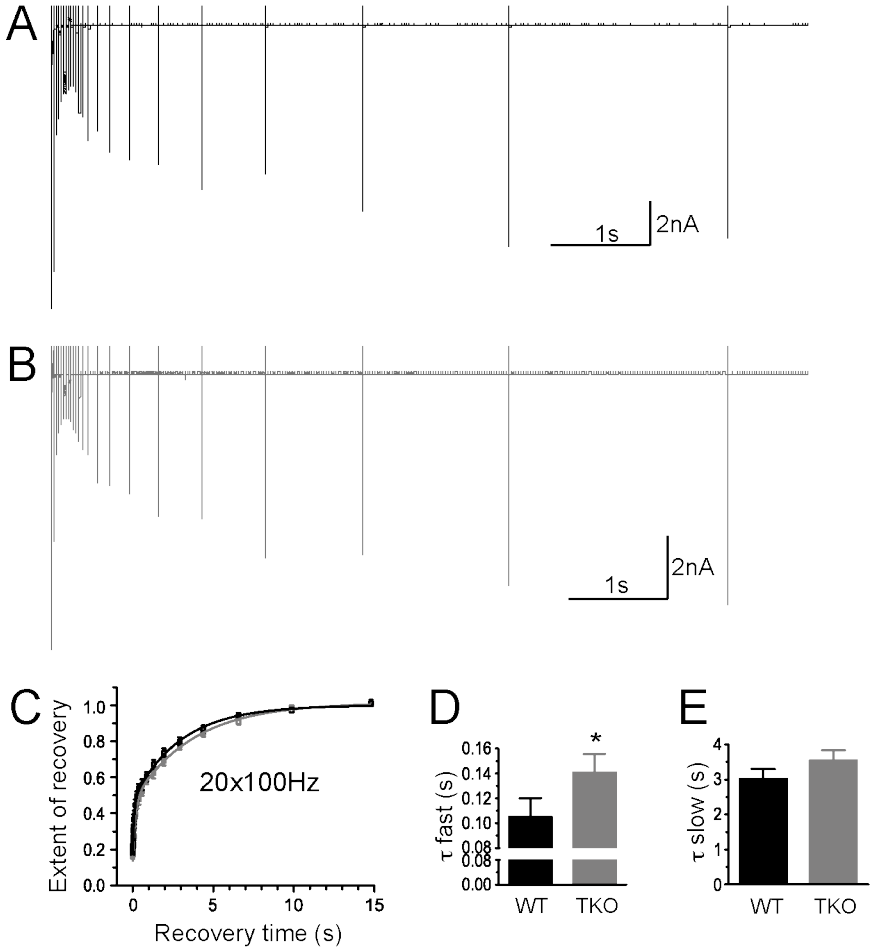

Figure 3.26: Recovery from depression was slowed down in TKO mice. A: Representative traces showing an initial depressing 20x100 Hz train and subsequent recovery of the EPSC amplitudes in WT (black) and TKO (gray) calyces. Superposition of 20 sweeps, each recording a single EPSC at intervals between 10 ms and 14.8 s after the depression train. B: Recovery from the depression train in WT and TKO terminals. Peak amplitudes are shown as fraction of the first EPSC in the stimulation train. The time course of the recovery was fitted by a biexponential function with a fast (C) and a slow time constant (D). The fast component of the recovery was delayed. In contrast, the slow component of the recovery remained intact. N = 29 WT and 26 TKO synapses). WT – black, TKO – gray, data points are presented as mean ± s.e.m., (*) for $p < 0.05$.

3.2.10. Summary – synapsins control the biogenesis and immobilization of synaptic vesicles and hence maintain the replenishment of the readily releasable pool during high-frequency transmission at the calyx of Held

We could show that synapsins control the number of SVs in the calyx of Held. TKO calyces had approximately 50 % reduction in the total vesicle number. The level of vesicle-associated proteins was decreased, while that of other presynaptic proteins remained intact upon deletion of synapsins. On ultrastructural level, the deletion of synapsins led to enlargement of the AZs and to a decrease of the SV density at the active zone. Although, larger vesicles were present

in TKO terminals, the total number of SVs associated with a given AZ was comparable to than in WT controls. The overall morphology of the mutant terminal was not altered and its size and presynaptic compartment was comparable to than observed in WT.

The vesicles, remaining in synapsin deficient terminals were sufficient to maintain close-to-normal levels of basal synaptic transmission, but failed to support release during the late phase of prolonged stimulation trains at high frequency (> 100 Hz). Therefore, synapsin lacking calyces showed pronounced short-term depression, which was accelerated and reached higher rate in comparison to WT controls. The size of the RRP, estimated from the depression trains, was not changed but its replenishment was slower in TKO terminals. Accordingly, the process of recovery from depression, which occurred in two phases reflecting vesicles with different recovery kinetics, took place slower than in WT calyces. Therefore, we could conclude that synapsins control a pool of vesicles, which are recruited to the active zones during prolonged presynaptic activity but do not seem to be important for maintaining basal levels of neurotransmitter release.

4. Discussion

In the present study we investigated the involvement of synapsins in the physiological functions at the calyx of Held *in vivo*. We employed both microscopical and electrophysiological methods to examine the consequences of acute genetic perturbation and chronic gene deletion of all known synapsin genes in an intact properly developed CNS synapse.

The first method involved the overexpression of synapsin I isoforms in the naïve rodent calyx of Held. For this purpose, we first obtained an overview of the expression pattern of the endogenous synapsin isoforms and constructed adeno-associated viruses coding for the two synapsin I isoforms, both of which are properly trafficked to the presynaptic boutons in WT preparations but differ in their dimerization properties. Contrary to our expectations, based on the ability of the two isoforms to form hetero- or homodimers (Gitler et al., 2004b) both isoforms had similar effects on the properties of the presynaptic terminal. Overexpression of either synapsin Ia or synapsin Ib led to vesicle redistribution within the calyx, which underlined enhanced and accelerated short-term depression. Although the proximal vesicle cluster in synapsin Ia overexpressing calyces was disrupted, the density of anatomically docked vesicles remained unchanged. Additionally, overexpression of synapsin I isoforms introduced a fast kinetic component in the course of recovery from STD, resulting in faster recovery compared to control terminals.

The second approach embraced on characterization of global synapsin knock-out, previously generated by crossing single knock-out lines (Gitler et al., 2004a). Previous attempts to characterize the functional effects of synapsin gene deletion failed to provide a complete characterization of the functional and structural alterations that ensue at *in vivo* developed and matured CNS synapses and led to the conclusion that synapsins are differentially involved in the regulation of neurotransmitter release at different synapses. Various studies have been conducted either in primary cultures (Baldelli et al., 2007; Gitler et al., 2008; Gitler et al., 2004a; Orenbuch et al., 2012a) or in dopaminergic (Kile et al., 2010; Venton et al., 2006) and cholinergic systems (Gaffield and Betz, 2007). Studies done in the hippocampus have examined either the morphological (Siksou et al., 2007) or the functional consequences of synapsin deletion (Farisello et al., 2012) without establishing a direct correlation between morphological and functional alterations which follow the deletion of all three synapsin genes. We could show that TKO calyces contained approximately 50 % less SVs, which resulted in enhanced STD and slower recovery compared to WT terminals.

Although both synapsin perturbations resulted in a reduction in the number of vesicles and increased and accelerated short-term depression at high stimulus frequencies, perturbation of synapsin function did not have dramatic effect on the spontaneous quantal release or on the postsynaptic current in response to single APs. Additionally, we did not detect effects on the size of the RRP or the P_r. However, the rate at which SVs were recruited to the readily releasable pool during trains of intense stimulation was decreased. These findings assign a key role of synapsins in the presynaptic mechanisms counteracting synaptic depression. Synapsins maintain the size of a portion of the vesicle pool and the vesicle transfer to the RRP, when the local recycling pathways are outcompeted by extensive exocytosis.

The synapsin gene deletion led to a global downregulation of vesicle-associated presynaptic proteins, which was reflected in the low number of functional SVs formed, similar to the observation in the hippocampus of single and double knock out mice (Rosahl et al., 1995). From this we conclude that synapsins might be involved in the biogenesis of vesicle precursor molecules. It was not possible to examine similar effect in the synapsin I overexpressing calyces, due to the synapse specific effect of the overexpression. However, since we did the genetic perturbation at p 6, we would expect that the global concentration of proteins would remain unchanged. Therefore, another molecular mechanism might underline the decrease in SV number within the presynaptic vesicle clusters in this case.

The number of physically docked vesicles in synapsin knock-out mice remained unchanged, explaining the unchanged levels of basal neurotransmission in the genetically altered calyces. However, overexpression of synapsin I isoforms led to reduction of the number of docked vesicles as well as reduction of the total SV number within the vesicle clusters without altering the quantal release and the size of the RRP, arguing for the presence of a surface pool, comprised of SVs physically attached to the membrane but not being part of the RRP (Denker, 2010). It is possible that overexpression of synapsin I isoforms led to a defect in the endocytosis and/or the vesicle recycling and integration into the different pools.

In the two sets of experiments, there was a clear correlation between the synapsin concentration in the calyx of Held and three presynaptic parameters: (1) active zone size, (2) synaptic vesicle diameter and (3) recovery from short-term depression. Acute overexpression of synapsin Ia led to decrease in the size of AZs and SVs, while the chronic absence of synapsin in the TKO terminals enlarged both AZs and SVs. Although short-term depression under both experimental conditions was accelerated and enhanced compared to controls, recovery from trains of high-frequency activity was differentially controlled by synapsins.

Overexpression of synapsin I isoforms introduced a fast component to the recovery kinetics leading to speeding of this process, whereas deletion of synapsins led to the opposite effect.

All this indicates that, at least at the calyx of Held, two distinct populations of vesicles co-exist – synapsin – dependent and synapsin – independent. Synapsin – independent vesicles remain close to the active zones and maintain release under basal conditions. Synapsin – dependent vesicles are involved in the synaptic response to high-frequency activity, when the capacity of the RRP is exhausted and the pool needs to be replenished with either newly endocytosed vesicles or reserve vesicles. Although, a large proportion of vesicles (~ 50 %) was absent from the TKO presynaptic terminal, the synapsin-dependent vesicles accounted for only ~ 20 % of the neurotransmitter release during repetitive trains of high-frequency activity. This indicates that not all of the vesicles present in the wild type calyx of Held are used during activity (Denker et al., 2011). In addition to the widely accepted role of synapsins in immobilization reserve vesicles within presynaptic terminals, our results propose non-canonical functions of synapsins – (1) role in vesicle precursor biogenesis; (2) maintenance the size of active zones and clear-core vesicles; (3) role in endocytosis and vesicle recycling.

4.1. Subcellular localization of endogenous synapsin isoforms within the rodent calyx of Held

Synapsins are broadly expressed within various brain regions (Südhof et al., 1989) and the vast majority of nerve terminals in the CNS express at least one synapsin isofom (De Camilli et al., 1983). It is highly probable that the synapsin composition varies between synapses with different functions and that different members of the family exhibit different expression patterns (Südhof et al., 1989). As shown previously, synapsin expression varies between synaptic populations in the thalamic dorsal lateral geniculate nucleus. Synapsin I and II are not present in retinogeniculate terminals, which transmit primary afferent input at high frequencies and show synaptic depression, whereas both are present in corticogeniculate terminals, which provide modulatory feedback at lower frequencies and show synaptic facilitation (Kielland et al., 2006). We presented a proof that each of the three synapsin genes was expressed in the calyx of Held at p 16 with synapsin Ia, synapsin Ib, synapsin IIb and synapsin IIIa showing the most robust expression (Fig. 3.1 and Supplementary Figure 1). To our surprise, we could not detect synapsin IIa within the calyx of Held (Fig. 3.2), an isoform that has been suggested to play a major role in synapses of cultured hippocampal neurons (Gitler et al., 2008). In the hippocampus of age-matched littermates synapsin IIa was broadly expressed, implying a region specific role for this isoform (Fig. 3.2). The lack of expression

in the calyx may suggest that synapsin IIa provides a specific function not necessary for normal synaptic transmission at the calyx or that the other a-isoforms present in the calyx might compensate for its function. Particularly synapsin IIIa (Fig. 3.1) may transiently take over this function until it is downregulated at later stages of maturation (Ferreira et al., 2000; Hosaka and Südhof, 1998a). It might be possible that synapsin IIIa is gradually exchanged for synapsin IIa during adulthood. All examined isoforms showed similar distribution patterns within the membrane of the presynaptic terminal – large fluorescent clusters inside the terminal, representing the densest SV population. Different synapsin isoforms do not populate different sub-compartments of the terminal with exception of synapsin Ia and synapsin Ib, which, although rarely, were found to be localized to mutually exclusive puncta (Fig. 3.3). This might lead to the conclusion that these two isoforms are differentially bound to SVs. The different localization of synapsin I isoforms could be a consequence of their dimerization properties, with synapsin Ia being able to form homo- and heterodimers and synapsin Ib only heterodimers in order to be able to bind to SVs in the WT situation (Gitler et al., 2004b). Therefore, synapsin Ib distribution pattern might be more restricted than that of synapsin Ia and there might be presynaptic subdomains that express either synapsin Ia or synapsin Ib, possibly delineating different SV pools within the calyx.

Synapsins, as expected, followed the SVs distribution into donuts, highly ordered ring-like assemblies (Wimmer et al., 2006), along the presynaptic membrane facing the MNTB principal cell. All synapsin isoforms tested showed almost complete overlap with vGluT1, suggesting that there is no systematic spatial segregation of synapsin isoforms within synaptic vesicle clusters. Although colocalizing with vGluT1, the synapsin staining was more diffuse and extended outside the boundaries of the vesicle cluster (Fig. 3.3). This shows that synapsin molecules, which are not bound to vesicles, remain close to the vesicle cluster. Outside the boundaries of the calyx of Held vGluT1 failed to co-localize with synapsin isoforms, suggesting that the other synaptic contacts on the MNTB principal cell do not contain vGluT1. These extracalyceal synapses might be both inhibitory (Awatramani et al., 2005; Lenn and Reese, 1966; Nakajima, 1971) and excitatory (Guinan and Li, 1990; Hamann et al., 2003) and hence might contain either no or glutamate transporters, different than vGluT1.

We detected all major isoforms found in the rat calyx of Held in the mouse as well (Fig. 3.15), excluding putative variations between species. In the mouse calyx the expression pattern of synapsin isoforms also followed the general distribution of SVs, visualized with vGluT1 stain.

4.2. Effects of overexpression of synapsin I isoforms on the structure of the calyx of Held

The role of separate synapsin isoforms in maintaining the integrity of the SV clusters *in vivo* was examined via rAAV-mediated gene transfer, which maintained constant overexpression of either synapsin Ia or synapsin Ib in the near-to-mature rat calyx of Held. Although the level of the protein overexpression in the presynaptic terminal depends on the number of viral particles, which have infected a given GBC, we obtained robust expression pattern for both proteins of interest. They were transported successfully to the presynaptic terminal and co-localized with SVs (Fig. 3.6), similar to observations in autaptic hippocampal cultures (Gitler et al., 2004b). Along the axon, both the overexpressed proteins were transported in large packets, which filled up the entire axon. This is in accordance with the fact that synapsins are transported as a part of slow component b macromolecular complexes, which shuffle diverse proteins from the cell body along the axon to the axonal tip at average rates of 2 – 8 mm/day, powered by microtubule motors (Roy et al., 2007, 2008). This transport mechanism is different from the mechanism of typical SV transmembrane proteins, which are transported in small vesicle-like compartments to the terminal, and it also differs from that of AZ proteins, which are part of PTVs (Goldstein et al., 2008; Gundelfinger and Fejtova, 2011). We can also exclude that the overexpressed synapsins are transported through mere diffusion to the calyx, similar to the transport of ectopic proteins such as cytosolic EGFP (M. Vasileva, unpublished observations).

Although, overexpression of synapsin I isoforms did not lead to major structural malformations of the presynaptic terminal, overexpression of synapsin Ia resulted in a slightly decreased volume of the presynaptic compartment (Fig. 3.7). However, we would attribute this result to the structural and functional differences of the terminals within the MNTB (Grande and Wang, 2011), rather than to direct consequences of the synapsin Ia overexpression.

4.2.1. Redistribution of SVs upon overexpression of synapsin I isoforms

Within the calyx of Held the overexpressed synapsin isoforms overlapped with vGluT1 immunofluorescence, similar to the wild type synapsins (Fig. 3.6 and 3.7). EYFP-synapsins were properly targeted and hence, had the potential to interfere with SV trafficking and immobilization. There was a diffuse component of EYFP-synapsin distribution, which is likely to be caused by overexpression and may correspond to free-floating or cytomatrix-bound cytoplasmic localizations. Furthermore, donut-like swellings were present (Wimmer et

al., 2006) and the 3D architecture of the terminal was unchanged. The overexpression resulted, however, in a significant redistribution of SV clusters, assessed by vGluT1 staining (Fig. 3.7). The excess of synapsin molecules may increase the chance of synapsins to form dimers without being linked to synaptic vesicles (Gitler et al., 2004b), thereby interfering with SV clustering. It is possible that vesicle immobilization is impaired and SVs are more mobile in synapsin-overexpressing terminals. In the latter case, vesicles might disperse from the clusters in close proximity to the AZs to more distant locations. Consistent with our results, a recent study reported an enlarged resting pool of SVs upon overexpression of synapsin in Aplysia sensorimotor neuron co-cultures (Fioravante et al., 2007). Hence, the increased SV cluster volume could be explained by an addition of SVs to the resting pool mediated by the overexpressed synapsin isoform.

4.2.2. Ultrastructure of the calyx of Held upon overexpression of synapsin Ia

Serial sectioning scanning electron microscopy after photooxidation of EGFP into electron-dense material revealed that overexpression of EGFP-synapsin Ia starting at p 6 did not perturb the development and maturation of the calyx of Held (Fig. 3.12 and 3.13). The overall SV population was intact and synapsin Ia overexpression did not introduce rearrangements of vesicle distribution within the reconstructed presynaptic segments. The vesicle pool localized away from the active zones remained intact, thus synapsin Ia did not alter the number of vesicles immobilized within the distal vesicle cluster. This disagreement with the fluorescence microscopy data might arise from the fact that only partial segments were reconstructed, which did not comprise the entire volume of the presynaptic terminal. Overexpression of synapsin Ia did not modify the SV density, leading to the conclusion that overexpression of synapsin Ia does not interfere with the SV biogenesis or the traffic of SV components to the terminal.

When focusing on SV clusters associated with identified AZs (Fig. 3.14), we found a strongly decreased AZ surface, decreased number of associated SVs and a decrease in the number of docked SVs. The SVs associated with an AZ may belong to any of the three SV pools and hence overexpression of synapsin Ia might affect SVs in all three pools. SVs might escape from the AZ and move into the bulk volume of the calyx – shifting SVs within the terminal but not between the different pools. However, we did not observe any changes in the SV distribution away from the AZs. Therefore, we conclude that synapsin Ia controls the SV number locally within the proximal vesicle cluster. We cannot exclude that the SVs leave the clusters close to the AZs and join a more distal vesicle pools, whose size is controlled by

synapsins. If interference with synapsins leads to dispersion of the vesicle pool, which is preferentially localized away from AZs, the SVs that escape from the boundaries of the proximal cluster might move towards the back of the presynaptic terminal and be fed into the distal pool. This hypothesis might explain the lack of effect of synapsin Ia overexpression on the vesicle distribution within the distal pool at the calyx of Held. To conclude synapsin Ia might control the number of vesicles in both the proximal and distal pools. Overexpression of synapsin Ia might lead to a reduction in the SV number within the distal pool, which is however compensated by proximal vesicles that escape the boundaries of the cluster at the AZ.

Overexpression of synapsin Ia led to an alteration of the architecture of the AZs – smaller AZs, which contained less and smaller in size SVs in infected calyces (Fig. 3.14). This hints towards a defect in the endocytosis of vesicular material and/or trafficking of newly endocytosis vesicles to the vesicle cluster. It might be also possible that the stabilization of the lipid bilayer is compromised leading to smaller SVs. There is an indication that synapsin I might lead to increased membrane stability and thus preserving the size and the shape of SVs and preventing multivesicular fusion (Pera et al., 2004). The decreased vesicle size might be a homeostatic compensatory change in response to synapsin Ia overexpression. Another possibility is that vesicle reuptake and recycling upon exocytosis might be impaired leading to smaller SVs. Synapsin could might interact with actin within the endocytic zone of active nerve terminals, thus playing a role in vesicle recycling (Bloom et al., 2003) and a direct connection between endocytosis and synapsin dispersion within the presynaptic terminal has been shown previously (Orenbuch et al., 2012b).

4.2.3. Synapsin I overexpression does not affect basal neurotransmitter release and RRP function

Overexpression of synapsins in the calyx of Held did not lead to alterations in the RRP, consistent with observations made in cultured hippocampal neurons from TKO mice (Gitler et al., 2004a). Spontaneous release of SVs was not altered (Fig. 3.9) and the size and the quantal content of evoked EPSCs were not changed in synapsin I isoform-overexpressing synapses (Table 3.1). The size of the RRP remained unaltered, implying that synapsin I isoforms are not involved in the regulation of the vesicle pool in close proximity to the active zone. Although the number of SV per AZ was decreased density of the docked vesicles was unchanged in synapsin Ia overexpressing terminals compared to control (Fig. 3.14), leading to unaltered size of the RRP compared to control situation. It seems that SVs belonging to the

RRP, maintained by local recycling at the active zone, are sufficient to sustain neurotransmitter release in response to isolated action potentials.

The lack of effect on size and kinetics of the evoked responses apparently contradicts experiments performed using a peptide derived from the E domain, present in synapsin Ia and absent from synapsin Ib. Injection of a domain E-derived peptide in the squid giant terminal decreased the size and slowed the kinetics of evoked EPSCs (Hilfiker et al., 1998). This discrepancy may be explained by the presence of the entire synapsin Ia protein in our preparation, which may compensate for the effects of the isolated E-domain by properly localizing to the terminal through interactions with other synapsin isoforms and SV. Alternatively, the overexpression levels achieved with rAAV-mediated expression are likely to be smaller than those obtained with peptide injections into the presynaptic giant terminal of the squid. If a low affinity interaction of the E-domain with the unknown target structure mediates the kinetic effect, it may not be apparent with the overexpression approach used here.

4.2.4. Synapsin I isoforms accelerate short-term depression

Overexpression of synapsin I isoforms enhanced the rate of activity-induced synaptic depression at the calyx of Held (Fig. 3.10). STD at the calyx of Held is predominantly mediated by a reduction and depletion of the number of RRP vesicles (von Gersdorff and Borst, 2002; Wang and Kaczmarek, 1998). At the end of a high-frequency stimulus train, when the RRP is depleted, SVs away from the plasma membrane belonging to the recycling and reserve pools need to be recruited. After overexpression of synapsin I isoforms we observed a significant decrease of the decay times and steady-state levels of depression at all tested stimulation frequencies. The effect was most pronounced at 100 Hz stimulation, leading to the conclusion that overexpression of synapsin I isoforms abolishes a pool of SVs which is fed into the RRP upon high-frequency stimulation but otherwise is not needed for maintenance of normal release. The paired-pulse ratio in synapsin Ia overexpressing terminals was also significantly reduced, however, synapsin Ib overexpressing synapses showed only a tendency towards a decrease in paired-pulse ratio. The recruitment process and the rate of replenishment of the RRP might be impaired, suggesting that synapsin isoforms might control SV immobilization within the resting pool and their ability to join the recycling pool in an activity-dependent manner. Similar results have been observed in hippocampal cultures from TKO mice (Gitler et al., 2004a), at the calyx of Held of synapsin I and II double knock-out mice (Sun et al., 2006) and in TKO mice (Fig. 3.23 and 3.24). The data strongly supports a

model in which both synapsin I isoforms participate in organizing the resting pool of SVs and control the activity-dependent transition of SVs from the reserve pool into the cycling pool or the RRP. Overexpression of EYFP-synapsin Ia or Ib may hinder the shuffling of vesicles between different pools, thereby accelerating short-term depression. Therefore, both synapsins I isoforms might be part of a rescue mechanism that is activated when the synapse is exposed to high-frequency activity and their main function is to supply SVs to the active zone.

4.2.5. Accelerated recovery from depression after EYFP-synapsin Ia/Ib overexpression

Overexpression of the both synapsin I isoforms accelerated recovery from short-term depression. Terminals expressing synapsin I not only depressed to a greater extent but they also recovered faster, compared to non-infected terminals (Fig. 3.11). The faster recovery rate might be explained by increased mobility of SVs due to enhanced resupply mechanisms during exhaustive use. Presynaptic studies at immature rats have shown that recovery from synaptic depression is frequency dependent (von Gersdorff et al., 1997). The recovery after moderate stimulation (10 – 100 Hz) follows a monoexponential time course, (Wang and Kaczmarek, 1998). Upon introduction of synapsin I isoforms in the calyx, fast and slow components of replenishment were introduced. The fast component of recovery from depletion is Ca^{2+} dependent. Increase in Ca^{2+} influx during repetitive firing is the key element that enhances replenishment. Synapsin I binding to ATP is Ca^{2+} dependent and increase in the Ca^{2+} concentration would lead to increase in the ATP binding ability of synapsin I (Hosaka and Südhof, 1998b). Under conditions of overexpression, the level of phosphorylated synapsin at any moment is higher than in control conditions. The phosphorylated synapsin I would unbind from vesicles rendering them more mobile. Additionally, dephosphorylated synapsin I is an actin-nucleating agent and can affect the dynamics of actin filament assembly (Benfenati et al., 1992; Greengard et al., 1993; Valtorta et al., 1992). The actin-nuacleating activity of synapsin I is maintained while it is bound to SVs and results in the embedding of vesicles in the cytoskeletal meshwork (Benfenati et al., 1992). Therefore, synapsin phosphorylation not only maintains the release of SVs from the actin cytoskeleton but also prevents their recapture within the meshwork (Greengard et al., 1993) thus accelerating the recovery of the RRP during periods of rest after depletion. Additionally, synapsins might play a role in the late phase of the SVs cycle. It has been shown that part of the synapsin proteins does not dissociate from SVs, and remains in the RRP, (Bloom et al., 2003; Torri Tarelli et al., 1992). Synapsins might stimulate actin polymerization after endocytosis of SVs and might

help to recruit the recently endocytosed SVs to the actin cytoskeleton, consistent with the observation that refilling of the vesicle pool requires polymerized actin (Sakaba and Neher, 2003). Hence, overexpression of synapsin I isoforms may introduce or potentiate an existing mechanism that translates the Ca^{2+} signal into faster endocytotic SV retrieval.

The compromised tethering of SVs to the cytoskeleton in the synapsin Ia and synapsin Ib infected terminals might be another explanation for the faster recovery rate. Since the overexpressed synaspin I isoforms might limit the crosslinking of SV, SVs are not completely immobile and might need less time to refill the RRP after prolonged depression trains compared to control synapses. It is also possible that newly endocytosed vesicles are not properly integrated into the cytoskeletal meshwork and hence are more mobile. Surprisingly, we could show that both synapsin I isoforms share similar functions, despite the structural difference, which lead to formation of homomers in case of synapsin Ia overexpression and heteromers, in case of synapsin Ib and to differential binding to SVs.

4.2.6. Synapsin Ia/Ib overexpression and the synapsin dimerization hypotheis

The consequences of the synapsin Ia/Ib overexpression in the calyx of Held are consistent with the dimerization hypothesis (Gitler et al., 2004b). The genetic manipulation may result in the formation of mixed population of hetero- and homodimer of overexpressed synapsin Ia/Ib and endogenous synapsins. Upon saturation of the endogenous synapsin isoforms, synapsin Ia- but not synapsin Ib homodimers will be successfully targeted to the presynaptic compartmnet (Gitler et al., 2004b). Synapsin Ia homodimers will outcompete the eight synapsin binding sites on the SVs (Takamori et al., 2006), while synapsin Ib homodimers would be unable to associate with SVs. SV might be more mobile and might distribute more widely within the calyx upon overexpression of the two synaspin I isoforms. The impaired vesicle mobility will lead to functional consequences, such as increased short-term depression, which is consistent with the decreased vesicle number at the AZs in synapsin Ia overexpressing calyces. Thus, synapsin I isofom overexpression reduces the replenishment of the vesicle pool during high frequency activity. While the number of docked SVs was decreased per AZ, the relative ‘concentration’ of docked SVs remained the same, explaining the lack of effect of synapsin Ia overexpression on the readily releasable pool. The synapsin-dependent SVs within the proximal vesicle cluster might not be required for basal neurotransmitter release but is fed into the RRP during periods of intense neuronal stimulation. It is possible that synapsin I maintains the integration of newly endocytosed SVs

within specific vesicle pools (Denker, 2010; Rizzoli and Betz, 2005). Accordingly, we showed that higher synapsin concentration leads to faster pool refilling at rest.

We provide evidence that not all SVs, included in the SV cluster at the AZs are actively involved in neurotransmission. A synapsin-dependent pool coexists with synapsin-independent pool in close proximity to the AZ, arguing for the spatial intermixing of vesicles with different release probabilities (Denker, 2010). Several lines of evidence indicate that the synapsin-independent SVs are sufficient to maintain normal basal transmission. First, the properties of spontaneous and evoked EPSC were not changed upon overexpression. Second, the RRP size and the release probability were comparable between genetically perturbed and control calyces. Finally, albeit slightly impaired, neurotransmission upon high-frequency stimulation was not abolished by the overexpression of synapsin isoforms. We cannot exclude the possibility that through binding to the endogenous synapsin isoforms, the overexpressed proteins are properly allotted to the SVs within the presynaptic compartment and a more severe effect is occluded.

4.3. Consequences of synapsin gene deletion that ensue at the mature calyx of Held

The second part of the study examined the structural and functional consequences at the calyx of Held after deletion of all three synapsin genes. Deletion of synapsins resulted in the loss of approximately half of the synaptic vesicles in the calyx of Held, however, this pronounced structural change caused only a modest functional phenotype. Although basal synaptic activity remained largely unaltered, short-term depression and replenishment of the readily releasable pool were significantly impaired in TKO compared to WT mice. Our observations demonstrate that synapsins define a pool of SVs that feeds into the RRP during high-frequency stimulation but is dispensable for a close-to-normal function of the calyx of Held synapse.

4.3.1. Synapsins define the resting pool of SVs and may function upstream of presynaptic terminals

In calyces lacking synapsins SVs were selectively reduced while the number of bassoon positive clusters was normal. Bassoon staining, however, will underestimate the actual number of AZs within the presynaptic terminal, because some AZs express either bassoon or piccolo (Dondzillo et al., 2010). We provide several arguments that synapsins control the number of SVs in the calyx. First, the presynaptic volume occupied by vGluT1

immunoreactivity in entirely reconstructed calyces was reduced in the absence of synapsins (Fig. 3.17). Second, quantitative electron microscopy of representative calyceal segments demonstrated that the number of SVs in TKO was reduced by ~ 50 % compared to WT (Fig. 3.18). SVs situated distally from the AZs were strongly decreased in number while those localized at the AZs remained unchanged. This coincides with the hypothesis that synapsins immobilize a defined pool of SVs (Gitler et al., 2004a; Hilfiker et al., 1998; Humeau et al., 2001; Pieribone et al., 1995; Rosahl et al., 1995) and that this pool mostly represents the reserve pool of SVs (Denker, 2010; Orenbuch et al., 2012a; Rizzoli and Betz, 2005). Given that the reserve pool of the calyx represents approximately 95% of the SVs present in the calyx (Rizzoli and Betz, 2005), but only 50% of the SVs are lost in the absence of synapsins, another large fraction of the reserve pool must be defined by different molecular entities (Bourne et al., 2006; Gaffield and Betz, 2007; Gaffield et al., 2006; Shupliakov et al., 2002). The decrease of total SV number aligns well with the observation that vesicle-associated proteins were specifically decreased in brain lysates of TKO mice, while proteins of the AZ or postsynaptic proteins remained unchanged (table 3.5), in agreement with previous observations (Gitler et al., 2004a). Similar results were also reported in double knock-out mice lacking synapsin I and synapsin II (Rosahl et al., 1995).

Together, our observations demonstrate that a lack of synapsin causes a reduction of the number of synaptic vesicles in CNS neurons. This may involve putative synapsin functions at several key steps of the synaptic vesicle life cycle: (1) synapsins may be important for the biogenesis of SV precursor vesicles at the soma of the neuron and their trafficking to the nerve terminal, which is consistent with a global reduction of SV proteins. An involvement of synapsins in SV biosynthesis also agrees with our finding that TKO calyces contained SVs with larger diameters. Lack of synapsins would result in a decreased delivery of precursors to the presynaptic terminal and subsequent depletion of SVs from the terminal. (2) Synapsins may be required for the efficient reuptake and processing of precursor vesicles exocytosed into the presynaptic plasma membrane (Bradke and Dotti, 2000; Santos et al., 2009). In this model, absence of synapsins would cause an accumulation of precursor vesicles in the membrane of the terminal, which we did not observe. (3) Synapsin-dependent anchoring at the cytoskeleton (Evergren et al., 2007; Greengard et al., 1993; Pieribone et al., 1995) or their mutual crosslinking via dimerization (Gitler et al., 2004b) is required to keep SVs within the presynaptic terminal. In primary hippocampal cultures synapsins seem to be crucial for the dispersion of resting vesicles and might be involved in the control of lateral sharing of vesicles between boutons (Orenbuch et al., 2012a). Consistently, we found a strong

reduction of reserve pool vesicles at mutant synapses. A lack of synapsins might result in the dispersion of part of the resting pool SVs and their subsequent degradation. We could exclude the possibility that vesicles redistribute back to the axon. The calyx of Held contains both actin and tubulin filaments, with actin strongly localizing to the SV cluster and tubulin being located distally from the cluster (Perkins et al., 2010). Therefore, the calyceal compartment can be considered to have dual properties – axon and synaptic terminal.

We consider a combined contribution of model 1 and 3 to be a possible scenario. Lack of synapsin would reduce the production of SV precursors at the soma, the remaining precursor vesicles would suffice to maintain the RRP and parts of the recycling and reserve pools at the terminal, but not the synapsin-dependent part of the resting pool. This part of the pool would not assemble due to the absent synapsin-dependent immobilization of vesicles to the cytoskeleton of the terminal. This model does not depend on the assumption of an elusive mechanism required for sustained SV degradation and takes into account the global decrease in SV proteins in the brain. The recycling pool is distributed within all areas of the terminal (Rizzoli and Betz, 2005) and may represent, in addition to a synapsin-independent resting pool, the small number of SVs found throughout the calyx in TKO mice.

4.3.2. Synapsins do not control calyx maturation and morphology

Our results show that calyces developed and matured properly in the constitutive absence of synapsins. The morphology and size of almost mature calyces at p 14 – 18 was indistinguishable from wild type (Fig. 3.16 – 3.17) and donuts (Wimmer et al., 2006), were present in both genotypes. Furthermore, the number of bassoon-labeled active zones was unchanged while the average AZ size was increased in calyces lacking synapsins. The latter may reflect a homeostatic compensation possibly linked to the increase of the SV diameter in TKO calyces. An increase in SV diameter has been reported in SVs devoid of synapsin I (Awizio et al., 2007) and might be related to the stabilizing effect of synapsins on vesicle lipid bilayers (Pera et al., 2004). The opposite effect was observed in calyces overexpressing synaspin Ia isoform (Fig. 3.14), providing a direct link between synapsin concentration in the presynaptic terminal and vesicle size.

The lack of effect of synapsin gene deletion on the gross morphology of the terminal indicates that synapsins are unlikely to play a pivotal role in the development and maturation of the calyx of Held, in contrast to such a role found in other experimental systems and synapse types (Ferreira et al., 1998; Fornasiero et al., 2009; Kao et al., 2002). Most of the studies have used embryonic cell lines where synapsins apparently modulate the early phase

of neuronal development. Synapsin II might regulate the axonal outgrowth whereas synapsin I might be involved in synapse formation in hippocampal cultures (Ferreira et al., 1998). Experiments done in intact organisms show that the effect of synapsin deletion is highly specific and has varying extent between different brain regions. For example, interference with the PKA-dependent phosphorylation of synapsins leads to decreased neurite outgrowth in *X. laevis* embryos (Kao et al., 2002) and in the hippocampus of adult mice deletion of synapsin III alters neurogenesis and the proliferation of neural progenitor cells (Kao et al., 2008). However, the calyx of Held develops and matures properly in the absence of synapsins, adopting all the necessary morphological changes to allow high fidelity synaptic transmission at high frequencies (Borst & Soria van Hoeve, 2012), arguing against the proposal that synapsins are important for neuronal development and maturation (Chin et al., 1995; Ferreira et al., 1998).

4.3.3. Normal synaptic vesicle organization at active zones and putative compensatory effects

Although deletion of synapsins decreased the total vesicle number within the calyx of Held, vesicles located at different distances from the AZs were differentially affected. While the SVs comprising the synapsin-dependent pool were located more distally from the AZs, the remaining SVs in the TKO terminals primarily formed clusters close to the presynaptic membrane, opposing the soma of the principal cell (Fig. 3.19 and 3.20). Hence, these clusters are synapsin-independent. The number of anatomically docked SVs as well as the SV distribution within the proximal cluster in TKO terminals was normal, similar to a study performed on cultured hippocampal neurons, which also revealed unchanged number of vesicles (Gitler et al., 2004a). However, the SV density within the cluster was decreased, which we attribute to an enlarged surface area of the AZs. A similar phenotype was reported for corticogeniculate terminals of synapsin I/II double mutants (Kielland et al., 2006). The increase in AZ size may result from a compensatory adaptation in the chronic absence of synapsins that aims at keeping the vesicle number constant and alleviates the functional phenotype. Similarly, the increased SV diameter may reflect a compensatory adaptation, although an increase of the SV volume and increase of the amount of glutamate per SV will not necessarily increase the EPSC size. In fact, more glutamate release per vesicle could increase the desensitization of glutamate receptors and therefore would even contribute to synaptic depression. However, mGluR desensitization is present only in immature calyces (p 8 – 10), while absent from mature terminals (p 16 – 18) (Renden et al., 2005). The diffusional

barrier for glutamate at mature calyces is small due to the high fenestration of the presynaptic terminal in mature calyces and diffusion and glutamate transporter activation assure sufficiently fast clearance of presynaptically released glutamate (von Gersdorff and Borst, 2002). Therefore, we can exclude that receptor desensitization, due to release of larger amounts of glutamate per synaptic vesicle, contributes significantly to the increased STD in synapsin TKO terminals. It is more likely that the decreased number of vesicles and the impaired abilities of the remaining SVs to join the RRP under high frequency stimulation underlie the physiological phenotype.

4.3.4. Basal synaptic transmission – largely unaltered by the deletion of synapsins

Deletion of synapsins had only minor consequences on spontaneous and evoked EPSCs. The frequency of spEPSCs was decreased, which would argue for less SVs fusing spontaneously. This might be underlined by the lower SV density at AZs in TKO terminals and/or by the increased vesicle size. However, the number of docked SVs was similar in both genotypes, hence it might be possible that although anatomically docked, these vesicles were not ready to undergo exocytosis. The increased vesicle size might interfere with the dynamics of the SNARE machinery (Rizo and Südhof, 2002). The slowed rise time of the eEPSCs might be related to desynchronization of synaptic transmission (Hilfiker et al., 1998). Altered kinetics of release has been observed also in cholinergic synapses of *Aplysia californica* injected with antibody specific to snail synapsins (Humeau et al., 2001). The rise time of the evoked postsynaptic currents was significantly slowed while the decay time and the amplitude of the currents remained unaffected, similar to our findings. The kinetic changes produced by the deletion of synapsins could result from slowing the reaction that leads to fusion of individual synaptic vesicles, or from desynchronization of the fusion events (Schweizer et al., 1998). Slowing of individual fusion events might result from changes in the dilation of the fusion pore (Rahamimoff and Fernandez, 1997), whereas desynchronization of fusion could arise from the reduction in the number of functional fusogenic particles (Hong et al., 1994; Vogel et al., 1996).

In double knock out mice spontaneous and evoked neurotransmitter release at the calyx of Held was comparable to that in wild type (Sun et al., 2006), raising the possibility that synapsin III may participate in the control of spEPSC frequency and eEPSC rise time at mammalian synapses. Alternatively, this difference may arise from comparing immature (p 9 – 11) and mature (p 14 – 18) synaptic terminals.

4.3.5. Altered short-term plasticity at the calyx of Held in TKO animals

Deletion of all synapsin genes similar to overexpression of synapsin I isoforms led to accelerated and increased short-term depression. The importance of synapsins in short-term depression at the calyx of Held depended on the rate of presynaptic stimulation. At low stimulation frequencies up to 50 Hz WT and TKO calyces did not differ, however, at frequencies exceeding 100 Hz TKO synapses exhibited faster rates and an increased extent of depression (Fig. 3.23 and 3.24). Similar results have been reported for hippocampal cultures from TKO mice (Gitler et al., 2004a) and for immature calyces lacking only synapsins I and II (Sun et al., 2006). These observations match well with the strong decrease of the pool of SVs distal to the AZ, assuming that at high stimulation frequencies the RRP can only be fully maintained through transfer of SVs from both the synapsin-dependent and possible synapsin-independent resting pool, while at lower frequencies the RRP can be maintained by the recycling pool of SVs (de Lange et al., 2003). Several results are consistent with this interpretation: (1) The difference in extend of depression between TKO and WT calyces becomes only evident later (approximately 100 ms at 100 Hz) in the stimulation train (Fig. 3.23); (2) the size of RRP was unchanged in synapsin-deficient terminals (Fig. 3.25); (3) the rate of replenishment of the RRP was decreased (Fig. 3.25); (4) the fast component of recovery from synaptic depression was slowed (Fig. 3.26). This fast component reflects both a calcium-dependent increase in SV replenishment and an increase in the release probability of "reluctant", rapidly replenishing SVs (Hosoi et al., 2007; Müller et al., 2010; Sakaba and Neher, 2001b; Wang and Kaczmarek, 1998; Wu et al., 1999). Nevertheless, the magnitude of the effects of synapsin deletion on refilling the RRP are rather small and active on a time scale of tens of milliseconds after onset of the stimulus, while on a time scale of seconds, synapsin-deficient calyces recover completely and indiscriminately from wild-type synapses (Fig. 3.26 C). Still, 50% of the total number of SVs is lost. This constellation predicts that the resting pool supplies vesicles into the RRP even under conditions of high frequency stimulation, yet the capacity of this process is limited.

In conclusion, synapsins are required to maintain a large portion of SV pools in central glutamatergic terminals, comprising primarily of reserve vesicles. We propose that this could be due to a combined impairment of precursor vesicle biosynthesis at the soma and lack of synaptic vesicle immobilization within the terminal. Surprisingly, this very pronounced structural alteration has only moderate functional consequences: the calyx of Held functions almost normally, apart from a slightly increased short-term depression at transmission frequencies exceeding 100 Hz caused by a reduced rate of SV replenishment and some small

alterations presumed to reflect compensatory mechanisms. The results reported here suggest that a putative synapsin-independent part of the reserve and the recycling pools is capable to maintain a fraction of SVs required for high-frequency transmission by local SV trafficking and recycling. The synapsin-dependent reserve pool, irrespective of constituting 50 % of all SVs in a calyx terminal, contributes only modestly to the refilling of the RRP at high stimulation frequencies. Therefore, the question of why a resting pool is needed, or in other words, why synapsins are needed for sustained synaptic transmission, remains unresolved.

4.4 Summary – mechanisms of synapsins action at the calyx of Held

We could show using two different experimental approaches that synapsins regulate the number of vesicles that are fed into the RRP. Therefore, interaction with synapsins reduces excitatory postsynaptic responses during periods of high-frequency synaptic activity. Synapsins maintain the stability of the vesicle population within the calyx of Held. The synapsin-dependent vesicle pool would provide strategically localized reserve vesicles buffering the depletion of the RRP when sustained and repetitive release overrides the tonic SV-recycling capacity of the terminal through direct (kiss and run or kiss and stay) and/or clathrin-mediated endocytosis (Greengard et al., 1993, Hilfiker et al., 1999). However, the molecular mechanisms behind this phenotype might be different in the two examined cases. While the genetic deletion of the three synapsin genes leads to general failure in the synthesis of SV precursor molecules and concomitant decrease in the number of functional clear core vesicles, the overexpression of synapsin I isoforms at the calyx of Held provokes redistribution of SVs within the proximal vesicle cluster. The overexpressed isoforms might form long protein chains, which fail to bind vesicles efficiently or if bound the distance between the vesicles would be larger. Hence, overexpression of synapsin I isoforms would render SVs more mobile and able to escape the constrains of the proximal vesicle cluster.

Synapsins might be important regulators of the size of the active zones and the associated vesicles. Synapsins determine the boundaries of the AZs – overexpression provoked decrease in the surface area of AZs, while deletion led to an increase. Alternatively, the change of the AZ might be result from the altered size of the SVs. Smaller vesicle diameter, as observed after overexpression would lead to less membrane material incorporated in the presynaptic membrane upon vesicle exocytosis, provided that vesicles undergo full fusion and collapse (Südhof et al., 2004). The opposite effect was observed in the TKO terminals – larger SVs led to larger AZs. Thus, synapsins regulate the stability of lipid bilayers and size of SVs *in vivo*.

Another parameter that is dependent on the synapsin concentration within the presynaptic terminal is the recovery of the RRP at rest following a depleting stimulus train. Although in both experimental paradigms the STD was increased and accelerated, recovery from the depressed state was faster after the introduction of synapsins and slower in the TKOs. This implies that the vesicle turn over at the active zones is differentially controlled by synapsins. We could show that synapsins maintain the faster refilling of the vesicle pool during periods of rest. We cannot exclude that synapsins control post-docking steps of the SV cycle. Vesicle endocytosis and the incorporation of newly endocytosed vesicles into the different pools might be dependent on the concentration or the phosphorylation state of synapsins (Orenbuch et al., 2012b). In both cases the recruitment of vesicles from the intracellular stores would be impaired, due to the decreased number of vesicles found in the terminals. However, synapsins have been also detected in association with SVs of the readily releasable pool and with uncoated recycled vesicles and with actin present at sites of intense SV recycling (Bloom et al., 2003). The overexpression of synapsin I isoforms would lead to higher synapsin concentration at these sites, which might accelerate the physiological function of the protein there.

In conclusion, the major function of synapsins at the calyx of Held is to immobilize SVs and maintain the refilling of the readily releasable pool upon high frequency activity. Genetic perturbations either acute (AAV-mediated overexpression of synapsin I isoforms) or chronic (genetic deletion of all three synapsin genes) did not result in severe malformation and malfunction of the presynaptic terminal, implying that although synapsin-dependent SV pool exists it is not vitally important for the normal synaptic transmission at this synapse. However, synapsins function to fine-tune presynaptic terminals during high-frequency activity when the capacity of the local recycling mechanisms at the active zone is exhausted and distal vesicles are fed into the readily releasable pool. Synapsin-independent local recycling at the presynaptic membrane and vesicle recruitment from a reserve pool defined by a molecular marker other than synapsins might be the dominant pathways for replenishment of the RRP during physiological activity at the calyx of Held.

4.5. Outlook

This study has shown that synapsins are not the only molecular players keeping synaptic vesicles immobile within the CNS terminals, similar to the neuromuscular junction (Gaffield and Betz, 2007). It will be vitally important to map the other proteins, which play role in this process and to unravel their interactions with the complex meshwork of vesicles and

presynaptic cytoskeleton. The vesicle population is decreased by 50 % in TKO animals but these SVs maintain only 20 % of the evoked response during high-frequency activity, provoking the question why does the synapse maintain a huge number of SVs while using only a fraction of them? Another interesting question to answer is how is the proximal vesicle cluster stabilized and how does the synapse distinguishes which vesicle should be associated with the defined pools upon recycling and is synapsin a vesicle landmark in this process? There are two rate-limiting mechanisms at mammalian CNS synapses – (1): baseline rate at which reserve vesicles are supplied to the RRP; (2): supply rate depression when synaptic transmission is driven hard for extended periods of time. Supply rate depresses faster in the synapsin I and II double knock-outs (Gabriel et al., 2011). Measurement of supply rate depression at the calyx of Held in TKO mice would help to estimate the role of the remaining SVs under even more intense stimulation paradigms than the ones used in this study.

The SVs that are used for the replenishment of the readily releasable pool during intense stimulation might originate from intracellular stores (e.g. the reserve pool) or might be recently endocytosed vesicles that are directly fed into the releasable pool. The dramatic reduction in the vesicle number in synapsin-manipulated CNS synapses, does not exclude failures in the endocytotic pathway. Direct capacitance measurements or ultrastructural reconstructions of HRP filled calyces would help to elucidate putative alterations in the vesicle endocytosis at TKO calyces.

Up to now, it was accepted that the decrease in the level of presynaptic proteins is a direct consequence of the decreased number of synaptic vesicles in synapsin-deficient terminals. Here we suggest that the failure in the synthesis of presynaptic proteins leads to less number of vesicles in mutant synapses. We rise the hypothesis that the synthesis of a specific population of presynaptic proteins – vesicle-associated proteins – directly depends on the presence of synapsin in the cells. It remains unclear how synapsins regulate this process and whether the vesicles in TKO terminals contain intact proteome, which will assure normal function. Additionally, it is not known if the alteration in the size of SVs and AZs is directly modulated by synapsins or is it a secondary effect aiming at homeostatic compensation. Thus, synapsins would be annotated a novel function in the control of biogenesis of presynaptic precursor molecules, which would be quite different from the well-established hypothesis of synapsins controlling vesicle immobilization within nerve terminals.

5. Appendix

5.1. Supplementary figures

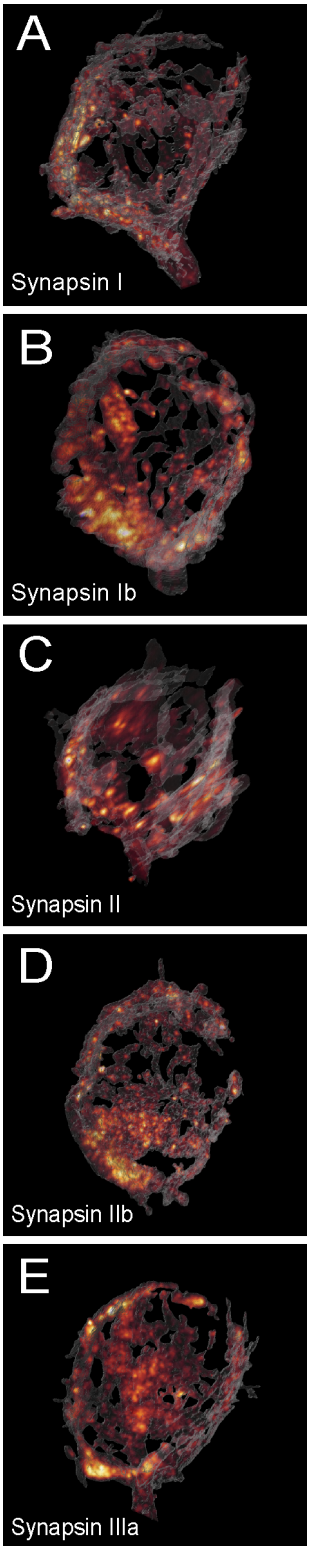

Supplementary figure 1: All synapsin isoforms are expressed within the entire volume of the calyx of Held. 3D reconstructions of the calyces shown in Fig. 3.1 reveal the localization of synapsin isoforms in the calyx of Held.

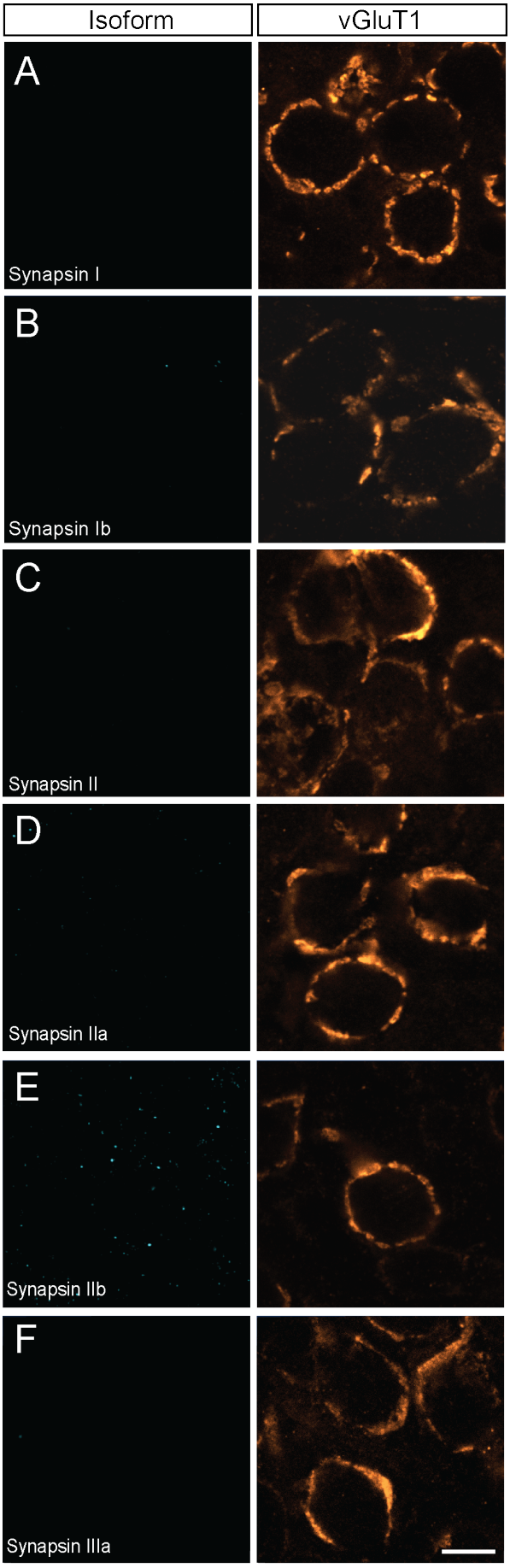

Supplementary figure 2: Synapsin staining is not present in TKOs. All tested synapsin antibodies (left panel) showed no signal when tested on MNTB tissue from TKO mice. vGluT1 stain (right panel) was used as a reference for the presynaptic terminal. Images are presented in pseudo colors. Scale bar: 10 μm.

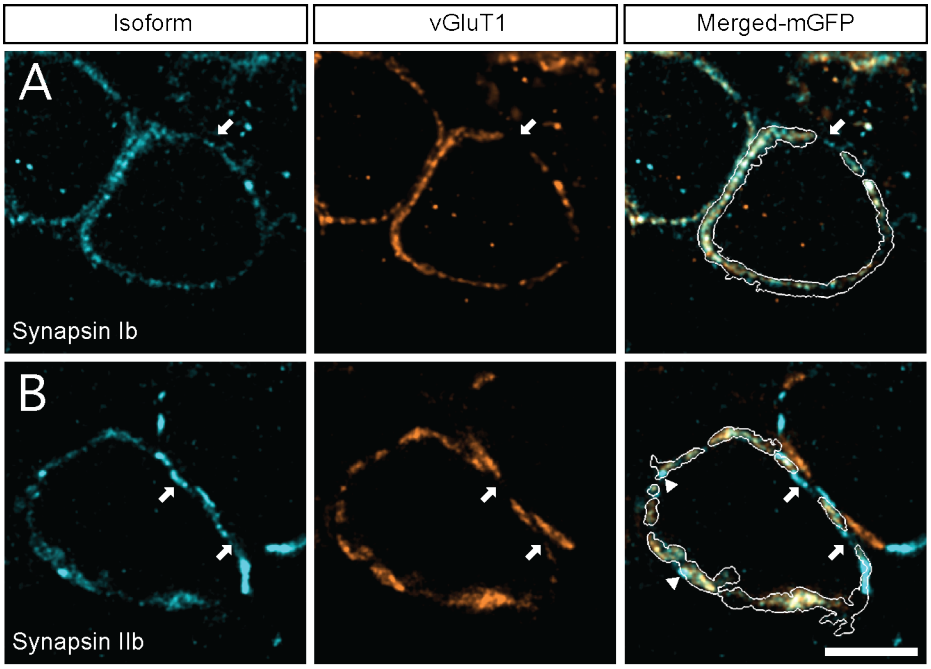

Supplementary Figure 3: Synapsin isoforms colocalize with synaptic vesicles within the calyx of Held. The presynaptic membrane was labeled with mGFP (white outline in the merged images). Distribution of synapsin isoforms (left panel) compared to a SV marker – vGluT1 (central panel), overlay of the corresponding images within the calyx of Held (right panel). Arrowheads indicate synapsin signal outside the vesicle cluster. White arrows point out synapsin-positive clusters outside the mGFP-outlined presynaptic membrane, which do not show vGluT1 positive immunofluorescence. A: synapsin Ib; B: synapsin IIb. Images are presented in pseudo-colors. Scale bars: 10 μm.

5.2. Abbreviations

rAAV	recombinant adeno-associated virus
AMPAR	α-amino-3-hydroxy-5-methyl-4-isoxazolepropionic acid receptor
AP	action potential
APV	D-(-)-2-amino-5-phosphonopentanoic acid
ATP	adenosine triphosphate
aVCN	anterior ventral cochlear nucleus
aCSF	artificial cerebrospinal fluid
AZ	active zone
CaMKI	calcium-calmodulin dependent kinase I
CaMKII	calcium-calmodulin dependent kinase II
CaMKIV	calcium-calmodulin dependent kinase IV
cAMP	cyclic adenosine monophosphate
CAZ	cytoskeletal matrix of the active zone
CNS	central nervous system
CSV	constitutive secretory vesicle
EGFP	enhanced green fluorescent protein
ELISA	enzyme-linked immunosorbent assay
EM	electron microscopy
EPSC	excitatory postsynaptic current
eEPSC	evoked excitatory postsynaptic current
spEPSC	spontaneous excitatory postsynaptic current
ER	endoplasmatic reticulum
EYFP	enhanced yellow fluorescent protein
Erk	extracellular signal regulated kinase
FCS	fetal calf serum
FP	fluorescence protein
GABA	γ-aminobutyric acid
GBC	globular bushy cell
GTP	guanine triphosphate
IPSC	inhibitory postsynaptic current
eIPSC	evoked inhibitory postsynaptic current
LSO	lateral superior olive

MAPK	mitogen-activated protein kinase
mGFP	membrane-bound green fluorescent protein
NA	numerical aperture
NMDAR	N-methyl-D-aspartate receptor
MNTB	medial nucleus of the trapezoid body
NGS	normal goat serum
NMJ	neuromuscular junction
NSF	N-ethylmaleimide-sensitive factor
p	postnatal
P_r	probability of release
PBS	phosphate buffered saline
PFA	paraformaldehyde
PKA	protein kinase A
PM	plasma membrane
PSD	postsynaptic density
PSD-95	postsynaptic density protein 95
PTP	post-tetanic potentiation
PTV	piccolo/bassoon transport vesicle
RIM	Rab3a-interacting molecule
RP	reserve pool
RRP	readily releasable pool
RSV	regulated secretory vesicle
SBC	spherical bushy cell
SEM	standard error of the mean
SD	standard deviation
SM-proteins	Sec1/Munc18-like family of proteins
SNARE	solube N-ethylmaleimide-sensitive factor attachment receptor
SNAP25	synaptosomal-associated protein 25
SOC	superior olivary complex
STD	short-term depression
STF	short-term facilitation
SV	synaptic vesicle
SYN	synapsin gene
TGN	trans Golgi network
TKO	triple knock out

vGluT	vesicular glutamate transporter
V_h	holding potential
WT	wild type

5.3. Acknowledgements

First of all, I would like to express my deepest gratitude to Prof. Dr. Thomas Kuner for giving me the opportunity to work in his lab and for providing the project topic and the financial resources for its fulfillment. His constant interest to the project and scientific discussions were very inspiring in the course of the project.

I would like to thank to Dr. Robert Renden for introducing me to the patch clamp procedure and the calyx of Held physiology, and for performing the electrophysiological experiments accompanying the overexpression project. I thank Heinz Horstmann and Dr. Constanze Geumann (Synaptic Systems) for the collaborations on the EM and ELISA experiments respectively, Dr. Kurt Sätzler for providing insights into the CAR and CARnEval programs.

Special thanks to Dr. Daniel Gitler for proving the synapsin knock-out mouse line and the initial plasmids containing the synapsin I isoforms.

Many thanks to the past and the present members of the Kuner lab as well as the rest of the Medical and Cell Biology department for creating a great working atmosphere, keeping track of lunch times and sunny afternoons in Café Botanik. Thanks to Christoph and Daniel for helpful discussions and technical support in all kinds of problems that I encountered in the lab.

Special thanks to Dr. Darius Schwenger and Franscico Urra for providing the initial IGOR algorithms, to Michaela Keiser and Claudia Kocksch for the excellent technical support that makes life in the lab possible.

And finally, I would like to thank to my family for the continuous support and belief in me.

5.4. References

Ahmari, S.E., Buchanan, J., and Smith, S.J. (2000). Assembly of presynaptic active zones from cytoplasmic transport packets. Nat Neurosci *3*, 445-451.

Akbergenova, Y., and Bykhovskaia, M. (2007). Synapsin maintains the reserve vesicle pool and spatial segregation of the recycling pool in Drosophila presynaptic boutons. Brain Res *1178*, 52-64.

Angleson, J.K., and Betz, W.J. (2001). Intraterminal Ca(2+) and spontaneous transmitter release at the frog neuromuscular junction. J Neurophysiol *85*, 287-294.

Atluri, P.P., and Regehr, W.G. (1996). Determinants of the Time Course of Facilitation at the Granule Cell to Purkinje Cell Synapse. The Journal of Neuroscience *16*, 5661-5671.

Atluri, P.P., and Regehr, W.G. (1998). Delayed release of neurotransmitter from cerebellar granule cells. The Journal of neuroscience : the official journal of the Society for Neuroscience *18*, 8214-8227.

Atwood, H.L., and Karunanithi, S. (2002). Diversification of synaptic strength: presynaptic elements. Nat Rev Neurosci *3*, 497-516.

Awatramani, G.B., Turecek, R., and Trussell, L.O. (2004). Inhibitory control at a synaptic relay. J Neurosci *24*, 2643-2647.

Awatramani, G.B., Turecek, R., and Trussell, L.O. (2005). Staggered development of GABAergic and glycinergic transmission in the MNTB. J Neurophysiol *93*, 819-828.

Awizio, A.-K., Onofri, F., Benfenati, F., and Bonaccurso, E. (2007). Influence of synapsin I on synaptic vesicles: an analysis by force-volume mode of the atomic force microscope and dynamic light scattering. Biophys J *93*, 1051-1060.

Bai, J., and Chapman, E.R. (2004). The C2 domains of synaptotagmin--partners in exocytosis. Trends Biochem Sci *29*, 143-151.

Baitinger, C., and Willard, M. (1987). Axonal transport of synapsin I-like proteins in rabbit retinal ganglion cells. J Neurosci *7*, 3723-3735.

Baldelli, P., Fassio, A., Valtorta, F., and Benfenati, F. (2007). Lack of synapsin I reduces the readily releasable pool of synaptic vesicles at central inhibitory synapses. J Neurosci *27*, 13520-13531.

Barbosa, J., Ferreira, L.T., Martins-Silva, C., Santos, M.S., Torres, G.E., Caron, M.G., Gomez, M.V., Ferguson, S.S.G., Prado, M.A.M., and Prado, V.F. (2002). Trafficking of the vesicular acetylcholine transporter in SN56 cells: a dynamin-sensitive step and interaction with the AP-2 adaptor complex. Journal of neurochemistry *82*, 1221-1228.

Barrett, E.F., and Stevens, C.F. (1972). The kinetics of transmitter release at the frog neuromuscular junction. J Physiol (Lond) *227*, 691-708.

Benfenati, F., Valtorta, F., Rubenstein, J.L., Gorelick, F.S., Greengard, P., and Czernik, A.J. (1992). Synaptic vesicle-associated Ca2+/calmodulin-dependent protein kinase II is a binding protein for synapsin I. Nature *359*, 417-420.

Betz, W.J. (1970). Depression of transmitter release at the neuromuscular junction of the frog. The Journal of physiology *206*, 629-644.

Blatow, M., Caputi, A., Burnashev, N., Monyer, H., and Rozov, A. (2003). Ca2+ Buffer Saturation Underlies Paired Pulse Facilitation in Calbindin-D28k-Containing Terminals. Neuron *38*, 79-88.

Blázquez, M., and Shennan, K.I. (2000). Basic mechanisms of secretion: sorting into the regulated secretory pathway. Biochem Cell Biol *78*, 181-191.

Bloom, O., Evergren, E., Tomilin, N., Kjaerulff, O., Löw, P., Brodin, L., Pieribone, V.A., Greengard, P., and Shupliakov, O. (2003). Colocalization of synapsin and actin during synaptic vesicle recycling. J Cell Biol *161*, 737-747.

Bogen, I.L., Jensen, V., Hvalby, O., and Walaas, S.I. (2009). Synapsin-dependent development of glutamatergic synaptic vesicles and presynaptic plasticity in postnatal mouse brain. Neuroscience *158*, 231-241.

Bonanomi, D., Benfenati, F., and Valtorta, F. (2006). Protein sorting in the synaptic vesicle life cycle. Prog Neurobiol *80*, 177-217.

Borst, J.G., and Sakmann, B. (1996). Calcium influx and transmitter release in a fast CNS synapse. Nature *383*, 431-434.

Borst, J.G.G., and Soria van Hoeve, J. (2012). The calyx of held synapse: from model synapse to auditory relay. Annu Rev Physiol *74*, 199-224.

Bourke, G.J., El Alami, W., Wilson, S.J., Yuan, A., Roobol, A., and Carden, M.J. (2002). Slow axonal transport of the cytosolic chaperonin CCT with Hsc73 and actin in motor neurons. J Neurosci Res *68*, 29-35.

Bourne, J., Morgan, J.R., and Pieribone, V.A. (2006). Actin polymerization regulates clathrin coat maturation during early stages of synaptic vesicle recycling at lamprey synapses. J Comp Neurol *497*, 600-609.

Bradke, F., and Dotti, C.G. (2000). Changes in membrane trafficking and actin dynamics during axon formation in cultured hippocampal neurons. Microsc Res Tech *48*, 3-11.

Brautigam, C.A., Chelliah, Y., and Deisenhofer, J. (2004). Tetramerization and ATP binding by a protein comprising the A, B, and C domains of rat synapsin I. J Biol Chem *279*, 11948-11956.

Ceccarelli, B., and Hurlbut, W.P. (1980). Vesicle hypothesis of the release of quanta of acetylcholine. Physiol Rev *60*, 396-441.

Ceccarelli, B., Hurlbut, W.P., and Mauro, A. (1973). Turnover of transmitter and synaptic vesicles at the frog neuromuscular junction. J Cell Biol *57*, 499-524.

Cesca, F., Baldelli, P., Valtorta, F., and Benfenati, F. (2010). The synapsins: Key actors of synapse function and plasticity. Progress in Neurobiology, 1-36.

Chi, P., Greengard, P., and Ryan, T.A. (2001). Synapsin dispersion and reclustering during synaptic activity. Nat Neurosci *4*, 1187-1193.

Chi, P., Greengard, P., and Ryan, T.A. (2003). Synaptic vesicle mobilization is regulated by distinct synapsin I phosphorylation pathways at different frequencies. Neuron *38*, 69-78.

Chiappalone, M., Casagrande, S., Tedesco, M., Valtorta, F., Baldelli, P., Martinoia, S., and Benfenati, F. (2009). Opposite changes in glutamatergic and GABAergic transmission underlie the diffuse hyperexcitability of synapsin I-deficient cortical networks. Cerebral Cortex *19*, 1422-1439.

Chin, L.S., Li, L., Ferreira, A., Kosik, K.S., and Greengard, P. (1995). Impairment of axonal development and of synaptogenesis in hippocampal neurons of synapsin I-deficient mice. Proc Natl Acad Sci USA *92*, 9230-9234.

De Camilli, P., Cameron, R., and Greengard, P. (1983). Synapsin I (protein I), a nerve terminal-specific phosphoprotein. I. Its general distribution in synapses of the central and peripheral nervous system demonstrated by immunofluorescence in frozen and plastic sections. J Cell Biol *96*, 1337-1354.

de Lange, R.P.J., de Roos, A.D.G., and Borst, J.G.G. (2003). Two modes of vesicle recycling in the rat calyx of Held. J Neurosci *23*, 10164-10173.

del Castillo, J., and Katz, B. (1954). Statistical factors involved in neuromuscular facilitation and depression. J Physiol *124*, 574-585.

Denker (2010). Synaptic vesicle pools: an update. Front Synaptic Neurosci, 1-12.

Denker, A., Bethani, I., Kröhnert, K., Körber, C., Horstmann, H., Wilhelm, B.G., Barysch, S.V., Kuner, T., Neher, E., and Rizzoli, S.O. (2011). A small pool of vesicles maintains synaptic activity in vivo. Proc Natl Acad Sci USA *108*, 17177-17182.

Denker, A., Kröhnert, K., and Rizzoli, S.O. (2009). Revisiting synaptic vesicle pool localization in the Drosophila neuromuscular junction. J Physiol (Lond) *587*, 2919-2926.

Dillman, J.F., Dabney, L.P., and Pfister, K.K. (1996). Cytoplasmic dynein is associated with slow axonal transport. Proc Natl Acad Sci USA *93*, 141-144.

Dondzillo, A., Satzler, K., Horstmann, H., Altrock, W.D., Gundelfinger, E.D., and Kuner, T. (2010). Targeted three-dimensional immunohistochemistry reveals localization of presynaptic proteins Bassoon and Piccolo in the rat calyx of Held before and after the onset of hearing. J Comp Neurol *518*, 1008-1029.

Elmqvist, D., and Quastel, D.M. (1965). A quantitative study of end-plate potentials in isolated human muscle. J Physiol (Lond) *178*, 505-529.

Esser, L., Wang, C.R., Hosaka, M., Smagula, C.S., Südhof, T.C., and Deisenhofer, J. (1998). Synapsin I is structurally similar to ATP-utilizing enzymes. EMBO J *17*, 977-984.

Evergren, E., Benfenati, F., and Shupliakov, O. (2007). The synapsin cycle: a view from the synaptic endocytic zone. J Neurosci Res *85*, 2648-2656.

Evergren, E., Zotova, E., Brodin, L., and Shupliakov, O. (2006). Differential efficiency of the endocytic machinery in tonic and phasic synapses. Neuroscience *141*, 123-131.

Farisello, P., Boido, D., Nieus, T., Medrihan, L., Cesca, F., Valtorta, F., Baldelli, P., and Benfenati, F. (2012). Synaptic and Extrasynaptic Origin of the Excitation/Inhibition Imbalance in the Hippocampus of Synapsin I/II/III Knockout Mice. Cerebral Cortex, 1-13.

Fassio, A., Merlo, D., Mapelli, J., Menegon, A., Corradi, A., Mete, M., Zappettini, S., Bonanno, G., Valtorta, F., D'Angelo, E.*, et al.* (2006). The synapsin domain E accelerates the exoendocytotic cycle of synaptic vesicles in cerebellar Purkinje cells. J Cell Sci *119*, 4257-4268.

Fatt, P., and Katz, B. (1952). Spontaneous subthreshold activity at motor nerve endings. J Physiol (Lond) *117*, 109-128.

Feldman, D.E. (2009). Synaptic mechanisms for plasticity in neocortex. Annu Rev Neurosci *32*, 33-55.

Feng, J., Chi, P., Blanpied, T.A., Xu, Y., Magarinos, A.M., Ferreira, A., Takahashi, R.H., Kao, H.-T., Mcewen, B.S., Ryan, T.A.*, et al.* (2002). Regulation of neurotransmitter release by synapsin III. Journal of Neuroscience *22*, 4372-4380.

Ferreira, A., Chin, L.S., Li, L., Lanier, L.M., Kosik, K.S., and Greengard, P. (1998). Distinct roles of synapsin I and synapsin II during neuronal development. Mol Med *4*, 22-28.

Ferreira, A., Kao, H.T., Feng, J., Rapoport, M., and Greengard, P. (2000). Synapsin III: developmental expression, subcellular localization, and role in axon formation. Journal of Neuroscience *20*, 3736-3744.

Ferreira, A., and Rapoport, M. (2002). The synapsins: beyond the regulation of neurotransmitter release. Cell Mol Life Sci *59*, 589-595.

Fioravante, D., Liu, R.-Y., Netek, A.K., Cleary, L.J., and Byrne, J.H. (2007). Synapsin regulates Basal synaptic strength, synaptic depression, and serotonin-induced facilitation of sensorimotor synapses in Aplysia. J Neurophysiol *98*, 3568-3580.

Fioravante, D., and Regehr, W.G. (2011). Short-term forms of presynaptic plasticity. Curr Opin Neurobiol *21*, 269-274.

Fletcher, T.L., Cameron, P., De Camilli, P., and Banker, G. (1991). The distribution of synapsin I and synaptophysin in hippocampal neurons developing in culture. J Neurosci *11*, 1617-1626.

Fornasiero, E.F., Bonanomi, D., Benfenati, F., and Valtorta, F. (2009). The role of synapsins in neuronal development. Cell Mol Life Sci.

Forsythe, I.D., Tsujimoto, T., Barnes-Davies, M., Cuttle, M.F., and Takahashi, T. (1998). Inactivation of Presynaptic Calcium Current Contributes to Synaptic Depression at a Fast Central Synapse. Neuron *20*, 797-807.

Fredj, N.B., and Burrone, J. (2009). A resting pool of vesicles is responsible for spontaneous vesicle fusion at the synapse. Nat Neurosci *12*, 751-758.

Futai, K., Okada, M., Matsuyama, K., and Takahashi, T. (2001). High-fidelity transmission acquired via a developmental decrease in NMDA receptor expression at an auditory synapse. J Neurosci *21*, 3342-3349.

Gabriel, T., García-Pérez, E., Mahfooz, K., Goñi, J., Martínez-Turrillas, R., Pérez-Otaño, I., Lo, D.C., and Wesseling, J.F. (2011). A new kinetic framework for synaptic vesicle trafficking tested in synapsin knock-outs. J Neurosci *31*, 11563-11577.

Gaffield, M.A., and Betz, W.J. (2007). Synaptic vesicle mobility in mouse motor nerve terminals with and without synapsin. Journal of Neuroscience *27*, 13691-13700.

Gaffield, M.A., Rizzoli, S.O., and Betz, W.J. (2006). Mobility of synaptic vesicles in different pools in resting and stimulated frog motor nerve terminals. Neuron *51*, 317-325.

Geumann, C., Grønborg, M., Hellwig, M., Martens, H., and Jahn, R. (2010). A sandwich enzyme-linked immunosorbent assay for the quantification of insoluble membrane and scaffold proteins. Anal Biochem *402*, 161-169.

Giovedì, S., Darchen, F., Valtorta, F., Greengard, P., and Benfenati, F. (2004a). Synapsin is a novel Rab3 effector protein on small synaptic vesicles. II. Functional effects of the Rab3A-synapsin I interaction. J Biol Chem *279*, 43769-43779.

Giovedì, S., Vaccaro, P., Valtorta, F., Darchen, F., Greengard, P., Cesareni, G., and Benfenati, F. (2004b). Synapsin is a novel Rab3 effector protein on small synaptic vesicles. I. Identification and characterization of the synapsin I-Rab3 interactions in vitro and in intact nerve terminals. J Biol Chem *279*, 43760-43768.

Giraudo, C.G., Eng, W.S., Melia, T.J., and Rothman, J.E. (2006). A clamping mechanism involved in SNARE-dependent exocytosis. Science *313*, 676-680.

Gitler, D., Cheng, Q., Greengard, P., and Augustine, G.J. (2008). Synapsin IIa controls the reserve pool of glutamatergic synaptic vesicles. Journal of Neuroscience *28*, 10835-10843.

Gitler, D., Takagishi, Y., Feng, J., Ren, Y., Rodriguiz, R.M., Wetsel, W.C., Greengard, P., and Augustine, G.J. (2004a). Different presynaptic roles of synapsins at excitatory and inhibitory synapses. Journal of Neuroscience *24*, 11368-11380.

Gitler, D., Xu, Y., Kao, H.-T., Lin, D., Lim, S., Feng, J., Greengard, P., and Augustine, G.J. (2004b). Molecular determinants of synapsin targeting to presynaptic terminals. Journal of Neuroscience *24*, 3711-3720.

Goldstein, A.Y.N., Wang, X., and Schwarz, T.L. (2008). Axonal transport and the delivery of pre-synaptic components. Curr Opin Neurobiol *18*, 495-503.

Grande, G., and Wang, L.-Y. (2011). Morphological and functional continuum underlying heterogeneity in the spiking fidelity at the calyx of Held synapse in vitro. The Journal of neuroscience : the official journal of the Society for Neuroscience *31*, 13386-13399.

Greengard, P., Valtorta, F., Czernik, A.J., and Benfenati, F. (1993). Synaptic vesicle phosphoproteins and regulation of synaptic function. Science *259*, 780-785.

Grimm, D., Kay, M.A., and Kleinschmidt, J.A. (2003). Helper virus-free, optically controllable, and two-plasmid-based production of adeno-associated virus vectors of serotypes 1 to 6. Mol Ther *7*, 839-850.

Groemer, T.W., and Klingauf, J. (2007). Synaptic vesicles recycling spontaneously and during activity belong to the same vesicle pool. Nat Neurosci *10*, 145-147.

Grothe, B., Pecka, M., and McAlpine, D. (2010). Mechanisms of sound localization in mammals. Physiol Rev *90*, 983-1012.

Guinan, J.J., and Li, R.Y. (1990). Signal processing in brainstem auditory neurons which receive giant endings (calyces of Held) in the medial nucleus of the trapezoid body of the cat. Hear Res *49*, 321-334.

Gundelfinger, E.D., and Fejtova, A. (2011). Molecular organization and plasticity of the cytomatrix at the active zone. Curr Opin Neurobiol.

Gundelfinger, E.D., Kessels, M.M., and Qualmann, B. (2003). Temporal and spatial coordination of exocytosis and endocytosis. Nat Rev Mol Cell Biol *4*, 127-139.

Hackett, J.T., Cochran, S.L., Greenfield, L.J., Brosius, D.C., and Ueda, T. (1990). Synapsin I injected presynaptically into goldfish mauthner axons reduces quantal synaptic transmission. J Neurophysiol *63*, 701-706.

Hamann, M., Billups, B., and Forsythe, I.D. (2003). Non-calyceal excitatory inputs mediate low fidelity synaptic transmission in rat auditory brainstem slices. Eur J Neurosci *18*, 2899-2902.

Hannah, M.J., Schmidt, A.A., and Huttner, W.B. (1999). Synaptic vesicle biogenesis. Annu Rev Cell Dev Biol *15*, 733-798.

Hanse, E., and Gustafsson, B. (2001). Vesicle release probability and pre-primed pool at glutamatergic synapses in area CA1 of the rat neonatal hippocampus. J Physiol (Lond) *531*, 481-493.

Hanse, E., and Gustafsson, B. (2002). Release dependence to a paired stimulus at a synaptic release site with a small variable pool of immediately releasable vesicles. J Neurosci *22*, 4381-4387.

Harata, N., Ryan, T.A., Smith, S.J., Buchanan, J., and Tsien, R.W. (2001). Visualizing recycling synaptic vesicles in hippocampal neurons by FM 1-43 photoconversion. Proc Natl Acad Sci USA *98*, 12748-12753.

Harris, K.M., Perry, E., Bourne, J., Feinberg, M., Ostroff, L., and Hurlburt, J. (2006). Uniform serial sectioning for transmission electron microscopy. J Neurosci *26*, 12101-12103.

He, L., Wu, X.-S., Mohan, R., and Wu, L.-G. (2006). Two modes of fusion pore opening revealed by cell-attached recordings at a synapse. Nature *444*, 102-105.

Held, H. (1893). Die zentrale Gehörleitung. Arch Anat Physiol Anat Abt, 201-248.

Heuser, J., and Reese, T. (1981). Structural changes after transmitter release at the frog neuromuscular junction. THE JOURNAL OF CELL BIOLOGY *88*, 564-580.

Heuser, J., Reese, T., Dennis, M., Jan, Y., Jan, L., and Evans, L. (1979). SYNAPTIC VESICLE EXOCYTOSIS CAPTURED BY QUICK FREEZING AND CORRELATED WITH QUANTAL TRANSMITTER RELEASE. J Cell Biology *81*, 275-300.

Heuser, J.E., and Reese, T.S. (1973). Evidence for recycling of synaptic vesicle membrane during transmitter release at the frog neuromuscular junction. J Cell Biol *57*, 315-344.

Hilfiker, S., Benfenati, F., Doussau, F., Nairn, A.C., Czernik, A.J., Augustine, G.J., and Greengard, P. (2005). Structural domains involved in the regulation of transmitter release by synapsins. Journal of Neuroscience *25*, 2658-2669.

Hilfiker, S., Pieribone, V.A., Czernik, A.J., Kao, H.T., Augustine, G.J., and Greengard, P. (1999). Synapsins as regulators of neurotransmitter release. Philos Trans R Soc Lond, B, Biol Sci *354*, 269-279.

Hilfiker, S., Schweizer, F.E., Kao, H.T., Czernik, A.J., Greengard, P., and Augustine, G.J. (1998). Two sites of action for synapsin domain E in regulating neurotransmitter release. Nat Neurosci *1*, 29-35.

Hirokawa, N., and Takemura, R. (2005). Molecular motors and mechanisms of directional transport in neurons. Nat Rev Neurosci *6*, 201-214.

Hodgkin, A.L., and Huxley, A.F. (1945). Resting and action potentials in single nerve fibres. The Journal of physiology *104*, 176-195.

Holt, M., Cooke, A., Neef, A., and Lagnado, L. (2004). High mobility of vesicles supports continuous exocytosis at a ribbon synapse. Curr Biol *14*, 173-183.

Holtzman, E. (1977). The origin and fate of secretory packages, especially synaptic vesicles. Neuroscience *2*, 327-355.

Hong, R.M., Mori, H., Fukui, T., Moriyama, Y., Futai, M., Yamamoto, A., Tashiro, Y., and Tagaya, M. (1994). Association of N-ethylmaleimide-sensitive factor with synaptic vesicles. FEBS Lett *350*, 253-257.

Horstmann, H., Körber, C., Sätzler, K., Aydin, D., and Kuner, T. (2012). Serial Section Scanning Electron Microscopy (S(3)EM) on Silicon Wafers for Ultra-Structural Volume Imaging of Cells and Tissues. PLoS ONE *7*, e35172.

Hosaka, M., Hammer, R.E., and Südhof, T.C. (1999). A phospho-switch controls the dynamic association of synapsins with synaptic vesicles. Neuron *24*, 377-387.

Hosaka, M., and Südhof, T.C. (1998a). Synapsin III, a novel synapsin with an unusual regulation by Ca2+. J Biol Chem *273*, 13371-13374.

Hosaka, M., and Südhof, T.C. (1998b). Synapsins I and II are ATP-binding proteins with differential Ca2+ regulation. J Biol Chem *273*, 1425-1429.

Hosaka, M., and Südhof, T.C. (1999). Homo- and heterodimerization of synapsins. J Biol Chem *274*, 16747-16753.

Hosoi, N., Holt, M., and Sakaba, T. (2009). Calcium dependence of exo- and endocytotic coupling at a glutamatergic synapse. Neuron *63*, 216-229.

Hosoi, N., Sakaba, T., and Neher, E. (2007). Quantitative analysis of calcium-dependent vesicle recruitment and its functional role at the calyx of Held synapse. Journal of Neuroscience *27*, 14286-14298.

Humeau, Y., Doussau, F., Vitiello, F., Greengard, P., Benfenati, F., and Poulain, B. (2001). Synapsin controls both reserve and releasable synaptic vesicle pools during neuronal activity and short-term plasticity in Aplysia. Journal of Neuroscience *21*, 4195-4206.

Inchauspe, C.G., Martini, F.J., Forsythe, I.D., and Uchitel, O.D. (2004). Functional compensation of P/Q by N-type channels blocks short-term plasticity at the calyx of held presynaptic terminal. J Neurosci *24*, 10379-10383.

Ishikawa, T., Kaneko, M., Shin, H.-S., and Takahashi, T. (2005). Presynaptic N-type and P/Q-type Ca2+ channels mediating synaptic transmission at the calyx of Held of mice. J Physiol (Lond) *568*, 199-209.

Iwasaki, S., and Takahashi, T. (2001). Developmental regulation of transmitter release at the calyx of Held in rat auditory brainstem. The Journal of physiology *534*, 861-871.

Janetzko, A., Zimmermann, H., and Volknandt, W. (1989). Intraneuronal distribution of a synaptic vesicle membrane protein: antibody binding sites at axonal membrane compartments and trans-Golgi network and accumulation at nodes of Ranvier. Neuroscience *32*, 65-77.

Job, C., and Lagnado, L. (1998). Calcium and protein kinase C regulate the actin cytoskeleton in the synaptic terminal of retinal bipolar cells. J Cell Biol *143*, 1661-1672.

Johnson, E.M., Ueda, T., Maeno, H., and Greengard, P. (1972). Adenosine 3',5-monophosphate-dependent phosphorylation of a specific protein in synaptic membrane fractions from rat cerebrum. J Biol Chem *247*, 5650-5652.

Joshi, I., and Wang, L.-Y. (2002). Developmental profiles of glutamate receptors and synaptic transmission at a single synapse in the mouse auditory brainstem. J Physiol (Lond) *540*, 861-873.

Kamin, D., Lauterbach, M.A., Westphal, V., Keller, J., Schönle, A., Hell, S.W., and Rizzoli, S.O. (2010). High- and low-mobility stages in the synaptic vesicle cycle. Biophys J *99*, 675-684.

Kandler, K., and Friauf, E. (1993). Pre- and postnatal development of efferent connections of the cochlear nucleus in the rat. J Comp Neurol *328*, 161-184.

Kao, H.-T., Li, P., Chao, H.M., Janoschka, S., Pham, K., Feng, J., Mcewen, B.S., Greengard, P., Pieribone, V.A., and Porton, B. (2008). Early involvement of synapsin III in neural progenitor cell development in the adult hippocampus. J Comp Neurol *507*, 1860-1870.

Kao, H.-T., Song, H.-j., Porton, B., Ming, G.-l., Hoh, J., Abraham, M., Czernik, A.J., Pieribone, V.A., Poo, M.-m., and Greengard, P. (2002). A protein kinase A-dependent molecular switch in synapsins regulates neurite outgrowth. Nat Neurosci *5*, 431-437.

Kao, H.T., Porton, B., Czernik, A.J., Feng, J., Yiu, G., Häring, M., Benfenati, F., and Greengard, P. (1998). A third member of the synapsin gene family. Proc Natl Acad Sci USA *95*, 4667-4672.

Katz, B. (1971). Quantal mechanism of neural transmitter release. Science *173*, 123-126.

Katz, B., and Miledi, R. (1968). The role of calcium in neuromuscular facilitation. J Phy8iol *195*, 481-492.

Katz, B., and Miledi, R. (1969a). Spontaneous and evoked activity of motor nerve endings in calcium Ringer. J Physiol (Lond) *203*, 689-706.

Katz, B., and Miledi, R. (1969b). Tetrodotoxin-resistant electric activity in presynaptic terminals. J Physiol (Lond) *203*, 459-487.

Kielland, A., Erisir, A., Walaas, S.I., and Heggelund, P. (2006). Synapsin utilization differs among functional classes of synapses on thalamocortical cells. J Neurosci *26*, 5786-5793.

Kile, B.M., Guillot, T.S., Venton, B.J., Wetsel, W.C., Augustine, G.J., and Wightman, R.M. (2010). Synapsins differentially control dopamine and serotonin release. J Neurosci *30*, 9762-9770.

Kim, S., Ko, J., Shin, H., Lee, J.-R., Lim, C., Han, J.-H., Altrock, W.D., Garner, C.C., Gundelfinger, E.D., Premont, R.T.*, et al.* (2003). The GIT family of proteins forms multimers and associates with the presynaptic cytomatrix protein Piccolo. J Biol Chem *278*, 6291-6300.

Klugmann, M., Symes, C.W., Leichtlein, C.B., Klaussner, B.K., Dunning, J., Fong, D., Young, D., and During, M.J. (2005). AAV-mediated hippocampal expression of short and long Homer 1 proteins differentially affect cognition and seizure activity in adult rats. Mol Cell Neurosci *28*, 347-360.

Kuromi, H., and Kidokoro, Y. (1998). Two distinct pools of synaptic vesicles in single presynaptic boutons in a temperature-sensitive Drosophila mutant, shibire. Neuron *20*, 917-925.

Kusano, K., and Landau, E.M. (1975). Depression and recovery of transmission at the squid giant synapse. J Physiol (Lond) *245*, 13-32.

Kushmerick, C., Renden, R., and von Gersdorff, H. (2006). Physiological temperatures reduce the rate of vesicle pool depletion and short-term depression via an acceleration of vesicle recruitment. J Neurosci *26*, 1366-1377.

Lee, J.S., Kim, M.-H., Ho, W.-K., and Lee, S.-H. (2008). Presynaptic release probability and readily releasable pool size are regulated by two independent mechanisms during posttetanic potentiation at the calyx of Held synapse. J Neurosci *28*, 7945-7953.

Leenders, A.G., Lopes da Silva, F.H., Ghijsen, W.E., and Verhage, M. (2001). Rab3a is involved in transport of synaptic vesicles to the active zone in mouse brain nerve terminals. Mol Biol Cell *12*, 3095-3102.

Lenn, N.J., and Reese, T.S. (1966). The fine structure of nerve endings in the nucleus of the trapezoid body and the ventral cochlear nucleus. Am J Anat *118*, 375-389.

Li, L., Chin, L.S., Greengard, P., Copeland, N.G., Gilbert, D.J., and Jenkins, N.A. (1995a). Localization of the synapsin II (SYN2) gene to human chromosome 3 and mouse chromosome 6. Genomics *28*, 365-366.

Li, L., Chin, L.S., Shupliakov, O., Brodin, L., Sihra, T.S., Hvalby, O., Jensen, V., Zheng, D., McNamara, J.O., and Greengard, P. (1995b). Impairment of synaptic vesicle clustering and of synaptic transmission, and increased seizure propensity, in synapsin I-deficient mice. Proc Natl Acad Sci USA *92*, 9235-9239.

Liley, A.W., and North, K.A. (1953). An electrical investigation of effects of repetitive stimulation on mammalian neuromuscular junction. J Neurophysiol *16*, 509-527.

Lisman, J.E., Raghavachari, S., and Tsien, R.W. (2007). The sequence of events that underlie quantal transmission at central glutamatergic synapses. Nat Rev Neurosci *8*, 597-609.

Llinás, R., McGuinness, T.L., Leonard, C.S., Sugimori, M., and Greengard, P. (1985). Intraterminal injection of synapsin I or calcium/calmodulin-dependent protein kinase II alters neurotransmitter release at the squid giant synapse. Proc Natl Acad Sci USA *82*, 3035-3039.

Mandell, J.W., Czernik, A.J., De Camilli, P., Greengard, P., and Townes-Anderson, E. (1992). Differential expression of synapsins I and II among rat retinal synapses. The Journal of neuroscience : the official journal of the Society for Neuroscience *12*, 1736-1749.

Mandell, J.W., Townes-Anderson, E., Czernik, A.J., Cameron, R., Greengard, P., and De Camilli, P. (1990). Synapsins in the vertebrate retina: absence from ribbon synapses and heterogeneous distribution among conventional synapses. Neuron *5*, 19-33.

Matus-Leibovitch, N., Nevo, I., and Vogel, Z. (1997). Differential distribution of synapsin IIa and IIb mRNAs in various brain structures and the effect of chronic morphine administration on the regional expression of these isoforms. Brain Res Mol Brain Res *45*, 301-316.

Matveev, V., Zucker, R.S., and Sherman, A. (2004). Facilitation through buffer saturation: constraints on endogenous buffering properties. Biophysical Journal *86*, 2691-2709.

Maximov, A., and Südhof, T.C. (2005). Autonomous function of synaptotagmin 1 in triggering synchronous release independent of asynchronous release. Neuron *48*, 547-554.

McPherson, P.S., Czernik, A.J., Chilcote, T.J., Onofri, F., Benfenati, F., Greengard, P., Schlessinger, J., and De Camilli, P. (1994). Interaction of Grb2 via its Src homology 3 domains with synaptic proteins including synapsin I. Proc Natl Acad Sci USA *91*, 6486-6490.

Meinrenken, C.J., Borst, J.G.G., and Sakmann, B. (2002). Calcium secretion coupling at calyx of held governed by nonuniform channel-vesicle topography. J Neurosci *22*, 1648-1667.

Mennerick, S., and Matthews, G. (1996). Ultrafast exocytosis elicited by calcium current in synaptic terminals of retinal bipolar neurons. Neuron *17*, 1241-1249.

Monaldi, I., Vassalli, M., Bachi, A., Giovedì, S., Millo, E., Valtorta, F., Raiteri, R., Benfenati, F., and Fassio, A. (2010). The highly conserved synapsin domain E mediates synapsin dimerization and phospholipid vesicle clustering. Biochem J *426*, 55-64.

Müller, M., Goutman, J.D., Kochubey, O., and Schneggenburger, R. (2010). Interaction between facilitation and depression at a large CNS synapse reveals mechanisms of short-term plasticity. J Neurosci *30*, 2007-2016.

Nakajima, Y. (1971). Fine structure of the medial nucleus of the trapezoid body of the bat with special reference to two types of synaptic endings. J Cell Biol *50*, 121-134.

Neher, E. (1998). Vesicle Pools and Ca2+ Microdomains: New Tools for Understanding Their Roles in Neurotransmitter Release. Neuron *20*, 389-399.

Neher, E. (2010). What is Rate-Limiting during Sustained Synaptic Activity: Vesicle Supply or the Availability of Release Sites. Front Synaptic Neurosci *2*, 144.

Neher, E., and Sakaba, T. (2001). Estimating transmitter release rates from postsynaptic current fluctuations. Journal of Neuroscience *21*, 9638-9654.

Neher, E., and Sakaba, T. (2008). Multiple roles of calcium ions in the regulation of neurotransmitter release. Neuron *59*, 861-872.

Neves, G., and Lagnado, L. (1999). The kinetics of exocytosis and endocytosis in the synaptic terminal of goldfish retinal bipolar cells. J Physiol (Lond) *515 (Pt 1)*, 181-202.

Ohtsuka, T., Takao-Rikitsu, E., Inoue, E., Inoue, M., Takeuchi, M., Matsubara, K., Deguchi-Tawarada, M., Satoh, K., Morimoto, K., Nakanishi, H.*, et al.* (2002). Cast: a novel

protein of the cytomatrix at the active zone of synapses that forms a ternary complex with RIM1 and munc13-1. J Cell Biol *158*, 577-590.

Onofri, F., Giovedì, S., Vaccaro, P., Czernik, A.J., Valtorta, F., De Camilli, P., Greengard, P., and Benfenati, F. (1997). Synapsin I interacts with c-Src and stimulates its tyrosine kinase activity. Proc Natl Acad Sci USA *94*, 12168-12173.

Onofri, F., Messa, M., Matafora, V., Bonanno, G., Corradi, A., Bachi, A., Valtorta, F., and Benfenati, F. (2007). Synapsin phosphorylation by SRC tyrosine kinase enhances SRC activity in synaptic vesicles. J Biol Chem *282*, 15754-15767.

Orenbuch, A., Shalev, L., Marra, V., Sinai, I., Lavy, Y., Kahn, J., Burden, J.J., Staras, K., and Gitler, D. (2012a). Synapsin selectively controls the mobility of resting pool vesicles at hippocampal terminals. J Neurosci *32*, 3969-3980.

Orenbuch, A., Shulman, Y., Lipstein, N., Bechar, A., Lavy, Y., Brumer, E., Vasileva, M., Kahn, J., Barki-Harrington, L., Kuner, T.*, et al.* (2012b). Inhibition of exocytosis or endocytosis blocks activity-dependent redistribution of synapsin. Journal of neurochemistry *120*, 248-258.

Pera, I., Stark, R., Kappl, M., Butt, H.-J., and Benfenati, F. (2004). Using the atomic force microscope to study the interaction between two solid supported lipid bilayers and the influence of synapsin I. Biophys J *87*, 2446-2455.

Perkins, G.A., Tjong, J., Brown, J.M., Poquiz, P.H., Scott, R.T., Kolson, D.R., Ellisman, M.H., and Spirou, G.A. (2010). The micro-architecture of mitochondria at active zones: electron tomography reveals novel anchoring scaffolds and cristae structured for high-rate metabolism. J Neurosci *30*, 1015-1026.

Petrucci, T.C., and Morrow, J.S. (1987). Synapsin I: an actin-bundling protein under phosphorylation control. J Cell Biol *105*, 1355-1363.

Pieribone, V.A., Porton, B., Rendon, B., Feng, J., Greengard, P., and Kao, H.-T. (2002). Expression of synapsin III in nerve terminals and neurogenic regions of the adult brain. J Comp Neurol *454*, 105-114.

Pieribone, V.A., Shupliakov, O., Brodin, L., Hilfiker-Rothenfluh, S., Czernik, A.J., and Greengard, P. (1995). Distinct pools of synaptic vesicles in neurotransmitter release. Nature *375*, 493-497.

Porton, B., Kao, H.T., and Greengard, P. (1999). Characterization of transcripts from the synapsin III gene locus. Journal of neurochemistry *73*, 2266-2271.

Prado, V.F., and Prado, M.A.M. (2002). Signals involved in targeting membrane proteins to synaptic vesicles. Cell Mol Neurobiol *22*, 565-577.

Rahamimoff, R., and Fernandez, J.M. (1997). Pre- and postfusion regulation of transmitter release. Neuron *18*, 17-27.

Ramirez, Denise M.O., Khvotchev, M., Trauterman, B., and Kavalali, Ege T. (2012). Vti1a Identifies a Vesicle Pool that Preferentially Recycles at Rest and Maintains Spontaneous Neurotransmission. Neuron *73*, 121-134.

Régnier-Vigouroux, A., Tooze, S.A., and Huttner, W.B. (1991). Newly synthesized synaptophysin is transported to synaptic-like microvesicles via constitutive secretory vesicles and the plasma membrane. EMBO J *10*, 3589-3601.

Reim, K., Mansour, M., Varoqueaux, F., McMahon, H.T., Südhof, T.C., Brose, N., and Rosenmund, C. (2001). Complexins regulate a late step in Ca2+-dependent neurotransmitter release. Cell *104*, 71-81.

Renden, R., Taschenberger, H., Puente, N., Rusakov, D.A., Duvoisin, R., Wang, L.-Y., Lehre, K.P., and von Gersdorff, H. (2005). Glutamate transporter studies reveal the pruning of metabotropic glutamate receptors and absence of AMPA receptor desensitization at mature calyx of held synapses. Journal of Neuroscience *25*, 8482-8497.

Rettig, J., and Neher, E. (2002). Emerging roles of presynaptic proteins in Ca++-triggered exocytosis. Science *298*, 781-785.

Richards, D.A., Guatimosim, C., and Betz, W.J. (2000). Two endocytic recycling routes selectively fill two vesicle pools in frog motor nerve terminals. Neuron *27*, 551-559.

Richards, D.A., Guatimosim, C., Rizzoli, S.O., and Betz, W.J. (2003). Synaptic vesicle pools at the frog neuromuscular junction. Neuron *39*, 529-541.

Rizo, J., and Rosenmund, C. (2008). Synaptic vesicle fusion. Nat Struct Mol Biol *15*, 665-674.

Rizo, J., and Südhof, T.C. (2002). Snares and Munc18 in synaptic vesicle fusion. Nat Rev Neurosci *3*, 641-653.

Rizzoli, S.O., and Betz, W.J. (2004). The structural organization of the readily releasable pool of synaptic vesicles. Science *303*, 2037-2039.

Rizzoli, S.O., and Betz, W.J. (2005). Synaptic vesicle pools. Nat Rev Neurosci *6*, 57-69.

Rosahl, T.W., Geppert, M., Spillane, D., Herz, J., Hammer, R.E., Malenka, R.C., and Südhof, T.C. (1993). Short-term synaptic plasticity is altered in mice lacking synapsin I. Cell *75*, 661-670.

Rosahl, T.W., Spillane, D., Missler, M., Herz, J., Selig, D.K., Wolff, J.R., Hammer, R.E., Malenka, R.C., and Südhof, T.C. (1995). Essential functions of synapsins I and II in synaptic vesicle regulation. Nature *375*, 488-493.

Rosenmund, C., and Stevens, C.F. (1996). Definition of the readily releasable pool of vesicles at hippocampal synapses. Neuron *16*, 1197-1207.

Rowland, K.C., Irby, N.K., and Spirou, G.A. (2000). Specialized synapse-associated structures within the calyx of Held. J Neurosci *20*, 9135-9144.

Roy, S., Winton, M.J., Black, M.M., Trojanowski, J.Q., and Lee, V.M.-Y. (2007). Rapid and intermittent cotransport of slow component-b proteins. J Neurosci *27*, 3131-3138.

Roy, S., Winton, M.J., Black, M.M., Trojanowski, J.Q., and Lee, V.M.-Y. (2008). Cytoskeletal requirements in axonal transport of slow component-b. J Neurosci *28*, 5248-5256.

Ryan, T.A., Li, L., Chin, L.S., Greengard, P., and Smith, S.J. (1996). Synaptic vesicle recycling in synapsin I knock-out mice. J Cell Biol *134*, 1219-1227.

Sabatini, B.L., and Regehr, W.G. (1996). Timing of neurotransmission at fast synapses in the mammalian brain. Nature *384*, 170-172.

Sakaba, T. (2006). Roles of the fast-releasing and the slowly releasing vesicles in synaptic transmission at the calyx of held. Journal of Neuroscience *26*, 5863-5871.

Sakaba, T., and Neher, E. (2001a). Calmodulin mediates rapid recruitment of fast-releasing synaptic vesicles at a calyx-type synapse. Neuron *32*, 1119-1131.

Sakaba, T., and Neher, E. (2001b). Quantitative relationship between transmitter release and calcium current at the calyx of held synapse. Journal of Neuroscience *21*, 462-476.

Sakaba, T., and Neher, E. (2003). Involvement of actin polymerization in vesicle recruitment at the calyx of Held synapse. Journal of Neuroscience *23*, 837-846.

Sakaba, T., Schneggenburger, R., and Neher, E. (2002). Estimation of quantal parameters at the calyx of Held synapse. Neurosci Res *44*, 343-356.

Samigullin, D., Bill, C.A., Coleman, W.L., and Bykhovskaia, M. (2004). Regulation of transmitter release by synapsin II in mouse motor terminals. J Physiol (Lond) *561*, 149-158.

Sankaranarayanan, S., Atluri, P.P., and Ryan, T.A. (2003). Actin has a molecular scaffolding, not propulsive, role in presynaptic function. Nat Neurosci *6*, 127-135.

Santos, M.S., Barbosa, J., Veloso, G.S., Ribeiro, F., Kushmerick, C., Gomez, M.V., Ferguson, S.S., Prado, V.F., and Prado, M.A. (2001). Trafficking of green fluorescent protein tagged-vesicular acetylcholine transporter to varicosities in a cholinergic cell line. Journal of neurochemistry *78*, 1104-1113.

Santos, M.S., Li, H., and Voglmaier, S.M. (2009). Synaptic vesicle protein trafficking at the glutamate synapse. Neuroscience *158*, 189-203.

Sara, Y., Virmani, T., Deák, F., Liu, X., and Kavalali, E.T. (2005). An isolated pool of vesicles recycles at rest and drives spontaneous neurotransmission. Neuron *45*, 563-573.

Sätzler, K., Söhl, L.F., Bollmann, J.H., Borst, J.G.G., Frotscher, M., Sakmann, B., and Lübke, J.H.R. (2002). Three-dimensional reconstruction of a calyx of Held and its postsynaptic principal neuron in the medial nucleus of the trapezoid body. Journal of Neuroscience *22*, 10567-10579.

Schaub, J.R., Lu, X., Doneske, B., Shin, Y.-K., and McNew, J.A. (2006). Hemifusion arrest by complexin is relieved by Ca2+-synaptotagmin I. Nat Struct Mol Biol *13*, 748-750.

Schneggenburger, R., and Forsythe, I.D. (2006). The calyx of Held. Cell Tissue Res *326*, 311-337.

Schneggenburger, R., Meyer, A.C., and Neher, E. (1999). Released fraction and total size of a pool of immediately available transmitter quanta at a calyx synapse. Neuron *23*, 399-409.

Schneggenburger, R., and Neher, E. (2000). Intracellular calcium dependence of transmitter release rates at a fast central synapse. Nature *406*, 889-893.

Schneggenburger, R., Sakaba, T., and Neher, E. (2002). Vesicle pools and short-term synaptic depression: lessons from a large synapse. Trends Neurosci *25*, 206-212.

Schoch, S., Deák, F., Königstorfer, A., Mozhayeva, M., Sara, Y., Südhof, T.C., and Kavalali, E.T. (2001). SNARE function analyzed in synaptobrevin/VAMP knockout mice. Science *294*, 1117-1122.

Schweizer, F.E., Dresbach, T., DeBello, W.M., O'Connor, V., Augustine, G.J., and Betz, H. (1998). Regulation of neurotransmitter release kinetics by NSF. Science *279*, 1203-1206.

Schwenger, D.B., and Kuner, T. (2010). Acute genetic perturbation of exocyst function in the rat calyx of Held impedes structural maturation, but spares synaptic transmission. Eur J Neurosci *32*, 974-984.

Shapira, M., Zhai, R.G., Dresbach, T., Bresler, T., Torres, V.I., Gundelfinger, E.D., Ziv, N.E., and Garner, C.C. (2003). Unitary assembly of presynaptic active zones from Piccolo-Bassoon transport vesicles. Neuron *38*, 237-252.

Shupliakov, O., Bloom, O., Gustafsson, J.S., Kjaerulff, O., Low, P., Tomilin, N., Pieribone, V.A., Greengard, P., and Brodin, L. (2002). Impaired recycling of synaptic vesicles after acute perturbation of the presynaptic actin cytoskeleton. Proc Natl Acad Sci USA *99*, 14476-14481.

Siksou, L., Rostaing, P., Lechaire, J.-P., Boudier, T., Ohtsuka, T., Fejtová, A., Kao, H.-T., Greengard, P., Gundelfinger, E.D., Triller, A.*, et al.* (2007). Three-dimensional architecture of presynaptic terminal cytomatrix. Journal of Neuroscience *27*, 6868-6877.

Sommer, I., Lingenhöhl, K., and Friauf, E. (1993). Principal cells of the rat medial nucleus of the trapezoid body: an intracellular in vivo study of their physiology and morphology. Exp Brain Res *95*, 223-239.

Stevens, C.F., and Williams, J.H. (2007). Discharge of the readily releasable pool with action potentials at hippocampal synapses. J Neurophysiol *98*, 3221-3229.

Stone, L.M., Browning, M.D., and Finger, T.E. (1994). Differential distribution of the synapsins in the rat olfactory bulb. The Journal of neuroscience : the official journal of the Society for Neuroscience *14*, 301-309.

Südhof, T.C. (2004). The synaptic vesicle cycle. Annu Rev Neurosci *27*, 509-547.

Südhof, T.C., Czernik, A.J., Kao, H.T., Takei, K., Johnston, P.A., Horiuchi, A., Kanazir, S.D., Wagner, M.A., Perin, M.S., and De Camilli, P. (1989). Synapsins: mosaics of shared and individual domains in a family of synaptic vesicle phosphoproteins. Science *245*, 1474-1480.

Sun, J., Bronk, P., Liu, X., Han, W., and Südhof, T.C. (2006). Synapsins regulate use-dependent synaptic plasticity in the calyx of Held by a Ca2+/calmodulin-dependent pathway. Proc Natl Acad Sci USA *103*, 2880-2885.

Sun, J., Pang, Z.P., Qin, D., Fahim, A.T., Adachi, R., and Südhof, T.C. (2007). A dual-Ca2+-sensor model for neurotransmitter release in a central synapse. Nature *450*, 676-682.

Sun, J.Y., and Wu, L.G. (2001). Fast kinetics of exocytosis revealed by simultaneous measurements of presynaptic capacitance and postsynaptic currents at a central synapse. Neuron *30*, 171-182.

Takamori, S., Holt, M., Stenius, K., Lemke, E.A., Grønborg, M., Riedel, D., Urlaub, H., Schenck, S., Brügger, B., Ringler, P.*, et al.* (2006). Molecular anatomy of a trafficking organelle. Cell *127*, 831-846.

Takei, Y., Harada, A., Takeda, S., Kobayashi, K., Terada, S., Noda, T., Takahashi, T., and Hirokawa, N. (1995). Synapsin I deficiency results in the structural change in the presynaptic terminals in the murine nervous system. J Cell Biol *131*, 1789-1800.

Tang, Y.-g., Schlumpberger, T., Kim, T.-s., Lueker, M., and Zucker, R.S. (2000). Effects of Mobile Buffers on Facilitation: Experimental and Computational Studies. Biophysical Journal *78*, 2735-2751.

Taschenberger, H., Leão, R.M., Rowland, K.C., Spirou, G.A., and von Gersdorff, H. (2002). Optimizing synaptic architecture and efficiency for high-frequency transmission. Neuron *36*, 1127-1143.

Taschenberger, H., and von Gersdorff, H. (2000). Fine-tuning an auditory synapse for speed and fidelity: developmental changes in presynaptic waveform, EPSC kinetics, and synaptic plasticity. J Neurosci *20*, 9162-9173.

Terada, S., Tsujimoto, T., Takei, Y., Takahashi, T., and Hirokawa, N. (1999). Impairment of inhibitory synaptic transmission in mice lacking synapsin I. J Cell Biol *145*, 1039-1048.

Timofeev, I. (2011). Neuronal plasticity and thalamocortical sleep and waking oscillations. Prog Brain Res *193*, 121-144.

Torri Tarelli, F., Bossi, M., Fesce, R., Greengard, P., and Valtorta, F. (1992). Synapsin I partially dissociates from synaptic vesicles during exocytosis induced by electrical stimulation. Neuron *9*, 1143-1153.

Torri-Tarelli, F., Villa, A., Valtorta, F., De Camilli, P., Greengard, P., and Ceccarelli, B. (1990). Redistribution of synaptophysin and synapsin I during alpha-latrotoxin-induced release of neurotransmitter at the neuromuscular junction. J Cell Biol *110*, 449-459.

Ueda, T., Maeno, H., and Greengard, P. (1973). Regulation of endogenous phosphorylation of specific proteins in synaptic membrane fractions from rat brain by adenosine 3':5'-monophosphate. J Biol Chem *248*, 8295-8305.

Vaccaro, P., Dente, L., Onofri, F., Zucconi, A., Martinelli, S., Valtorta, F., Greengard, P., Cesareni, G., and Benfenati, F. (1997). Anti-synapsin monoclonal antibodies: epitope mapping and inhibitory effects on phosphorylation and Grb2 binding. Brain Res Mol Brain Res *52*, 1-16.

Valtorta, F., Benfenati, F., and Greengard, P. (1992). Structure and function of the synapsins. J Biol Chem *267*, 7195-7198.

Venton, B.J., Seipel, A.T., Phillips, P.E.M., Wetsel, W.C., Gitler, D., Greengard, P., Augustine, G.J., and Wightman, R.M. (2006). Cocaine increases dopamine release by mobilization of a synapsin-dependent reserve pool. The Journal of neuroscience : the official journal of the Society for Neuroscience *26*, 3206-3209.

Verhage, M., Maia, A.S., Plomp, J.J., Brussaard, A.B., Heeroma, J.H., Vermeer, H., Toonen, R.F., Hammer, R.E., van den Berg, T.K., Missler, M.*, et al.* (2000). Synaptic assembly of the brain in the absence of neurotransmitter secretion. Science *287*, 864-869.

Vogel, S.S., Blank, P.S., and Zimmerberg, J. (1996). Poisson-distributed active fusion complexes underlie the control of the rate and extent of exocytosis by calcium. J Cell Biol *134*, 329-338.

von Gersdorff, H., and Borst, J.G.G. (2002). Short-term plasticity at the calyx of held. Nat Rev Neurosci *3*, 53-64.

von Gersdorff, H., Schneggenburger, R., Weis, S., and Neher, E. (1997). Presynaptic depression at a calyx synapse: the small contribution of metabotropic glutamate receptors. J Neurosci *17*, 8137-8146.

Wadel, K., Neher, E., and Sakaba, T. (2007). The coupling between synaptic vesicles and Ca2+ channels determines fast neurotransmitter release. Neuron *53*, 563-575.

Wang, L.Y., and Kaczmarek, L.K. (1998). High-frequency firing helps replenish the readily releasable pool of synaptic vesicles. Nature *394*, 384-388.

Wang, Y., and Manis, P.B. (2008). Short-Term Synaptic Depression and Recovery at the Mature Mammalian Endbulb of Held Synapse in Mice. Journal of Neurophysiology *100*, 1255-1264.

Wilhelm, B.G., Groemer, T.W., and Rizzoli, S.O. (2010). The same synaptic vesicles drive active and spontaneous release. Nat Neurosci *13*, 1454-1456.

Wimmer, V.C., Horstmann, H., Groh, A., and Kuner, T. (2006). Donut-like topology of synaptic vesicles with a central cluster of mitochondria wrapped into membrane protrusions: a novel structure-function module of the adult calyx of Held. Journal of Neuroscience *26*, 109-116.

Wimmer, V.C., Nevian, T., and Kuner, T. (2004). Targeted in vivo expression of proteins in the calyx of Held. Pflugers Arch *449*, 319-333.

Wölfel, M., Lou, X., and Schneggenburger, R. (2007). A mechanism intrinsic to the vesicle fusion machinery determines fast and slow transmitter release at a large CNS synapse. J Neurosci *27*, 3198-3210.

Wölfel, M., and Schneggenburger, R. (2003). Presynaptic capacitance measurements and Ca2+ uncaging reveal submillisecond exocytosis kinetics and characterize the Ca2+ sensitivity of vesicle pool depletion at a fast CNS synapse. J Neurosci *23*, 7059-7068.

Wu, L.G., Westenbroek, R.E., Borst, J.G., Catterall, W.A., and Sakmann, B. (1999). Calcium channel types with distinct presynaptic localization couple differentially to transmitter release in single calyx-type synapses. The Journal of neuroscience : the official journal of the Society for Neuroscience *19*, 726-736.

Wu, W., and Wu, L.-G. (2007). Rapid bulk endocytosis and its kinetics of fission pore closure at a central synapse. Proc Natl Acad Sci USA *104*, 10234-10239.

Wu, W., Xu, J., Wu, X.-S., and Wu, L.-G. (2005). Activity-dependent acceleration of endocytosis at a central synapse. J Neurosci *25*, 11676-11683.

Xu, J., and Wu, L.-G. (2005). The decrease in the presynaptic calcium current is a major cause of short-term depression at a calyx-type synapse. Neuron *46*, 633-645.

Yamashita, T., Eguchi, K., Saitoh, N., von Gersdorff, H., and Takahashi, T. (2010). Developmental shift to a mechanism of synaptic vesicle endocytosis requiring nanodomain Ca2+. Nat Neurosci *13*, 838-844.

Yang-Feng, T.L., DeGennaro, L.J., and Francke, U. (1986). Genes for synapsin I, a neuronal phosphoprotein, map to conserved regions of human and murine X chromosomes. Proc Natl Acad Sci USA *83*, 8679-8683.

Yuste, R., and Bonhoeffer, T. (2001). Morphological changes in dendritic spines associated with long-term synaptic plasticity. Annu Rev Neurosci *24*, 1071-1089.

Zhai, R.G., Vardinon-Friedman, H., Cases-Langhoff, C., Becker, B., Gundelfinger, E.D., Ziv, N.E., and Garner, C.C. (2001). Assembling the presynaptic active zone: a characterization of an active one precursor vesicle. Neuron *29*, 131-143.

Ziv, N.E., and Garner, C.C. (2004). Cellular and molecular mechanisms of presynaptic assembly. Nat Rev Neurosci *5*, 385-399.

Zucker, R.S., and Regehr, W.G. (2002). Short-term synaptic plasticity. Annu Rev Physiol *64*, 355-405.